UNIVERSITÀ DEGLI STUDI DELL'AQUILA
DIPARTIMENTO DI INGEGNERIA E SCIENZE DELL'INFORMAZIONE E MATEMATICA

Dottorato di Ricerca in Ingegneria e Scienze dell'Informazione

Curriculum Systems engineering, telecommunications and HW/SW platforms

XXXV ciclo

Titolo della tesi

Multilevel battery systems for electric mobility and smart grids: from cell models to system behavior

SSD ING/IND-32

Dottorando

Roberta Di Fonso

Coordinatore del corso

Prof.Vittorio Cortellessa

Tutor

Prof. Carlo Cecati

A.A. 2021/2022

Summary

The storage of electric energy is a key process in mobility applications but is also essential in fixed smart grids for the time-shifting of energy production/consumption. The storage unit is usually a battery pack with adequate power factors and with requirements concerning energy density, lightweight and long life cycle. The high voltage of the battery is obtained by a series connection of elementary cells and the low internal impedance of the battery is obtained by parallel connections of cells or streams of cells. In many applications, the battery is seen as a raw energy source, unsuitable to directly power the load. Thus, a converter/inverter is usually put as an interface between the battery and the final load to assure the required quality of output voltage. The first part of this thesis explores the advantages that can be gained by including the multilevel solutions of inverters inside the battery architecture. Instead of a fixed stream of cells, the battery contains a stream of modules. Each module has insert/bypass power switches and one or a group of battery cells. By properly driving the switches at sampling times, the battery can synthesize a desired DC or even an AC output voltage. The number of modules can be redundant in order to assure fault tolerance against cell failures and/or to accommodate a greater total charge capacity. Batteries are governed by complex internal chemical reactions, that are not completely reversible. Thus continuously charging and discharging the battery gives rise to what is commonly known as ageing. Ageing implies changes in the internal impedance of the battery and a decrease in the to-

tal charge capacity over time. The internal impedance is usually observed experimentally, and this requires expensive equipment and delicate test procedures. Moreover, observing the effects of ageing on real batteries is very time-consuming, since many charge-discharge cycles need to be performed. These operations can take months in the lab and, moreover, require special equipment to ensure safety. Batteries are complex non-linear systems that must be run under the supervision of a Battery Management System (BMS) to assure safe charge/discharge operations. The development of a complete autonomous system requires fine-tuning of many algorithms, which include the SoC/SoH estimation algorithms from voltage and currents signals at the battery terminals. Thus precise simulations of various components play a crucial role in the successful design of an efficient BMS. Therefore, a robust battery model is required for field applications. Depending on the desired level of abstraction, a multitude of models have been developed by researchers worldwide. Among these, ECM models represent an effective and computationally light solution to capture the battery behavior. The behavior of the cell is described by common circuit elements whose properties represent the internal chemical processes. ECM are usually static models, but to make them more realistic, dynamic circuit parameters can be considered. In recent years, many high-end laboratories have released datasets with battery experimental data, making them publicly available for researchers worldwide. Although these data are very useful for the scientific community, they are necessarily limited to a few working conditions of selected battery cells.
The second part of this thesis aims at developing a Battery Digital Twin (BDT) that receives normalized state of charge, state of heath parameters as inputs, and produces a realistic voltage output signal in response to a load current waveform of any shape. This characteristic allows to use the BDT for many purposes: (i) for the validation of SoC and SoH estimation algorithms (ii) for battery monitoring or diagnostic when run in parallel with the real battery.

This BDT is very useful in smart batteries where the single cells inside the pack can be used according to their states (SoC, SoH), possibly leading to a longer lifetime of the battery. It is therefore essential, especially in SB, to have a tool that is able to simulate cells at different SoC and SoH. Since the BDT allows to simulate a smart battery pack with cells at different charge and ageing states, it can be used for the validation of different SB balancing algorithms, consequently allowing to test the optimization of the lifetime of the SB. The BDT is developed in the Matlab-Simulink-Simscape environment. The non-linear ECM parameters depending on SoC/SoH values are based on feed-forward Neural Networks (NN) trained with real data from the NASA Prognostic Repository, publicly available online.

Acknowledgments

First and foremost I would like to thank my esteemed Supervisor Professor Carlo Cecati for his supervision and support and I would like to extend my gratitude also to Professor Concettina Buccella. I thank them for all the advice and for the opportunities they offered me and for their kindness. I would like to express my deepest appreciation to Professor Remus Teodorescu who supervised my work at Aalborg University. He made me feel like I was a part of his research group. His constant hunger to seek new challenges and reach new goals helped me expand my mind. I thank him for all the interesting meetings, for sharing with me his valuable knowledge and for supporting me. I deeply appreciated his friendly nature and his dedication to creating a cohesive and happy work team. A special and heartfelt thank to Professor Pallavi Bharadwaj who also supervised my work at Aalborg University. I cannot begin to express my gratitude for all her advice and for profoundly believing in my abilities. This encouraged me to work harder. Her brilliant mind and sparkling enthusiasm for research are one of a kind. I would like to thank the DISIM Department of the University of L'Aquila and MUR for giving me the chance to pursue my PhD and for funding my scholarship. On a personal level, I would like to express my deepest appreciation to my loyal, supportive and caring family, especially my sister Alessia, whom I shared my PhD experience with. None of this would have been possible without all their love and unwavering support in every possible way. I thank them for always undestanding my decisions, for all the sacrifices they made to help

me to flourish and for being the shoulder I could lean on whenever I needed it. I would like to extend my sincere thanks to all my colleagues, both in L'Aquila and in Aalborg. I was lucky enough to find valuable friends among them! Especially thanks to Francesco, Morteza, Sobhan, Pallavi, Hannah and Daniela. I thank them for all the time spent together, the travels, the coffee breaks, the concerts and all the laughter. Their warmth, generosity and thoughtfulness meant a lot to me. Many thanks to my cousins and best friends who always supported me, lifted me up and pushed me to be better: Mara, Giuseppe, Alessandro, Marco and Alessio. Their joy, good heart and radiance light up my life and I am very grateful to have them in it.

Nomenclature

AI	Artificial Intelligence
BDT	Battery Digital Twin
BMS	Battery Management System
BP	Battery Pack
CC-CV	Constant Current - Constant Voltage
CHB	Chained H-Bridge
CPE	Constant Phase Element
CWT	Continuous Wavelet Transform
DoD	Depth of Discharge
ECM	Equivalent Circuit Model
EIS	Electrochemical Impedance Spettroscopy
EV	Electric Vehicle
IR	Internal Resitance
Li-ion	Lithium-Ion
LIB	Lithium-ion Battery

LUT	Look-Up Table
MKNA	Multidimensional K-nearest control algorithm
ML	Machine Learning
MSE	Mean Squared Error
NN	Neural Network
OCV	Open Circuit Voltage
PEV	Pure Electric Vehicle
PMSM	Permanent Magnet Synchronous Motor
RW	Random Walk
SB	Smart Battery
SBP	Smart Battery Pack
SEI	Solid Electrolyte Interphase
SoC	State of Charge
SoH	State of Health
VCVS	Variable Controlled Voltage Source
WLTC	Worldwide harmonized Light duty driving Test Cycle

List of Figures

Contents

Introduction

Background

The storage of electric energy is a key process in mobility applications but is also essential in fixed smart grids for the time-shifting of energy production/consumption. One of the key features of a smart grid is its capacity to handle various distributed storage alternatives and renewable energy sources. To distribute electricity to customers more effectively, the smart grid combines cutting-edge sensor technologies, control techniques, and communication technologies into existing power distribution systems[10]. A significant part of the generation in the smart grid comes from renewable energy resources such as wind and solar. The unpredictability and intermittent nature of these renewable sources pose serious challenges to the network during energy generation, transmission, and distribution. The smart grid operation can be of two types: power applications and energy applications. Power applications require the management of short bursts of high power, ranging from a few seconds to a few minutes. Energy applications require a system able to store a large amount of energy and discharge it over a longer period of time. In both applications, Li-ion Batteries (LIB) turned out to be a valuable and effective solution[14]. Despite the rapid evolution of battery technologies, several factors need to be taken into account to achieve a successful application of battery-powered solutions in smart grids. There are still concerns regarding the total cost (including manufacturing, management

and replacement), lifetime, power delivery and environmental impact[18].

Battery packs and related issues

Thanks to their high energy density (up to 200 Wh/kg), high energy efficiency (more than 95%) and long cycle life (3000 cycles at deep discharge of 80%) [10], LIBs are employed in a broad range of applications: they are an effective solution for the integration of renewable energy sources in the smart grid and they are the preferred solution for electric mobility, ranging from Electric Vehicles (EVs) to mobile robots. Every class of application will require a tailored battery solution. To obtain a battery of the required voltage and charge capacity, elementary battery cells are connected in series/parallel. Cells can also be arranged in modules that can in turn be connected in series and/or parallel. The ensemble of cells/modules forms the battery pack (BP). The cells inside the battery pack are not perfectly equal. The cells can have different charge capacities and this could happen for various reasons: it could be a result of the manufacturing process or the results of the ageing mechanism that affects the cells differently[19]. Moreover, leakage currents and different working conditions can impact the cells, causing State of Charge (SoC) imbalances that lead to different Depth of Discharge (DoD) of the cells[9]. Temperature gradient inside the battery pack is another important issue and can be the result of parameter variation of the cells (internal resistance and/or thermal resistance variation) and temperature variation of the coolant of the EV. As a result, the cells in the pack are not equally utilized, and the weakest cell in a series-connected battery can stop the whole operation due to overcharge or over-discharge, so it is not possible to use all the energy stored in the battery. Furthermore, the battery lifetime is heavily affected by SoC imbalance and high temperature. To circumvent these issues, strategies are needed for balancing SoC and limiting the temperature gradient. A crucial component of a battery pack is the Battery Manage-

ment System (BMS): it ensures safe and reliable operation of the battery and it provides an estimation of the battery states, namely SoC and State of Health (SoH). BMS are also crucial in EVs, where Li-ion battery safety is a non-negotiable requirement to prevent the risk of fire and hazard to the vehicle passengers. The BMS main features are: (1) cell monitoring (voltage, current and temperature measurements) (2) battery safety and protection (3) cell balancing (4) SoC and SoH estimation (5) charge control (6) thermal management.

Battery models

Depending on the desired level of abstraction, a multitude of models have been developed by researchers worldwide. There are three big categories of battery models: (i) physics and multi-physics models that aim at describing the complex internal chemical phenomena of batteries[11]; these can be considered lower-level models (ii) empirical models that use past experimental data to develop a strategy for predicting future behavior[8]; (iii) Equivalent Circuit Models (ECM) aim at simulating the battery behavior using circuit elements[17], these models can be considered to be at higher level. ECM models are usually static, but research shows that using dynamic circuit elements, tuned with look-up tables (LUTs) allows to achieve high-fidelity model of the battery behavior[13].

Multilevel battery solutions

In many applications, the battery is seen as a raw energy source, unsuitable to directly power the load. Thus, a converter/inverter is usually put as an interface between the battery and the final load to assure the required quality of output voltage. Innovative battery topologies that integrate the multilevel inverter concept have been developed in literature[16, 15]. Instead

of a fixed stream of cells, the battery contains a stream of modules. Each module has insert/bypass power switches and one or more battery cells. By properly driving the switches at sampling times, the battery can synthesize a desired DC or even an AC output voltage, as well as performing cell balancing, charge control and subsequent thermal management. The number of modules can be redundant in order to assure fault tolerance against cell failures and/or to accommodate a greater total charge capacity. Among these battery solutions, the Smart Battery (SB) is an innovative concept that combines advanced power electronics, Artificial Intelligence (AI) and wireless communication with the goal of developing a new generation of battery solutions for e-mobility and grid storage [20]. The SB topology is based on the series connection of modules. Each module has a cell with an insertion/bypass circuit and a local processor that monitors the cell states[12]. The SB has more cells than strictly necessary to synthesize the desired nominal voltage, so the whole battery has a higher total charge capacity compared to a standard battery. By strategically exploiting the insertion/bypass mechanism, it is possible to design a control algorithm that uses the cells in the battery uniformly, according to their SoC, temperature and possibly SoH, thus extending the lifetime of the battery[3]. When a cell is bypassed, it has time to rest. This rest time can be used to allow a cell to cool off when its temperature is too high so it can be inserted again when it has in-the-range temperature values. The insertion/bypass circuit can also be used to: (i) bypass a low-charge cell, putting it to rest until the next charge (ii) bypass a faulted cell, so the SB can keep working.

This work has been developed under the Programma Operativo Nazionale 2014-2020 (CCI 2014IT16M2OP005), Fondo Sociale Europeo, Azione I.1 “Dottorati Innovativi con caratterizzazione industriale”. The project was developed in collaboration with Aalborg University, Denmark and Digipower ltd.

Thesis motivation

Batteries are the energy source for a wide range of electrical applications. However, there are still challenges that need to be addressed to develop effective solutions:

- **Need for a flexible battery architecture:** at present batteries are built from a fixed stream of series/parallel cells However, the cells inside the battery are not perfectly equal. As a result, the weakest cell in a series-connected stream can be overcharged or over-discharged, lowering the whole battery's performance. To maximize the battery charge capacity, cell balancing is needed. Cell balancing can be either passive or active: passive balancing techniques dissipate the energy of higher SoC cells through resistors. Classical active balancing techniques use additional circuits like DC/DC converters to distribute the charge among the cells. In both cases, part of the energy of the battery is lost. Strategies are thus needed to use the cells in the battery pack optimally, with also benefits on the battery lifetime. Moreover, in many applications, the battery is seen as a raw energy source, unsuitable to directly power the load due to the changing of voltage as the cells discharge and age. A flexible architecture could compensate for these effects and enable the synthesis of a stabilized DC or even an AC output voltage.
- **Need for a dynamic cell/Battery model for realistic simulations:** batteries exhibit a non-linear behavior during charge-discharge cycles and lifetime. The successful design of a complex system, such as a BMS, requires a realistic simulation model of the battery. The battery's internal parameters depend on SoC and SoH and are usually observed performing expensive and time-consuming laboratory experiments, usually at fixed SoC and SoH values. Thus, a model with fixed

parameters cannot successfully fit the wide range of battery SoC and SoH. Hence the need for a dynamic battery model that can simulate a specific cell at different SoC and ageing times.

Thesis objectives

To address the above-mentioned challenges, the main objectives are the following:

- **explore the advantages of multilevel battery systems for cell balancing and load management.**
- **develop cell models as a function of SoC and SoH.**

Thesis outline

The thesis is organized as follows:

The first part of the thesis will focus on the applications of multilevel-based battery systems. Chapter 1 presents a multilevel battery solution for the synthesis of the AC driving voltage to power a PMSM motor inside an electric car. Each module has a half bridge and an ideal cell. The proposed topology is exploited to develop a regenerative braking system to recover the kinetic energy of the car during braking. Chapter 2 addresses the issue of Soc and temperature imbalances of battery cells that constitute battery packs. The SB topology is introduced. An intelligent algorithm based on Machine Learning (ML) is proposed, with the aim of choosing in real time which cells need to be connected/bypassed, according to their states and temperatures.

The goal is to synthesize a stabilized DC output voltage of a SB, while simultaneously balancing the SOC and reducing the temperature spread among the cells.

The second part of the thesis will focus on cell models. Chapter 3 presents the Li-ion basic operation and ageing effects. Chapter 4 introduces the issues related to battery modelling and focuses on the ECM models of a battery cell showing the correlation of RC components with internal electrochemical processes. Chapter 5 presents a method to parametrize a Simulink predefined model using a data-driven approach. Two different ways of computing the parameters are explored: using datasheets provided by the manufacturer and using more extensive laboratory measurements. Chapter 6 presents an innovative methodology to extract the ECM model as a function of the SoC and SoH of the cell from pulsed discharge signals. Furthermore, a methodology for OCV extraction is provided. Chapter 7 shows how to use the results presented in Chapter 6 to synthesize a NN-based Battery Digital Twin (BDT). The BDT receives normalized SoC, SoH parameters as inputs, and produces a realistic voltage output signal in response to a load current waveform of any shape. Chapter 8 summarizes the main contributions and gives an overview of future work.

List of publications

[1] Roberta Di Fonso and Carlo Cecati. Navigation and motors control of a differential drive mobile robot. In *2023 International Conference on Control, Automation and Diagnosis (ICCAD)*, pages 1–6, 2023.

[2] Roberta Di Fonso and Carlo Cecati. Test cycle simulation of an electric car with regenerative braking. In *2020 AEIT International Conference of Electrical and Electronic Technologies for Automotive (AEIT AUTOMOTIVE)*, pages 1–5, 2020.

[3] Roberta Di Fonso, Xin Sui, Anirudh Budnar Acharya, Remus Teodorescu, and Carlo Cecati. Multidimensional machine learning balancing in smart battery packs. In *IECON 2021 47th Annual Conference of the IEEE Industrial Electronics Society*, pages 1–6, 2021.

[4] Roberta Di Fonso, Pallavi Bharadwaj, Remus Teodorescu, and Carlo Cecati. Internal resistance estimation of li-ion batteries using wavelet analysis. In *2022 IEEE 13th International Symposium on Power Electronics for Distributed Generation Systems (PEDG)*, pages 1–5, 2022.

[5] Roberta Di Fonso, Pallavi Bharadwaj, Remus Teodorescu, and Carlo Cecati. A battery digital twin based on neural network for testing soc/soh algorithms. In *2022 IEEE 20th International Power Electronics and Motion Control Conference (PEMC)*, pages 655–660, 2022.

[6] Roberta Di Fonso, Remus Teodorescu, Daniel-Ioan Stroe, Carlo Cecati, and Pallavi Bharadwaj. Data-driven modeling of li-ion battery based on the manufacturer specifications and laboratory measurements. In *2022 IEEE Power Electronics, Drives and Energy Systems (PEDES)*, 2022.

[7] Roberta Di Fonso, Remus Teodorescu, Carlo Cecati, and Pallavi Bharadwaj. A battery digital twin from pulsed laboratory data using wavelet analysis and neural networks. *Submitted for publication to IEEE Transaction on Industrial Informatics*, 2023.

References

[8] Empirical modeling of lithium-ion batteries based on electrochemical impedance spectroscopy tests. *Electrochimica Acta*, 160:169–177, 2015.

[9] Faisal Altaf. *Thermal and State-of-Charge Balancing of Batteries using Multilevel Converters*. PhD thesis, Mar. 2014.

[10] Tianmei Chen, Yi Jin, Hanyu Lv, Antao Yang, Meiyi Liu, Bing Chen, Ying Xie, and Qiang Chen. Applications of lithium-ion batteries in grid-scale energy storage systems. *Transactions of Tianjin University*, 26, 02 2020.

[11] W. B. Gu and C. Y. Wang. Thermal electrochemical modeling of battery systems. *2000 J. Electrochem. Soc. 147 2910.*

[12] Xinrong Huang, Anirudh Budnar Acharya, Jinhao Meng, Xin Sui, Daniel-Ioan Stroe, and Remus Teodorescu. Wireless smart battery management system for electric vehicles. In *IEEE Energy Conv. Congr. Expo. (ECCE)*, pages 5620–5625, 2020.

[13] Tarun Huria, Massimo Ceraolo, Javier Gazzarri, and Robyn Jackey. High fidelity electrical model with thermal dependence for characterization and simulation of high power lithium battery cells. In *2012 IEEE International Electric Vehicle Conference*, pages 1–8, 2012.

[14] Alireza Khaligh and Zhihao Li. Battery, ultracapacitor, fuel cell, and hybrid energy storage systems for electric, hybrid electric, fuel cell, and

plug-in hybrid electric vehicles: State of the art. *IEEE Transactions on Vehicular Technology*, 59(6):2806–2814, 2010.

[15] Branko Majmunovic, Radhika Sarda, Remus Teodorescu, Cristian Lascu, and Mattia Ricco. Highly efficient smart battery pack for ev drivetrains. In *IEEE Veh. Power Propuls.Conf.(VPPC)*, pages 1–5, 2017.

[16] Antonio Manenti, Andrea Abba, Alessandro Merati, Sergio M. Savaresi, and Angelo Geraci. A new bms architecture based on cell redundancy. *IEEE Trans. Ind. Electron.*, 58(9):4314–4322, 2011.

[17] Gregory Plett. *Battery Management Systems, Volume II: Equivalent-Circuit Methods.* 2015.

[18] Habiballah Rahimi-Eichi, Unnati Ojha, Federico Baronti, and Mo-Yuen Chow. Battery management system: An overview of its application in the smart grid and electric vehicles. *IEEE Industrial Electronics Magazine*, 7(2):4–16, 2013.

[19] Mattia Ricco, Jinhao Meng, Tudor Gherman, Gabriele Grandi, and Remus Teodorescu. Smart battery pack for electric vehicles based on active balancing with wireless communication feedback. *Energies*, 12(20), 2019.

[20] Remus Teodorescu, Xin Sui, Soren B. Vilsen, Pallavi Bharadwaj, Abhijit Kulkarni, and Daniel-Ioan Stroe. Smart battery technology for lifetime improvement. *Batteries*, 8(10), 2022.

Chapter 1

Synthesis of an AC power signal for driving a PMSM motor

1.1 Background

Electric propulsion can be adopted in a wide class of applications such as cars, trucks, vehicles for mobility-impaired people, industrial robots and much more [4]. Multilevel inverters are a class of power electronics converters that are able to operate at high voltages and allow to create stepped output voltages [1, 2, 6, 7, 9, 12, 14, 15]. They are mainly employed in high [13] medium voltage industry and traction applications [14], but their use can be effectively extended to road transportation [11]. Multilevel converters output voltages that better approximate the ideal sinusoidal reference that an electric machine should have as input [13]. These sinusoidal-like voltages make the PMSM motor perform more closely to the ideal operation, creating less heat and vibrations and diminishing torque ripples [11]. The converter itself has better operations due to low-frequency operations, lower dv/dt and di/dt [8]. The higher the number of levels, the better the approximation, hence operations [5, 10], but the higher the converter complexity. A critical aspect of electric vehicles is the energy management which is directly corre-

lated to battery energy depletion. The so-called "range anxiety", i.e. the fear that the vehicle will not have enough energy to reach the desired destination, is one of the biggest deterrents in the diffusion of EVs. It is therefore essential to find a way to extend the autonomy of the vehicle and one promising approach consists of reducing energy consumption and recovering as much energy as possible. Electric machines, including PMSM motors, have the attractive ability to work both as motor (during acceleration, steady state) and, if properly supplied, as a generator during deceleration. This capability can be exploited to recover part of the kinetic energy during deceleration which is then capable of partially recharging the car battery pack. This type of operation requires a bidirectional DC-AC Multilevel converter [3]. In this chapter, a regenerative braking system for an EV will be developed and combined with the usage of multilevel converters. The underlying idea is that from one side multilevel converters power more efficiently the PMSM machine (thus having lessened motor losses), and from the other side, the regenerative braking systems allows to recover as much kinetic energy as possible. These two approaches combined allow to improve the energy management of the car. In this chapter, we will show: (i) the development of a regenerative braking system for the vehicle making use of the quarter car model; (ii) the comparison between a conventional braking system and proposed regenerative braking system (iii) the analysis for the energy consumption.

1.2 Quarter-car model

An electric vehicle can be modelled by a combination of a mechanical and electrical subsystems exchanging energy. The whole car model contains both a mechanical and an electrical subsystem in order to better simulate the energy exchange between the two domains. All simulations have been carried out in the Matlab-Simulink-Simscape development environment so it seems appropriate to use their symbols to describe the subsystems.

The mechanical model considered to pose the motor control problem of the car is the so-called "quarter car model" which consists of a wheel and its attachments and the mass of one-fourth of the total mass of the car. It has been assumed that there is no rotational motion in the body and the wheel in always in contact with the ground. The classical quarter car model assumes no friction, but in this work a rotational damper has been introduced to take into account the rotational loss. Fig. 1.1 shows the mechanical model of a quarter-car. The translational mass represents one-fourth of the car mass and is coupled to a wheel-and-axle mechanism. A rotational input to the axle (port A) produces a translational motion of the wheel periphery (port P). The wheel is simulated by a rotational inertia and the viscous friction is simulated by the rotational damper.

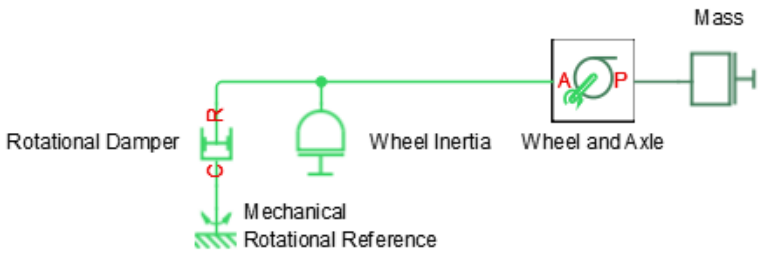

Figure 1.1: Quarter car mechanical model

Assuming that the wheel does not slip, the system is governed by the following equation:

$$T = \left(J + m \cdot r^2\right)\dot{\omega} + D \cdot \omega; \tag{1.1}$$

T	torque on the axle $[\mathrm{N}\cdot\mathrm{m}]$
J	wheel inertia $[Kg\cdot m^2]$
r	wheel radius $[m]$
m	quarter car mass $[Kg]$
ω	wheel angular speed $[\mathrm{rad}/\mathrm{sec}]$
D	damping coefficient $\left[\frac{\mathrm{N}\cdot\mathrm{m}}{\mathrm{rad}/\mathrm{sec}}\right]$

Fig.1.2 shows a portion of the electrical subsystem.

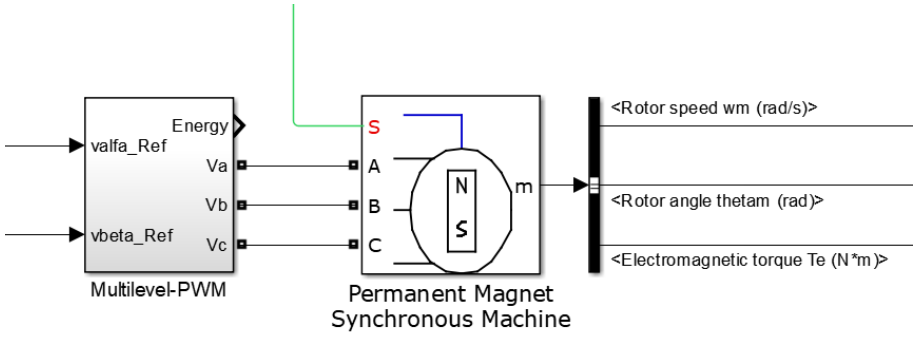

Figure 1.2: Electrical subsystem

The PMSM block is the interface between the electrical and the mechanical domain. Ports A, B and C are linked to a multilevel three-phase converter, port m is a bus for measurements and port S is a rotational shaft directly coupled to the wheel axle. The PMSM operates in either generator or motor mode. The mode of operation is dictated by the sign of the mechanical torque (positive for motor mode, negative for generator mode).

1.2.1 Multilevel battery system topology

The three-phase converter is a bidirectional 9-level DC-AC with PWM between levels in order to mitigate the transitions. The converter has four Chained-H-Bridge (CHB) per phase: each cell is powered by an isolated battery. This seems difficult to realize, but thinking of a wireless recharge systems, it can be accepted. Moreover, the chained architecture can allow

battery SoC balancing. It is assumed that the batteries and switches are nearly ideal, as the focus is on energy flow between the electrical and mechanical subsystems. The multilevel converter provides also an Energy output signal whose meaning is the total energy exchanged from 0 to t with the PMSM block. The Energy signal E is computed as the integral of the instantaneous power of the three phases, where $d\tau$ is the sampling period:

$$E(t) = \int_0^t (v_a(\tau) \cdot i_a(\tau) + v_b(\tau) \cdot i_b(\tau) + v_c(\tau) \cdot i_c(\tau)) d\tau \tag{1.2}$$

Fig. 1.3 shows one phase maximum voltage output from the multilevel converter. Each battery has a $V_{peak}/4$ voltage.

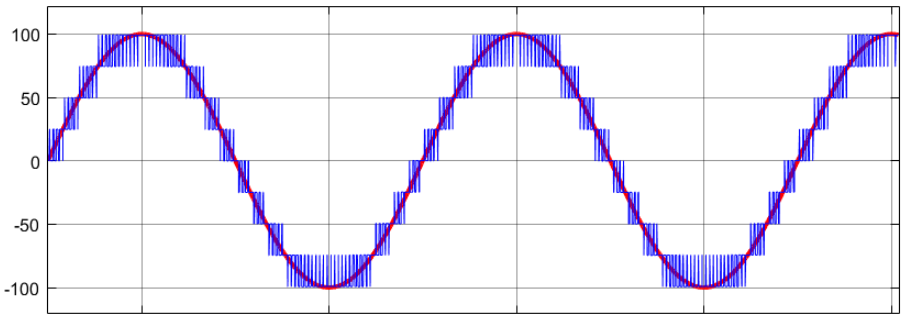

Figure 1.3: Maximum voltage output of the multilevel converter

The converter is driven by two-phase reference voltages v_α^*, v_β^* computed by the higher level control loops, as shown in Fig. 1.2.

1.3 PMSM control

Fig. 1.4 shows the inner loop to control the Iq, Id currents in the rotor reference frame. Id is controlled to zero (no flux weakening) so there is only one

input Iqref from higher levels. The PMSM is configured to be round rotor, sinusoidal back Emf, four pole pairs. The rotor angle is thus multiplied by 4, being the electrical speed four times the mechanical speed.

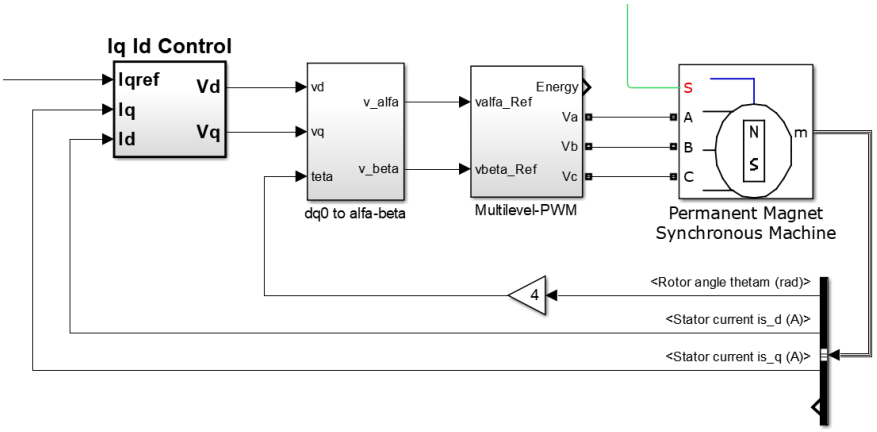

Figure 1.4: PMSM control: inner loop

Fig. 1.5 shows the outer loop that controls the rotor angular speed and thus the wheel and the car longitudinal speed.

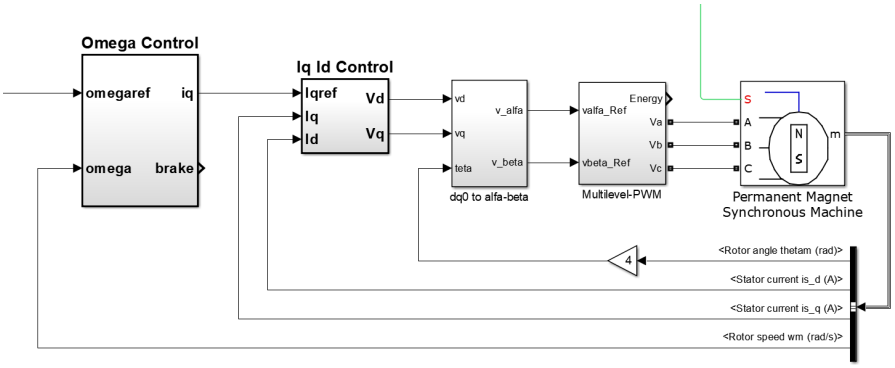

Figure 1.5: PMSM control: outher loop

The two control blocks are Matlab user defined functions, containing simple proportional-integral (PI) controllers.

1.4 Regenerative braking

The PMSM can be used in generator mode to brake the car and recharge the batteries. The following parameters have been chosen for the simulations:

Table 1.1: Simulation parameters

Quarter-car mass	400 Kg
Wheel radius	0.316 m
Wheel inertia	1 $[\mathrm{Kg}\cdot \mathrm{m}^2]$
Viscous dumper	0.1 $\left[\frac{\mathrm{N}\cdot\mathrm{m}}{\mathrm{rad/sec}}\right]$
Gear box ratio	3

The parameters in 1.1 are relative to an average electric car. The gearbox ratio value has been set to 3 for simulation purposes: a higher value would require less torque from the motor, but also a higher functioning frequency from the multilevel converter. The PMSM machine parameters are from model n.16 of the Simscape Power Systems Library:

Table 1.2: PMSM parameters

Stator phase resistance	0.05 Ω
Flux linkage	0.192 $[\mathrm{V}\cdot \mathrm{s}]$
Pole pairs	4
Torque constant	1.152 $\left[\frac{\mathrm{N}\cdot\mathrm{m}}{\mathrm{A}}\right]$

Fig. 1.6 shows a trapezoidal speed test of the quarter-car at the rotor level.

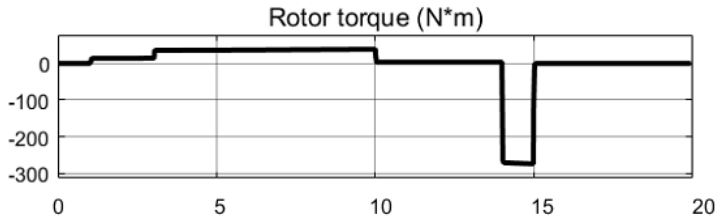

(a) Rotor torque

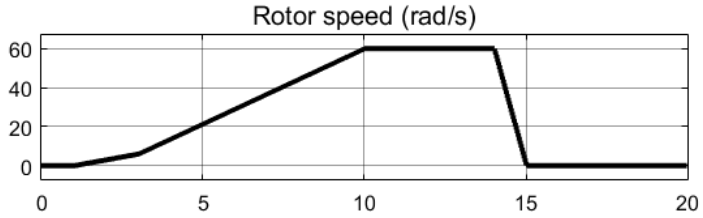

(b) Rotor speed

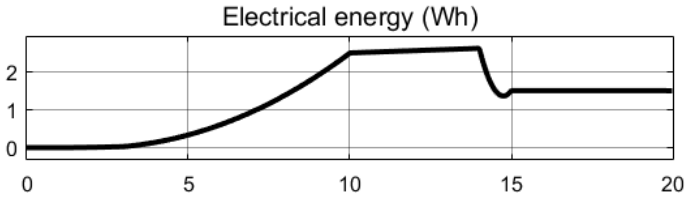

(c) Electrical energy

Figure 1.6: Trapezoidal speed test of the quarter-car at the rotor level

The rotor torque is positive and slightly increasing (due to the viscous damper) during constant acceleration and negative during braking. The electrical energy from the multilevel converter is decreasing during braking as the batteries are recharging. However, there are two problems with this simple solution:

- currents can be very high during braking with consequential excessive PMSM dissipation;
- at low speed the back Emf is not sufficient to assure the required braking torque. Thus energy is drown from batteries and the energy graph

rises before rotor stops.

A better and safer solution is to use a mix of electrical and mechanical braking. The mechanical brake is used to avoid high negative torque to the PMSM and for stopping the car. The PMSM brake is highly beneficial at high speed to recover the kinetic energy and to avoid excessive brake pad wear. The maximum instantaneous current during braking is $i_q = {}^{back\ Emf}/_{2 \cdot R}$, where R is the stator resistance. The corresponding braking torque is $T_b = (Torque\ constant) \cdot i_q$. This solution is shown in Fig. 1.7 , where $i_{q\,max}$ is limited to 80 A. The mechanical braking torque is superimposed.

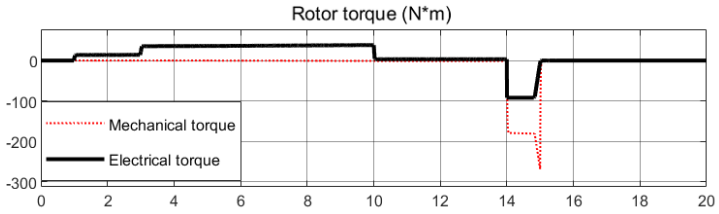

(a) Rotor torque

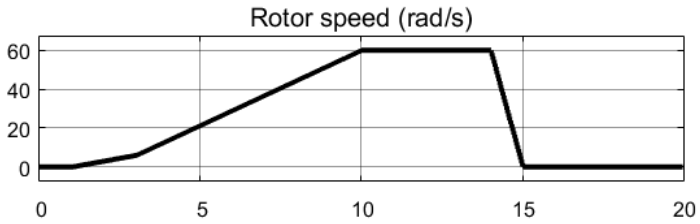

(b) Rotor speed

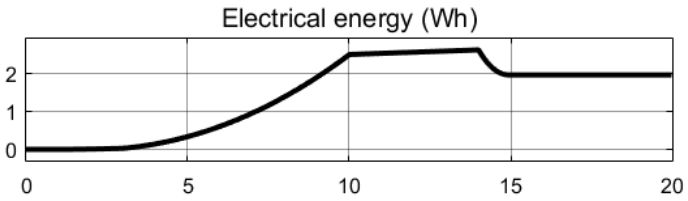

(c) Electrical energy

Figure 1.7: Regenerative and mechanical braking for the PMSM motor

1.5 WLTC test cycle results

The United Nations Economic Commission for Europe (UN-ECE) has developed a World-wide harmonized Light duty driving Test Cycle (WLTC) to represent typical driving characteristics around the world. The Test Cycle is useful to assess the performance of vehicles in terms of emissions, fuel and/or energy consumption. The WLTC contains four phases of time-speed data points ((Low, Medium, High and Extra-high). The applicable test for Pure Electrical Vehicles (PEV) is WLTC class 3, version

5.1. The following results are relative to the medium phase test: duration 433 s, maximum speed 76.6 [Km/h], distance 4.72 [Km]. Simulations are carried out with Matlab, Simulink and Simscape. To simulate air drag loss, a negative brake torque is applied to the wheel axle by a controlled Torque Source block, as shown in Fig. 1.8.

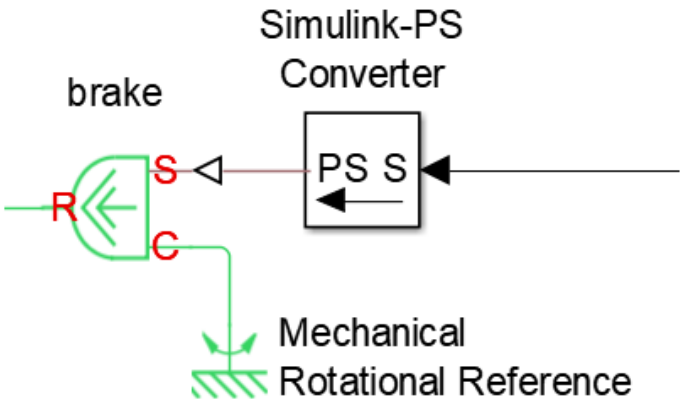

Figure 1.8: Controlled Torque Source block

The control signal is computed by the following formula:

$$Air\ drag\ torque = \frac{1}{2}\left(C \cdot A \cdot \rho \cdot (\omega \cdot r)^2\right) \tag{1.3}$$

where:

$C = 0.25$	air drag coefficient
$A = 0.5$	cross section quarter-car [m^2]
$\rho = 1.29$	air density [Km/m^3]
ω	wheel speed [rad/s]
$r = 0.316$	wheel radius [m]

Fig. 1.9 shows the results seen from the point of view of the PMSM rotor shaft (the [Km/h] data points of WLTC have been converted to rotor angular speed, taking into account wheel radius and the gear-box ratio of

3). The amount of rotor torque has to overcome viscous friction, air drag and car acceleration-deceleration to perfectly track the WLTC data points.

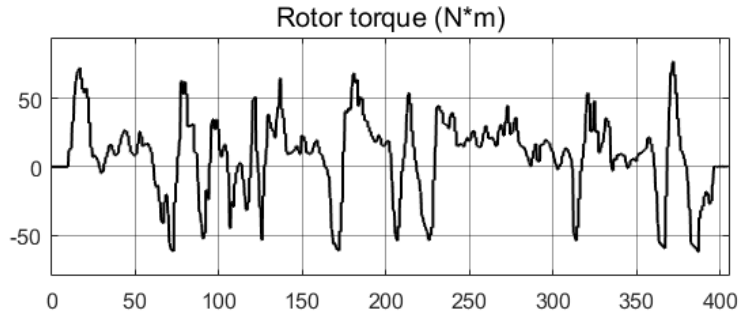

(a) Rotor torque

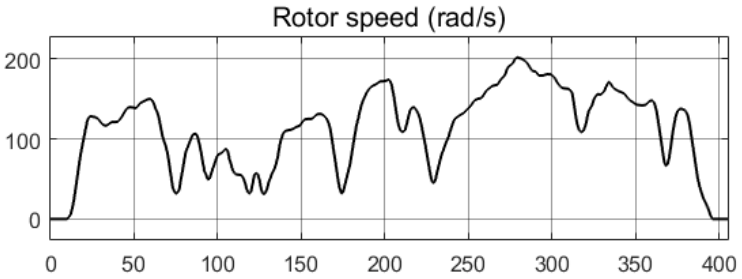

(b) Rotor speed

Figure 1.9: Rotor torque and speed

The corresponding energy balance is shown in Fig. 1.10a. The electrical energy (E-energy) is measured at the three-phase bus of PMSM. The mechanical energy (M-energy) is measured at the rotor shaft. The difference is due to the PMSM loss (mainly stator resistance). The E-energy rises during acceleration and decays during regenerative braking (battery recharge). The air-drag energy loss is substantially high and also the viscous friction loss cannot be neglected. At the end of the test cycle, the quarter-car has drawn about 100 [Wh] of energy from batteries to overcome the total losses (the full car would have drawn 400 [Wh]of energy

from the batteries). The [Wh/Km] for the quarter car is 21 [Wh/Km] (for the full car it would have been about 84 [Wh/Km]) (test cycle distance of 4.72 Km). It is interesting to see the energy lost in the case of pure mechanical braking, as shown in Fig. 1.10b. At the end of the test cycle, the energy drawn from batteries is about 170 Wh. The regenerative braking system can thus save up to 41% of electrical energy.

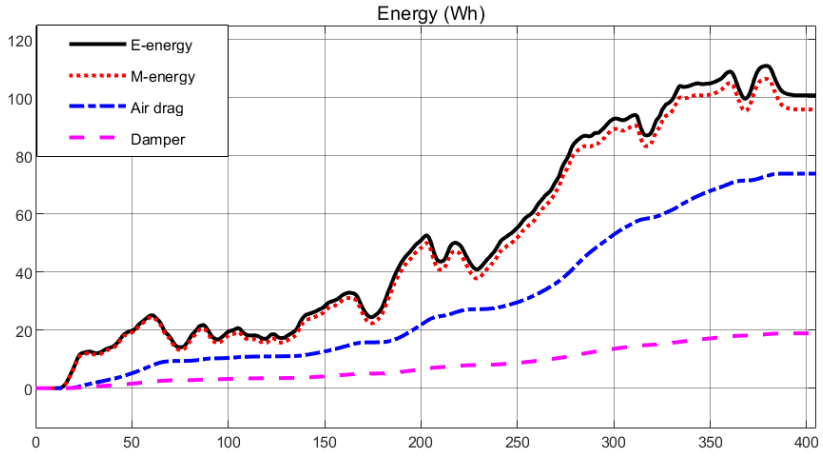

(a) Regenerative braking

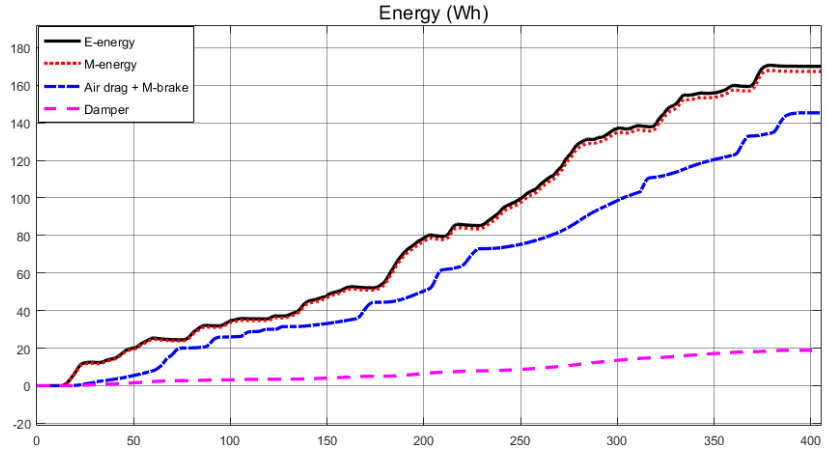

(b) Pure mechanical braking

Figure 1.10: Regenerative braking vs. pure mechanical braking

1.6 Summary

Electric cars must be able of long-range operations. This goal can be reached with high-capacity batteries but also by adopting suitable energy management. In this chapter, a multilevel battery system for Ev has been proposed. The goal is to recover the car's mass kinetic energy during braking to recharge the batteries. To simulate the flow of energy between the mechanical and the electric domain, in this chapter a complete model of an electric car has been developed. The interface between the two domains is a PMSM machine that operates as a motor during acceleration and as a generator during braking. The simulation model takes into account substantial viscous rotational friction and realistic air-drag losses. The simulations have been run through time-speed data points taken from the WLTC worldwide Test Cycle. Results show that the proposed regenerative braking system can save up to 41% of electrical energy versus pure mechanical braking.

References

[1] C. Cecati, A. Dell'Aquila, M. Liserre, and V.G. Monopoli. Design of h-bridge multilevel active rectifier for traction systems. *IEEE Transactions on Industry Applications*, 39(5):1541–1550, 2003.

[2] Carlo Cecati, Antonio Dell'Aquila, Marco Liserre, and Vito Giuseppe Monopoli. A passivity-based multilevel active rectifier with adaptive compensation for traction applications. *IEEE Transactions on Industry Applications*, 39:1404–1413, 2003.

[3] S D'Arco, L Piegari, M S Quraan, and P Tricoli. Battery charging for electric vehicles with modular multilevel traction drives. In *7th IET International Conference on Power Electronics, Machines and Drives (PEMD 2014)*, pages 1–6, 2014.

[4] Roberta Di Fonso and Carlo Cecati. Navigation and motors control of a differential drive mobile robot. In *2023 International Conference on Control, Automation and Diagnosis (ICCAD)*, pages 1–6, 2023.

[5] Rahul Kanchan, M.R. Baiju, K.K. Mohapatra, P.P. Ouseph, and K. Gopakumar. Space vector pwm signal generation for multilevel inverters using only the sampled amplitudes of reference phase voltages. *Electric Power Applications, IEE Proceedings* -, 152:297 – 309, 04 2005.

[6] Hassan Abdullah Khalid, Nasser Ahmed Al-Emadi, Lazhar Ben-Brahim, Adel Gastli, and Carlo Cecati. A novel control scheme for three-phase

seven-level packed u-cell based dstatcom. *Electric Power Systems Research*, 182:106201, 2020.

[7] Jih-Sheng Lai and Fang Zheng Peng. Multilevel converters-a new breed of power converters. *IEEE Transactions on Industry Applications*, 32(3):509–517, 1996.

[8] Sobhan Mohamadian, Mohammad Modarres, Francesco Simonetti, and Carlo Cecati. Modeling of switching power losses in cascaded h-bridges with unipolar pwm. *IEEE Journal of Emerging and Selected Topics in Power Electronics*, 11(3):3270–3280, 2023.

[9] Dhairyasheel S. Nikam and V. N Kalkhambkar. Statcom and multilevel vsc topology: A review. In *2018 International Conference on Current Trends towards Converging Technologies (ICCTCT)*, pages 1–7, 2018.

[10] Darshan Patel, R. Saravanakumar, K. K. Ray, and R. Ramesh. A review of various carrier based pwm methods for multilevel inverter. In *India International Conference on Power Electronics 2010 (IICPE2010)*, pages 1–6, 2011.

[11] Vidhi Patel, Mario Tinari, Concettina Buccella, and Carlo Cecati. Analysis on multilevel inverter powertrains for e-transportation. In *2019 IEEE 13th International Conference on Compatibility, Power Electronics and Power Engineering (CPE-POWERENG)*, pages 1–6, 2019.

[12] Fang Z. Peng, Wei Qian, and Dong Cao. Recent advances in multilevel converter/inverter topologies and applications. In *The 2010 International Power Electronics Conference - ECCE ASIA -*, pages 492–501, 2010.

[13] P. Pillay and R. Krishnan. Modeling of permanent magnet motor drives. *IEEE Transactions on Industrial Electronics*, 35(4):537–541, 1988.

[14] Jose Rodriguez, Leopoldo G. Franquelo, Samir Kouro, Jose I. Leon, Ramon C. Portillo, Ma Angeles Martin Prats, and Marcelo A. Perez. Multilevel converters: An enabling technology for high-power applications. *Proceedings of the IEEE*, 97(11):1786–1817, 2009.

[15] Yushu Zhang, G.P. Adam, T.C. Lim, Stephen J. Finney, and B.W. Williams. Voltage source converter in high voltage applications: Multilevel versus two-level converters. In *9th IET International Conference on AC and DC Power Transmission (ACDC 2010)*, pages 1–5, 2010.

Chapter 2

Multidimensional balancing in smart battery packs

2.1 Background

In recent years the interest in lithium batteries has grown enormously. The goal of reducing CO2 emissions has been the main reasoning behind the development of electric mobility and the effort to increase electricity production from sustainable sources. Lithium batteries find their main application area in the field of renewable energy sources, whose market penetration rate is expected to increase in the coming years. Lithium batteries will play a key role in the reliable and efficient integration of renewable energy sources with the electricity grid [2, 10]. Electric propulsion can be used in a wide range of applications (cars, trucks, industrial robots, vehicles for people with impaired mobility...). Thanks to the use of batteries as a driving force, purely electric vehicles are able to eliminate environmental emissions. In addition, unlike conventional vehicles, in which the kinetic (downhill) energy and braking energies of a vehicle are wasted, battery-powered electrified vehicles are able to store energy in the battery and use it later for propulsion. Therefore, the electrification of transport will have a positive social impact in economic and

environmental terms. Among the different types of batteries, lithium (Li-ion) batteries are the most promising, thanks to their higher energy density and a longer life cycle. The batteries consist of long strings of hundreds of cells connected in series and/or parallel to meet the required traction power and are currently the most expensive component of an electric vehicle's powertrain; Therefore, battery lifetime is a key factor in the success of electric vehicles. The need to extend the battery lifetime and ensure its correct use has attracted great research interest, both from an academic and industrial point of view. The battery lifetime is strongly influenced by the imbalance of the State of Charge SoC and the temperature between the cells that make up the battery pack. For these reasons, in recent years, new concepts of BMS have been proposed in the literature. The BMS is a critical component of a battery pack, as it ensures that the battery pack operates in the safe operating region, constantly monitors the battery pack status and records useful data. One of the fundamental tasks of the BMS is the estimation of the battery SoC and its balancing. Estimating the SoC is essential, as batteries can be damaged in both overcharging and over-discharging. Balancing allows you to use all the energy stored in the battery pack, avoiding the need to stop using the battery when one of its cells reaches the minimum SoC.

2.1.1 Causes of cell unbalancing

The unbalancing of the cells during discharge is due to the different internal resistances and capacities of the individual cells that make up the battery pack. The production processes of the cells are complex, and cannot ensure that the cells produced have the same capacity. Ageing processes also have an unpredictable impact on cells, resulting in a battery pack with cells that have a wide range of different capacities. Variations in cell capacities, cell leakage currents, and operating conditions cause SoC imbalance in cell strings. The SoC and capacity imbalance in turn results in DoD imbalance. Similarly, changes in the internal resistance of the cells and the temperature gradient

in the coolant, which is not negligible in electric vehicle battery packs, cause a thermal imbalance in the string. The SoC level and temperature of every single cell in a string during battery storage and the succession of charge-discharge cycles, have a great impact on the electrochemical ageing of the battery, while the DOD affects the life cycle of the cell. Therefore, the battery pack is subject to a serious problem of uneven ageing due to SoC, DOD and thermal imbalance. The battery pack may reach its end of life sooner due to premature failure of just one cell in the string, regardless of the high SoH of other cells.

2.1.2 Multidimensional control motivation

To circumvent these issues, strategies are needed for balancing SoC and limiting the temperature gradient. Classical active balancing techniques use additional circuits like DC/DC converters to exchange energy between cells [1, 3, 4, 5, 6, 9]. A more flexible and efficient option to achieve the active balancing of the battery pack is represented by the smart batteries (SB)[7, 8, 11]. SB topologies introduce modularity and reconfigurability in the battery pack thanks to the capability to insert/bypass single cells. This feature can be exploited to reach multidimensional control, that is simultaneous balancing of SoC and limiting temperature gradient inside the battery. A K-nearest-based control algorithm is developed to achieve the multidimensional balancing goal. The algorithm chooses at sampling time a subset of the cells to maintain the SB nominal output voltage. The cells are selected based on their sampled SoC and temperature values. The algorithm allows to trade off between the SOC and temperature spread of the cells during discharge. A lower temperature spread has also the effect to slow down the ageing of the cells and thus extending the lifetime of the battery pack.

2.2 The Smart Battery

Smart Battery (SB) is a new concept that combines advanced power electronics, wireless communication and artificial intelligence with the goal to develop a new generation of battery solutions for transportation and grid storage where the following new features are achieved: increased safety and reliability by fault-tolerant operation, user-controlled lifetime and software reconfiguration for 2nd-lifetime applications. The structure of SB is shown in Figure 2.1 and consists of a battery cell, a switching device, and a slave controller. The cell is not directly connected to the battery string but through

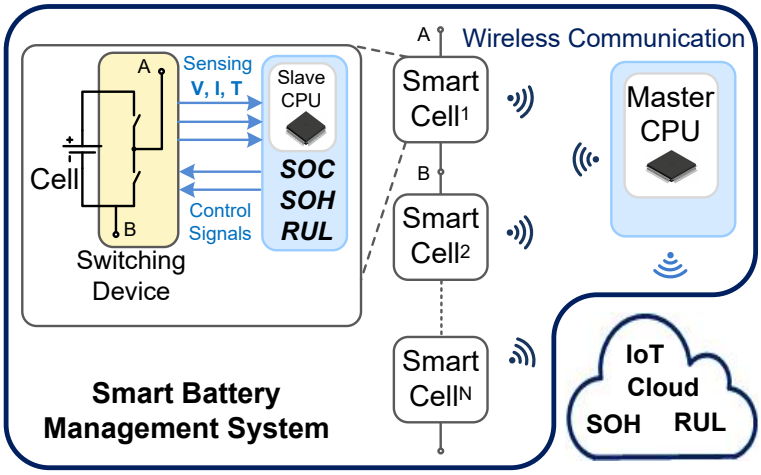

Figure 2.1: Smart Battery Structure.

the switching device which is implemented by a simple half-bridge MOSFET circuit and allows two operation modes: inserted or bypassed, as shown in Figure 2.2. The advantages of SB are many:

- The modularity of the structure allows to design a battery with a higher number of modules than those strictly necessary, adding redundancy to the battery and making it;
- Individual modules can be easily replaced in case of failure or ageing;

- The structure is easily scalable: starting from a battery it's possible to put together a more or less powerful battery pack for another application;
- The BMS which is usually a component external to the battery, is integrated into the structure;
- The structure adds "intelligence" to the single cell: parameters such as the SoC and the temperature can be locally evaluated;

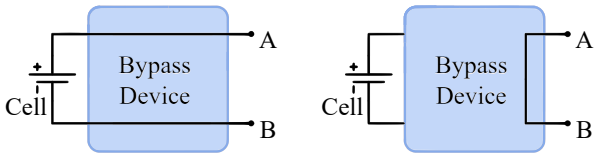

Figure 2.2: Operation mode of the switching device: inserted cell on the left, bypassed cell on the right.

The slave controller can monitor the voltage, current, and temperature of the cell and also estimate the SoC of the cell. All slaves are communicating wirelessly with a Master controller that is performing higher (package) level functions as SoH estimation and prediction using AI, SoC&SoH balancing and lifetime control. The balancing process is done by bypassing one cell at a time and thus not affecting the load current. In contrast to other active balancing methods, this balancing method is not requiring the use of DC/DC converters and is therefore an ultra-low energy balancing. The switching device is also used to permanently bypass faulted cells and thus adding fault-tolerant operation mode, increasing the safety and reliability at system level. When a cell is bypassed, it has time to rest. Cell rest time is used to: (i) allow a cell to cool off when its temperature is too high so it can be inserted again when it has in-the-range temperature values; (ii) bypass a faulted cell, so the SB can keep working; (iii) bypass a low charge cell, putting it to rest until next charge. In this way the whole battery can also be made fault tolerant.

By strategically exploiting the insertion/bypass mechanism, it is possible to design a control algorithm that uses the cells in the battery uniformly, according to their SoC, temperature and possibly SoH, thus extending the lifetime of the battery. The increase in the availability of data and the advances in Artificial Intelligence applications have contributed to pushing the batteries into the new "smart era".

2.3 Multidimensional K-nearest control algorithm

The SB has more cells than strictly necessary, so only a subset $n \leq N$ of the cells is needed to synthesize the output voltage. The redundancy and the reconfigurability of the topology allow us to dynamically choose among cells. A cell with low SoC (i.e. below 20%) can be bypassed in favour of cells with higher SoC; cells with out-of-range temperatures can be bypassed until they return to acceptable values. Since the algorithm is dynamic, cells can be inserted or bypassed based on the working condition. In this way, the bypassed cells have time to rest until they are either inserted again by the algorithm or until the next charge. Furthermore, in case of a cell fault, the cell is permanently excluded and the SB keeps working. Given the N cells of the SB, the goal is to optimally choose the subset $n \leq N$ of cells to balance both the SoC and temperatures. The algorithm chooses the cells with the highest SoC and lowest temperatures. The proposed control algorithm leverage on the K-nearest classification algorithm. Given a data set of points and one or more test examples, the K-nearest algorithm calculates the distances from all the points in the data set and the test example(s). These distances are then sorted and the k nearest neighbours (i.e the points with the minimum distances from the test examples) are returned. By properly choosing k, the test examples and the distance metric, we can use the K-nearest technique to optimally choose the n cells that need to be inserted in the SB. In this work

the data set is given by the N couples of SoC and temperatures $(SoC_i, T_i)\,, i = 1, \ldots, N$, the test example is given by the couple (SoC_{max}, T_{min}), $k = n$ and the metric used for the distance is a weighted Euclidean distance. The control algorithm receives as input the voltage, SoC and temperature values of the N cells and outputs the control signals for the Half-Bridges of the N cell modules. The voltage values are used to calculate the number n of cells to synthesize the desired output voltage, while the SoCs and the temperatures are used to choose which cells need to be inserted to achieve balancing.
The steps of the control algorithm are the following:

- given the SoC and temperature values of all cells create a virtual point v by choosing the highest SoC and the minimum temperature: $v = (SoC_{max}, T_{min})$;
- calculate the distance vector d *:*

$$d = \sum_{i=1}^{N} \left(k_S \left(SoC_i - SoC_{max} \right)^2 + k_T \left(T_i - T_{min} \right)^2 \right)$$

  where: k_S, k_T are weighting factors for the SoC and the temperature;

- sort the distances d in ascending order and find the index vector of the corresponding cells;
- scan the index vector and add the voltages of the corresponding cells until the desired output voltage is reached;
- compute the binary vector to drive the h-bridges that insert/bypass the cells (1 to insert a cell, 0 to bypass it).

2.4 Results

The SB system is simulated in Matlab-Simulink-Simscape. In order to reduce the simulation time to acceptable levels, the SB model is built with only 25 modules, instead of 150 needed for a real EV battery (a model scaled down by 6). At each sampling time, the control unit connects in series the right number of cells in order to output an average of 60 V (instead of 360 V). The battery cell parameters shown in Table 2.1 are from the preset model n. 6 from the Simscape Power System Library. With these cells, the parameters of the SB pack are shown in Table2.2.

Table 2.1: Cell parameters.

Nominal voltage	3.6 V
Cell capacity	48 Ah

Table 2.2: Smart Battery pack parameters.

Controlled output voltage	60 V
Energy stored	4.32 kWh

Case Study

In order to get meaningful results, it is useful to think to the following case study. A car is parked in a garage for a time long enough to have all the cells at the same initial ambient temperature, which is $25°C$. When the car starts for a test drive, the temperatures of the used cells will rise due to their internal resistance. The simulation is carried out thinking that the battery is contained in a box whose ambient temperature increases as the mean temperature of the cells. No cooling action has been considered. The initial SoC of the cells is set up between 80% and 90%, as shown in Fig. 2.3.

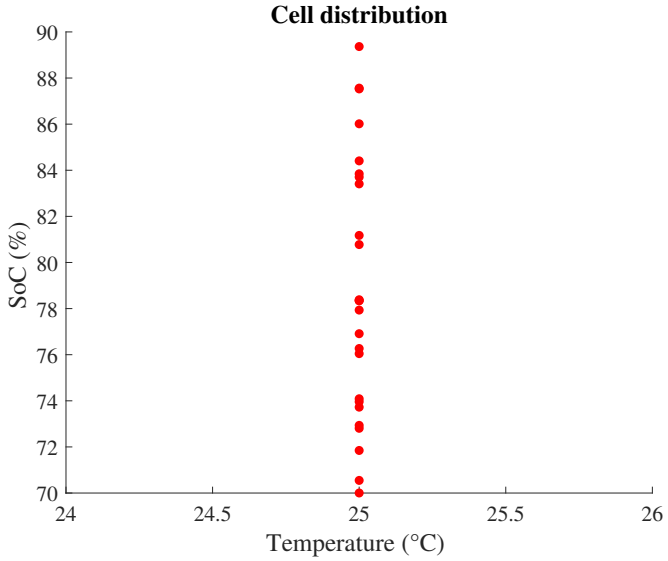

Figure 2.3: Cell distribution at the beginning of the test.

The SB performance depends on the control algorithms used to select the right cells at each sampling time. Their selection can be based on a single dimension, like SoC, or multiple dimensions, like SoC and temperature, or ageing, or other parameters. The following results are related to two distinct control algorithms: (i) an SoC Sorting algorithm, based on cell SoC only and, (ii) the proposed Multidimensional K-nearest control algorithm (MKNA), based both on cell SoC and temperature. Both algorithms maintain the desired output voltage close to $V_{des} = 60\,V$ using 16 or even more cells with discrete increments. The load is simulated by a 1.8 Ω resistor resulting in an average discharge current of about 33 A.

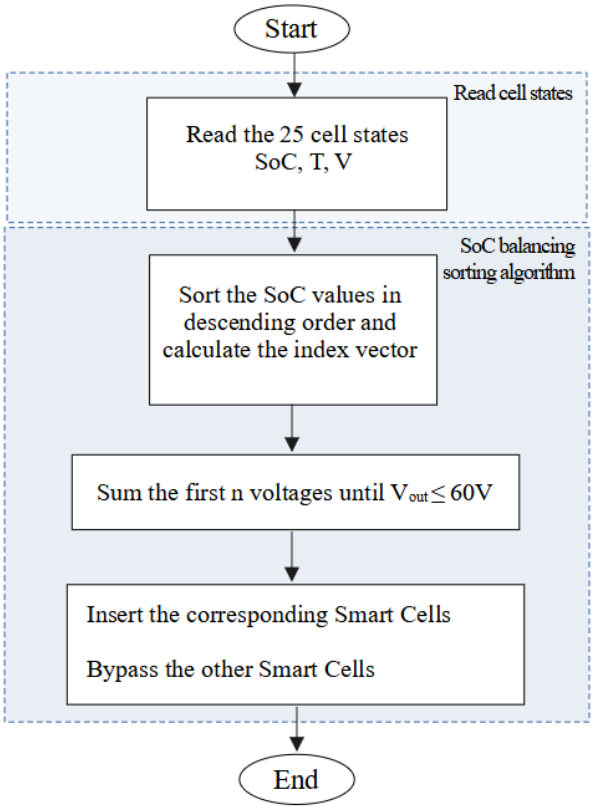

Figure 2.4: SoC balancing sorting algorithm flow chart.

SoC Balancing Sorting algorithm

This control algorithm is based on SoC sorting. At each step, the algorithm sorts the SoC of all the cells in descending order and chooses the first n cells to be inserted in the SB string. The number n is dynamically defined in order to synthesize the desired output voltage. A flow chart of the algorithm is shown in Fig. 2.4. The chosen cells have the relatively highest SoC, while the cells with the lowest SoC have time to rest. The algorithm action is best seen on an animated scatter plot (SoC vs. Temperature). Used cells are pushed down-right (SoC decrease and temperature increase) until all cells reach roughly the same SoC value (a flat line). From then on, the cells will be

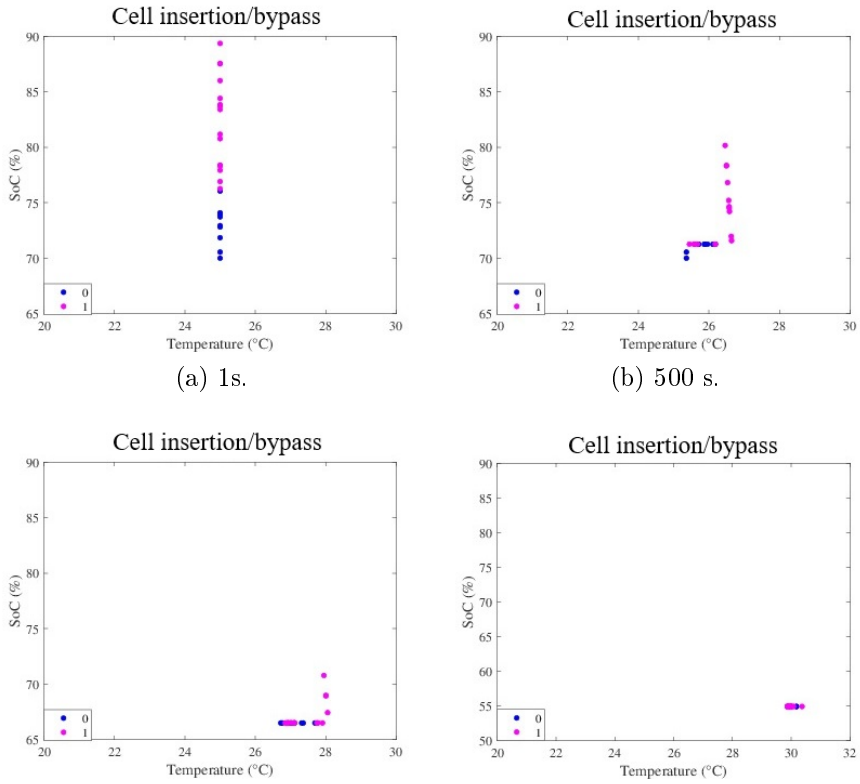

(a) 1s. (b) 500 s.

(c) 1000 s. (d) 2000 s.

Figure 2.5: Cell insertion/bypass choice - SoC balancing sorting algorithm.

used more uniformly and remain horizontally aligned. The total simulation time is 2000 s. Fig. 2.5 shows four screenshots of the scatter plot at 1 s, 500 s, 1000 s and 2000 s. Fig. 2.6a and 2.6b show SoC and temperature vs. time of all the 25 cells. The temperature of each cell varies according to its usage. At the beginning of the test, all cells are at 25°C and then the spread of temperatures increases as the temperature of the most inserted cells increases. The cells tend to reach the same higher temperature towards the end of the test. Fig. 2.5 shows how the cells to be inserted/bypassed are chosen by the algorithm at different time steps: a value of "1" corresponds to cell insertion, while a value of "0" corresponds to cell bypass.

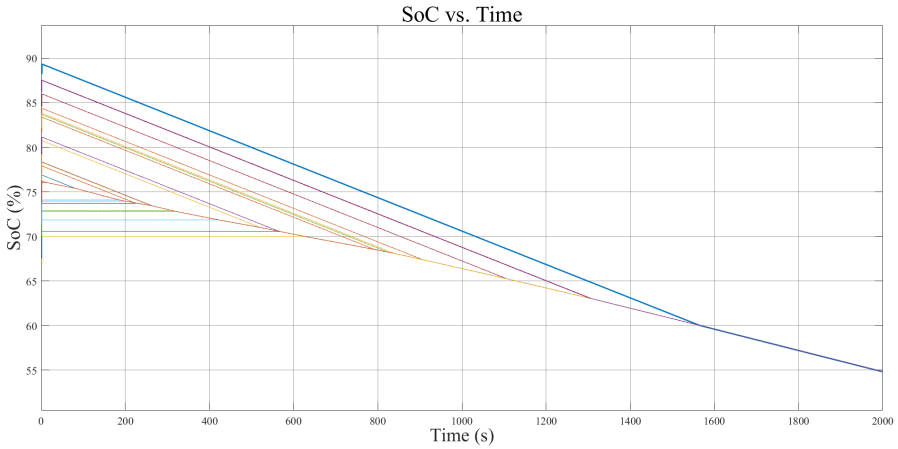

(a) SoC of the 25 cells.

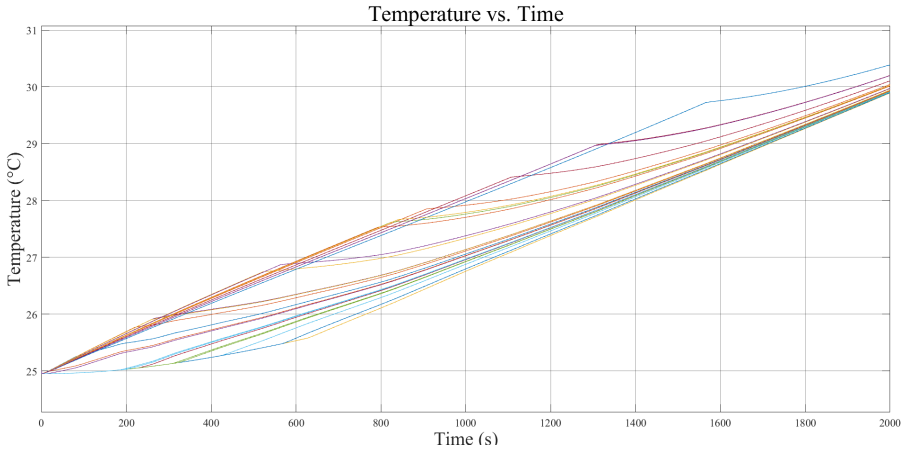

(b) Temperature of the 25 cells

Figure 2.6: SoC balancing sorting algorithm simulation results.

Multidimensional K-nearest control algorithm

The previous algorithm based only on SoC has the side effect of an uncontrolled spread of the cell temperatures. The idea here is to select cells both on their SoC and temperature in order to reduce the maximum temperature spread. The K-nearest algorithm selects the n cells that are nearest to the dynamic virtual point $\mathrm{SoC}_{\max}$, $T_{\min}$. The algorithm action could be best

seen on an animated scatter plot (SoC vs. Temperature). Used cells are

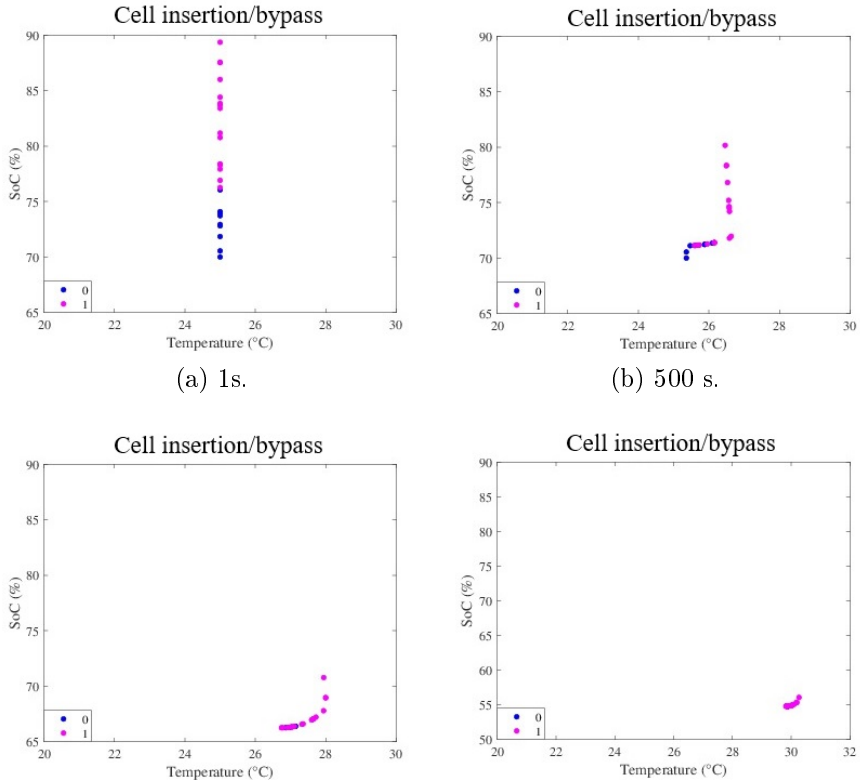

(a) 1s. (b) 500 s.

(c) 1000 s. (d) 2000 s.

Figure 2.7: Cell insertion/bypass choice - MKNA algorithm.

pushed down-right (SoC decrease and temperature increase) until all cells tend to converge on an arc centered on current $\mathrm{SoC}_{\max}$, $T_{\min}$. This means that the maximum temperature spread is reduced at the expense of a small SoC spread (the ray of the arc). The weighting factors k_S, k_T can be used to give more weight to SoC or to temperature. The limiting cases are: (i) $k_T = 0$, the arc changes to a horizontal line and the cells are pushed to have the same SoC (as the previous SoC Sorting); (ii) $k_S = 0$, the arc changes to a vertical line and the cells are pushed to have the same temperature. Fig. 2.7 shows four screenshots of the scatter plot at $1\,s$, $500\,s$, $1000\,s$ and $2000\,s$. Fig.

2.8a and 2.8b show SoC and temperature vs. time of all the 25 cells. Fig. 2.7 shows how the cells to be inserted/bypassed are chosen by the algorithm at different time steps: a value of "1" corresponds to cell insertion, while a value of "0" corresponds to cell bypass.

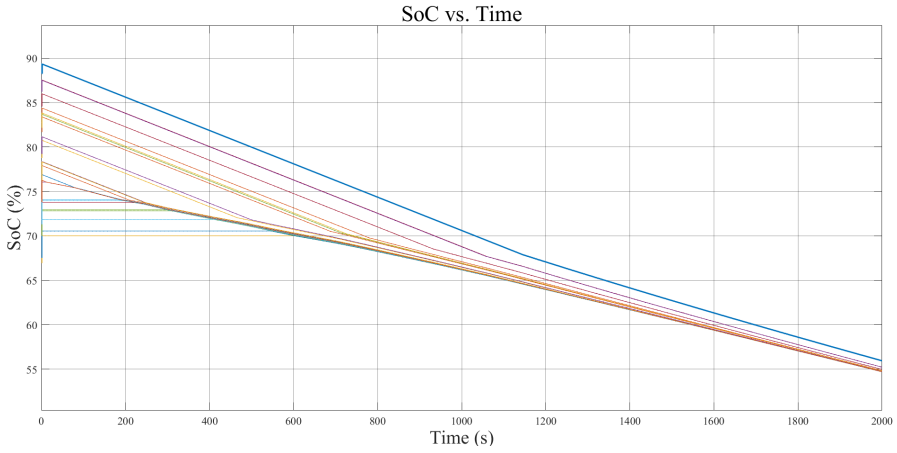

(a) SoC of the 25 cells.

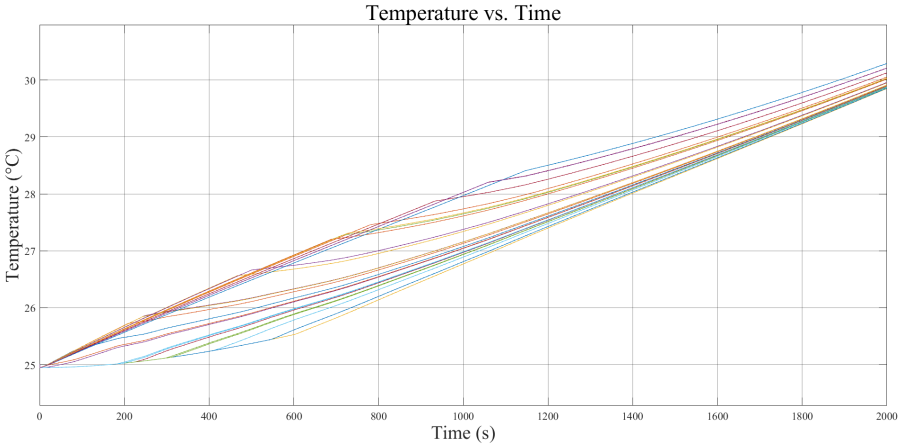

(b) Temperature of the 25 cells

Figure 2.8: MKNA algorithm simulation results.

Finally, Fig. 2.9 shows a comparison between the temperature spread of the two control algorithms vs. time. The SoC Sorting algorithm produces peak temperatures higher than the multidimensional algorithm.

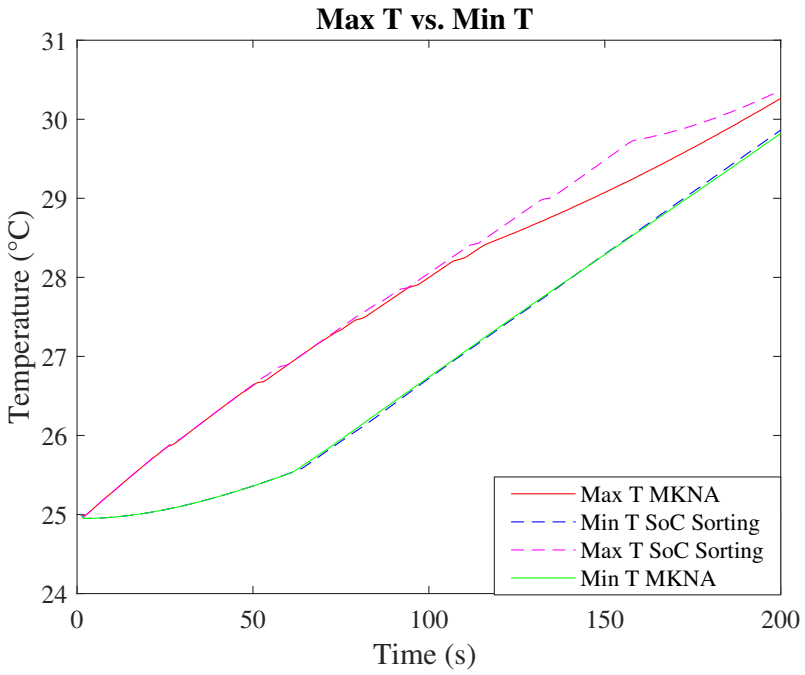

Figure 2.9: Comparison of maximum and minimum temperature.

2.5 Summary

The proposed SB architecture, where at a given time only $n < N$ cells are series-connected, has many useful features like modularity, reconfigurability, cell fault tolerance, greater useful capacity. In order to achieve optimal balancing in operation for both temperature and SoC, a multidimensional K-nearest control algorithm (MKNA) was developed and simulated with the aim to limit the spread of cell SoCs and temperatures. The MKNA algorithm chooses the cells to be inserted/bypasses based on their "distance" from a virtual point that is dynamically computed at sampling time. The algorithm uses weighting factors to give more importance to SoC or temperature. It turns out that the MKNA algorithm reduces itself to the SoC Sorting algorithm when the temperature is weighted out. Simulation results show that the maximum temperature spread is reduced in comparison with a simple SoC sort. This operation has the potential to extend the lifetime of the battery pack, which will be evaluated in future work. The structure of the MKNA algorithm allows to easily add other dimensions to the control strategy, such as the internal resistance or the SoH of the cells.

References

[1] Federico Baronti, Roberto Roncella, and Roberto Saletti. Performance comparison of active balancing techniques for lithium-ion batteries. *Journal of Power Sources*, 267:603–609, 2014.

[2] Tianmei Chen, Yi Jin, Hanyu Lv, Antao Yang, Meiyi Liu, Bing Chen, Ying Xie, and Qiang Chen. Applications of lithium-ion batteries in grid-scale energy storage systems. *Transactions of Tianjin University*, 26, 02 2020.

[3] Mohamed Daowd, Noshin Omar, Peter Van Den Bossche, and Joeri Van Mierlo. Passive and active battery balancing comparison based on matlab simulation. In *IEEE Veh. Power and Propuls. Conference*, pages 1–7, 2011.

[4] Markus Einhorn, Werner Roessler, and Juergen Fleig. Improved performance of serially connected li-ion batteries with active cell balancing in electric vehicles. *IEEE Trans. Veh. Techol.*, 60(6):2448–2457, 2011.

[5] Ye Li and Yehui Han. A module-integrated distributed battery energy storage and management system. *IEEE Trans. Power Electron.*, 31(12):8260–8270, 2016.

[6] Martin Lukasiewycz, Matthias Kauer, and Sebastian Steinhorst. Synthesis of active cell balancing architectures for battery packs. *IEEE Trans. Comput. Des. Int. Circuits Syst.*, 35(11):1876–1889, 2016.

[7] Branko Majmunovic, Radhika Sarda, Remus Teodorescu, Cristian Lascu, and Mattia Ricco. Highly efficient smart battery pack for ev drivetrains. In *IEEE Veh. Power Propuls.Conf.(VPPC)*, pages 1–5, 2017.

[8] Antonio Manenti, Andrea Abba, Alessandro Merati, Sergio M. Savaresi, and Angelo Geraci. A new bms architecture based on cell redundancy. *IEEE Trans. Ind. Electron.*, 58(9):4314–4322, 2011.

[9] Swaminathan Narayanaswamy, Matthias Kauer, Sebastian Steinhorst, Martin Lukasiewycz, and Samarjit Chakraborty. Modular active charge balancing for scalable battery packs. *IEEE Trans. Very Large Scale Int. Syst.*, 25(3):974–987, 2017.

[10] Habiballah Rahimi-Eichi, Unnati Ojha, Federico Baronti, and Mo-Yuen Chow. Battery management system: An overview of its application in the smart grid and electric vehicles. *IEEE Industrial Electronics Magazine*, 7(2):4–16, 2013.

[11] Mattia Ricco, Jinhao Meng, Tudor Gherman, Gabriele Grandi, and Remus Teodorescu. Smart battery pack for electric vehicles based on active balancing with wireless communication feedback. *Energies*, 12(20), 2019.

Chapter 3

Overview of battery cells

3.1 Battery Basics

Traditional electrochemical cells depend on redox reactions that chemically change the reacting species at the electrode surfaces. Lithium-ion cells working principle is different: lithium ions move from the electrolyte to the electrode (absorbed) or from the electrode to the electrolyte (expelled). The absorption of lithium is a process known as intercalation and the opposite process is referred to as deintercalation. In order for this process to work properly, the electrode materials must have a proper crystal structure and must be able to accept or deliver electrons to/from the external electric circuit. Each cell has 4 components [5]: the negative electrode (often a metal or an alloy or graphite), the positive electrode (often a metallic oxide, sulfide, or oxygen), the electrolyte (the ionic conductor) and the separator (that electrically isolates the positive and negative electrodes to avoid self-discharge of the cell). The electrolyte is the media that conducts ions between electrodes. The separator inside the electrolyte in a lithium-ion cell is a permeable membrane that allows lithium ions to pass through but avoids short circuits between negative and positive electrodes. Lithium-ion cells are fabricated in a completely discharged state (all of the lithium is in the positive

electrode). In order to activate the working materials, the cell must be put through at least one precisely controlled charge cycle, referred to as the formation process. The result is the formation of a passivating film on the surface of the graphite, known as the solid electrolyte interphase (SEI) layer which is electrically insulating yet provides sufficient ionic conductivity for lithium to move through the electrodes. Failures in Li-ion cells can happen due to poorly controlled manufacturing processes, aging, uncontrolled operations and abuse. Cell performance naturally deteriorates gradually with time and usage and it is generally irreversible, with detrimental effects on battery operativity. The causes for ageing are [1]: (i) corrosion, that is the deterioration due to chemical interaction with the environment; (ii) SEI growth; (iii) loss of capacity due to gases-leak and crystal formation. These chemical-related aging effects have in turn adverse effects on cell operativity and can lead to: (iv) increased internal impedance leading to power fade; (v) reduced capacity with continuous charge-discharge cycles, leading to charge capacity fade; (vi) increased self-discharge, further accelerated by elevated temperatures. Battery cells are thus not immune to failures. Using cells at unsuitable charging/discharging profiles and exposing it to high ambient or storage temperatures can shorten the battery life. The high voltage of a battery pack is obtained by series connection of elementary cells, and the high charge capacity is obtained by parallel connection of cells or stream of cells. Two important parameters must be known to assure that the battery always operates inside a safe area: the State of Charge (SoC) and State of Health (SoH). SoC is an indicator of the actual charge inside the cell and it can be computed by integrating the current exchanged with the external circuit. SoC is a relative measure of the actual charge, normalized to the full charge capacity. SoH instead, is a relative measure of the actual full charged capacity, normalized to the full charge capacity of a fresh cell. Both parameters are thus normalized in the range 1 to 0 to give compact information on battery states. To operate the battery pack optimally, usually a BMS is in charge of

the following features: (1) cell monitoring (voltage, current and temperature measurements) (2) battery safety and protection (3) cell balancing (4) SoC and SoH estimation (5) charge control (6) thermal management.

3.2 Internal electrochemical processes and their effects

When a battery cell is operated, a current flow alters the electrochemical equilibrium inside the cell. The electrochemical processes are not perfect, and there is a loss in the electrochemical energy conversion. This process is due to an effect called polarization. There are two main types of polarization: activation polarization and concentration polarization. If electrochemical parameters and the mass-transfer condition were known, it would be theoretically possible to estimate activation polarization and concentration polarization. Electrodes have very complex physical structures, so it would require complex mathematical modelling to derive equations to estimate activation and concentration polarization [4]. Therefore, it is very complex to get an accurate estimation. Furthermore, the output voltage of the cell is also influenced by the internal impedance of the cell. The total internal impedance of a cell is the sum of the electric resistance of the electrolyte (within the separator and the porous electrodes), the resistances of the electrodes and of the battery cell terminals. When the cell is under operation, there is an instantaneous voltage change proportional to the intensity of the current [6]. This effect is referred to as "ohmic polarization" and it is due to the above-mentioned resistances. Another electrochemical effect is known as the "electrical double layer" and it is referred to the presence of two separate layers of electric charge building up at the electrolyte-electrode surface. There are also complex ion diffusion processes that are responsible for slow dynamic effects on the output voltage. Since these electrochemical internal processes are not completely reversible, continuous usage of a battery results

in aging. A battery cell can face two types of aging: calendar ageing and cycling ageing [2, 3]. Calendar ageing is related to the time and conditions of storage. Cycling ageing is related to the charge/discharge of the cell. When a cell ages its full charged capacity decreases (capacity fade) and its internal resistance rises (power fade). In EVs applications, this capacity fade leads to the so-called range anxiety and the power fade leads to loss of performance in the driving experience and to higher battery temperature, with detrimental effects on battery lifetime. Li-ion batteries are governed by complex internal electrochemical processes. However, from an application point of view, the battery behavior can be summarized in a simpler equivalent model.

References

[1] Reddy Thomas B. and David Linden. *Linden's handbook of batteries.* 2011.

[2] S. Barcellona and L. Piegari. Effect of current on cycle aging of lithium ion batteries. *Journal of Energy Storage*, 29:101310, 2020.

[3] Peter Keil, Simon F. Schuster, Jorn Wilhelm, Julian Travi, Andreas Hauser, Ralph C. Karl, and Andreas Jossen. Calendar aging of lithium-ion batteries. *Journal of Electrochemical Society*, 2016.

[4] Z. Khalik, M.C.F. Donkers, J. Sturm, and H.J. Bergveld. Parameter estimation of the doyle fuller newman model for lithium-ion batteries by parameter normalization, grouping, and sensitivity analysis,. *Journal of Power Sources*, 499, 2021.

[5] Gregory Plett. *Battery Management Systems, Volume I: Battery Modeling.* 2015.

[6] Gregory Plett. *Battery Management Systems, Volume II: Equivalent-Circuit Methods.* 2015.

Chapter 4

ECM model

4.1 Battery Modeling

Lithium-ion batteries are the preferred energy source for the ever-expanding world of mobile applications, ranging from low power in smartphones to high power in electric vehicles (EVs). Such a wide spectrum of systems requires quite different battery models, based on different chemistry and with different behavior at the electrical terminals. Batteries are complex non-linear systems that must be run under the supervision of a BMS (Battery Management System) in order to assure safe charge/discharge operations. The development of a complete autonomous system requires the fine-tuning of many algorithms, which include the SoC/SoH estimation algorithms using voltage and currents at the battery terminals. Thus precise simulations of various components play a crucial role in the successful design of an efficient BMS. Depending on the desired level of abstraction, a multitude of models have been developed by researchers worldwide. There are three big categories of battery models: (i) Physics and Multiphysics models that aim at describing the complex internal chemical phenomena of batteries [5] ; these can be considered lower-level models (ii) empirical models that use past experimental data to develop a strategy for predicting future behavior [1]; (iii) Equiva-

lent Circuit Models that aim at simulating the battery behavior using circuit elements [4], these can be considered higher-level models. Physics models are the most accurate since they can capture the internal electrochemical behavior of the cell. The most famous among these models is the Doyle-Fuller-Newman model which describes the battery internal states using sets of Partial Differential Equations. These equations require a high number of parameters that are usually determined using complex and time-consuming experiments that usually involve cycling or tearing down of a cell in the laboratory. The literature on the DFN model is vast and researchers continue to put effort both in optimizing the estimation of the model parameters and in developing software solutions for making the model performance faster [6]. ECM models are instead computationally fast and simple. There are many techniques for the identification of equivalent circuit parameters such as the Electrochemical Impedance Spectroscopy (EIS) [2]. Traditional EIS is a technique to measure the real and imaginary parts of internal impedance Z as a function of frequency. EIS is an expensive lab activity that requires a scanning sine wave generator, powerful enough to stimulate the battery at different frequencies, from mHz to kHz. The result is a Nyquist plot that is only valid for well-defined values of T, SoC and SoH. The Nyquist plot is then fitted with a circuit containing resistors, capacitors and even exotic components like Warburg impedance or Constant Phase Element (CPE), Unfortunately, Z is a function of T, SoC, SoH and a complete estimation of the components would require a massive use of EIS. In [7] an alternative solution to the frequency scanning stimulus of EIS is provided, by the injection of a wide spectrum current signal to the battery. Then, the resulting voltage drop could be analyzed in frequency with signal processing techniques. However, EIS-based methodologies for impedance evaluation are not very useful for EVs because the identification is mainly offline. An online identification would provide real-time information that could be used to operate the battery optimally. The knowledge of the cell's actual internal impedance is also

very important in Smart Battery (SB) applications, in order to design better control algorithms.

4.2 Equivalent Circuit Model

Lithium-ion batteries are based on highly complex chemistry that is not easy to understand. However, from the perspective of the application, we need only to know how the battery behaves at the accessible terminals. The ECM is an electrical model based on common circuit elements, like voltage generator, resistors and capacitors. Fig. 4.1 shows the Randles circuit based

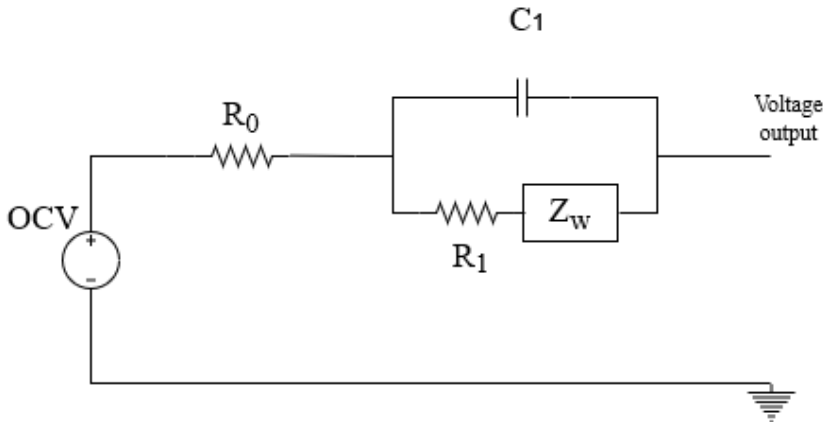

Figure 4.1: Randles circuit

on electro-chemical principles [3]:

- R_0 models the electrolyte resistance
- R_1 models the voltage drop over the electrode–electrolyte interface
- C_1 models the effect of charges building up in the electrolyte at the electrode surface
- Z_w is the Warburg impedance that models diffusion of lithium ions in the electrodes

The Warburg impedance $Z_w = {}^{A_w}/\sqrt{j\omega}$ is frequency-dependent and can be thought as the impedance of a semi-infinite transmission line composed only of resistance and capacitance per unit length [8]. Fig. 4.2 shows an equivalent circuit of a Warburg impedance.

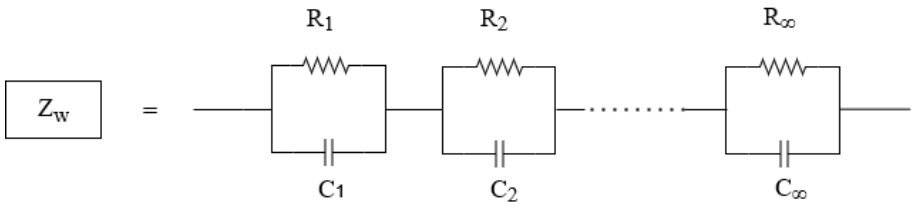

Figure 4.2: Equivalent circuit of the Warburg impedance

The precise simulation of a Warburg impedance requires an infinite number of RC pairs and is thus intractable. However, Z_w can be modelled well over some frequency range using a few RC pairs. The double-layer capacitance C_1 of the Randles circuit has little effect except at very high frequencies and can thus be often omitted. Substituting the Z_w with a small number of RC pairs, the Randles circuit becomes identical to what is shown in Fig.4.3. This cell/battery ECM model is adopted in Chapter 6. Note that the ideal

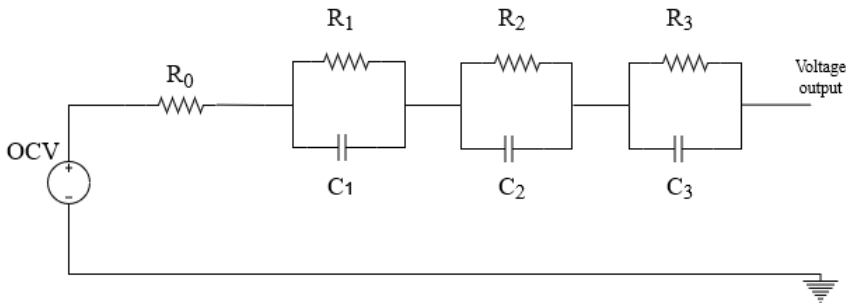

Figure 4.3: Complete 3RC ECM model

generator, labelled as OCV (Open Circuit Voltage) and all RC pairs are a non-linear function of temperature T, SoC and SoH. To simulate a specific

real cell/battery, it is first necessary to identify the functions of all elements of the ECM model by means of laboratory measurements. Regarding the OCV generator, as the name implies, it can be easily measured at zero or low currents, although the complete function characterization requires a time-consuming process in the lab. The identification of all RC elements is more challenging as they are not accessible from the battery's terminals. However, the collective effects of all the RC elements, i.e. of the battery internal impedance, is fully observable as an output voltage drop when the battery supplies current to an external load. The traditional identification method of the internal impedance is performed by using EIS, which requires special equipment and time-consuming measurements in the lab. In the next Chapters we will show that the identification of the internal complex impedance can be done in different ways, by means of signal processing of the battery voltage and current signals.

4.3 Summary

Li-ion batteries are governed by complex internal electrochemical processes but, from an application point of view, we need only a behavioral model to effectively simulate the battery. The ECM is a fast computationally model of the battery behavior that uses simple circuit elements. However, these elements are not fixed as they change as a non-linear function of SoC, SoH and temperature. To simulate a specific real cell/battery, it is first necessary to identify the functions of all elements of the ECM model. The task is challenging but it can be carried out in new ways compared to traditional EIS.

References

[1] Empirical modeling of lithium-ion batteries based on electrochemical impedance spectroscopy tests. *Electrochimica Acta*, 160:169–177, 2015.

[2] D. Andre, M. Meiler, K. Steiner, Ch. Wimmer, T. Soczka-Guth, and D.U. Sauer. Characterization of high-power lithium-ion batteries by electrochemical impedance spectroscopy. i. experimental investigation. *Journal of Power Sources*, 196(12):5334–5341, 2011.

[3] Analog Devices. Cn0510 electrochemical impedance spectroscopy(eis) for batteries, circuit notes, 2020.

[4] Roberta Di Fonso, Pallavi Bharadwaj, Remus Teodorescu, and Carlo Cecati. Internal resistance estimation of li-ion batteries using wavelet analysis. In *2022 IEEE 13th International Symposium on Power Electronics for Distributed Generation Systems (PEDG)*, pages 1–5, 2022.

[5] Z. Khalik, M.C.F. Donkers, J. Sturm, and H.J. Bergveld. Parameter estimation of the doyle fuller newman model for lithium-ion batteries by parameter normalization, grouping, and sensitivity analysis,. *Journal of Power Sources*, 499, 2021.

[6] Scott Moura. Fast doyle-fuller-newman (dfn) electrochemical-thermal battery model simulator. https://github.com/scott-moura/fastDFN.git, 2018.

[7] Gjorgji Nusev, Dani juricic, Miran Gaberscek, Joze moskon, and Pavle Boskoski. Fast impedance measurement of li-ion battery using discrete random binary excitation and wavelet transform. *IEEE Access*, 9:46152–46165, 2021.

[8] Gregory Plett. *Battery Management Systems, Volume II: Equivalent-Circuit Methods*. 2015.

Chapter 5

Data-driven Modeling of Li-ion Battery

5.1 Background

Researchers need a good battery model for the development of innovative performance optimization algorithms. The optimization of the battery model comes down to three elements: (i) ready to use in a small amount of developing time (ii) custom-made to a specific battery of interest (iii) good trade off between accuracy and complexity. The Datasheet Battery Block from Simulink [3] aims at developing an Equivalent Circuit Model of the battery, based on the datasheets provided by the battery manufacturer. This data, however, is not "ready to use", but need to be extracted in a precise way in order to be used successfully for which a systematic methodology is presented in this chapter. Configuring a Simulink model directly from the commercial datasheet is very useful and relatively fast. However, the datasheet data are collected using sets of C-rates and temperatures chosen by the manufacturer, and they could be very different from the ones that would be used in the laboratory for experiments or in real-life applications of the battery. In order to further enhance the robustness of the battery model for real field

applications experimental data is collected in the laboratory and used in further training of datasheet model: these controlled experiments allow us to add additional conditions of interest as are faced by battery in field applications. This chapter presents different paths and steps that can be followed to gather information about a specific battery model, looking first at the battery manufacturer datasheet and when specified data is not enough, resorting to dedicated laboratory data collection. The extracted information is further used to develop an accurate simulation model of the selected battery. This virtual battery model can be used in battery cell simulators that allow the testing of Battery Management Systems as Hardware-in-the-Loop systems (BMS HiL) among many other applications.

5.2 Datasheet Battery Block

One of the most readily available and basic tools of battery modelling is found in Matlab, called the Datasheet Battery Block which is contained in the Simulink Library and simulates a lithium-ion, lithium-polymer, or lead-acid battery cell. The model can be customized to the type of battery of interest, by using the manufacturer's data. The model is shown in Fig. 5.1. Internally the block is built using an ECM, as shown in Fig. 5.2. The inputs of the datasheet battery block are the battery initial charge capacity rated at nominal temperature, the battery current, and the battery temperature. The output voltage is computed using look-up tables for the Open Circuit Voltage (OCV) and the Internal Resistance (IR). These look-up tables are user-generated by using the discharge characteristics provided by the manufacturer. By using a standard procedure, the user can parameterize the OCV and IR depending on SoC and temperature, and thus the battery performance is characterized at different operating points. The Datasheet Battery Block can either represent a single cell, or a battery made up by combining cells in parallel or in series. As previously said, the internal structure of the block is

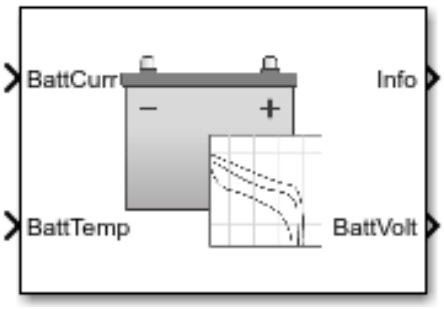

Figure 5.1: Datasheet Battery Block

an ECM and this can be either a basic model, that just considers OCV and IR, or a more complex model that also considers one RC branch. This can be done by selecting the option Filtered in the Output Battery Voltage box and choosing the RC time constant.

Lookup table generation procedure

In order to get the Datasheet Battery Block model running, we need to create the parameters to fill up the lookup tables for the OCV and IR that will be used by the block. The procedure is broken down into steps:

- import the datasheet data
- use curve-fitting techniques to obtain OCV and IR data at different temperatures
- validate the model comparing the simulated values to the datasheet data and verifying the behavior of IR
- specify the Datasheet Battery Block parameters: Rated capacity at nominal temperature, OCV table data, OCV breakpoints, IR table data, battery temperature breakpoints, battery capacity breakpoints and initial battery charge

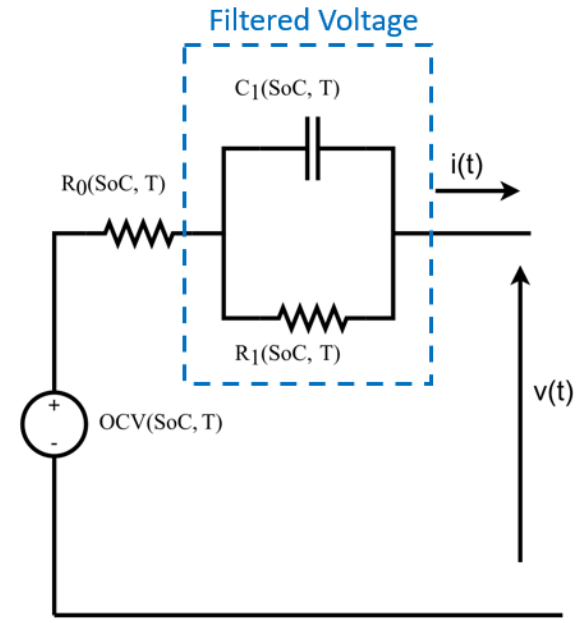

Figure 5.2: Datasheet Battery Block Internal Structure

5.3 Extracting Data from Datasheet

The Simulink "Datasheet Battery block" is a ready to use subsystem that can simulate an ECM model, customized with look-up tables. In particular, this block must be configured with the cell OCV and the cell internal resistance, both as a function of SOC and temperature T. Unfortunately, these data are not directly available from the cell manufaturers, but can be extracted from the official datasheets, mainly provided in graphic form. Therefore there is the need to extract the numerical data in some way. This data recovery process from graphs is not easy and naturally prone to errors. Many tools have been developed over the years to aid this process, and some of them are freely available online [4]. The sample points of interest can be extracted semi-automatically drawing a mask to isolate the curve of interest: Fig. 5.3 shows an example of sampling a signal from the datasheet of A123 batteries

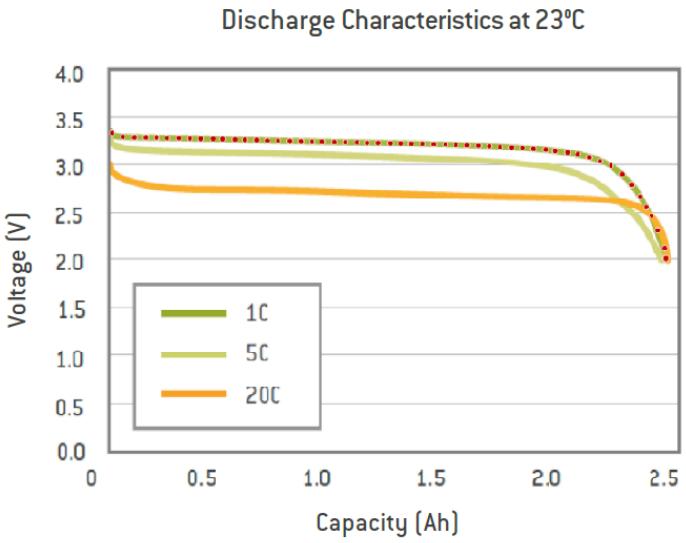

Figure 5.3: Sampling the graphic datasheet curves

recorder at 23°C. Fig. 5.4 shows the raw vectors imported in Matlab (i.e. the values extracted from the voltage vs. capacity curves using this procedure). The raw vectors are sampled semi-automatically and some points must be hand adjusted in the x,y coordinates. So the sampling period is not uniform and, moreover, the curves are not sampled synchronously. The synchronicity is needed in order to relate the curves algebraically. The solution is provided by the Matlab Interp1 function [1], which can interpolate and resample the curves. Fig. 6(a), 6(b) show the results after up-sampling to 101 points and lightly filtering the curves. The manufacturer provides two families of curves:

- curves at constant temperature and different discharge currents (Fig.6(a));
- curves at constant current and different temperatures (Fig.6(b))

We need the OCV curve at zero current. In order to extract this information, we can fit a surface to the curves of Fig. 5.5a, obtaining Fig. 5.6.

The black curves are the originals ones from Fig. 5.5a, at discharge currents 1C, 5C and 20C. Note that the surface can now be cut at any desired

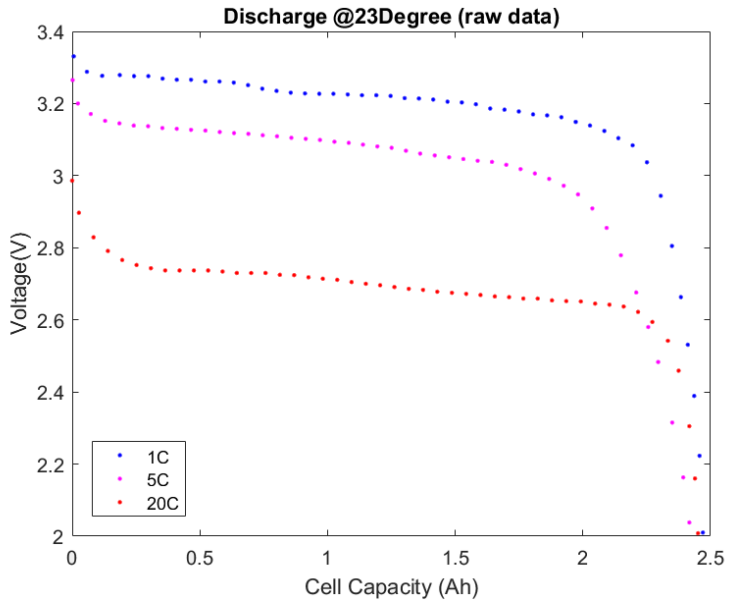

Figure 5.4: Imported raw vectors for voltage vs. cell capacity

value between 1C and 20C. However, to obtain the surface cut at zero current, i.e the OCV curve, we need to extrapolate the surface. Again, the solution is provided by the Matlab function Interp2 [2], using the extrapolation method spline. The final answer is the red curve, which can be directly used to configure the E_m parameter of the Datasheet Battery Block. From the OCV curve is now possible to compute the internal resistance R_0 at different temperature from the data $V(T)$ of Fig.5.5b. The curves can be related algebraically, elementwise, to obtain R_0 as a function of SOC and temperature:

$$R_0(SOC, T) = (OCV - V(T))/1C$$

The result is shown in Fig. 5.7: Unfortunately, OCV can be computed only at $23°C$ and not as a function of T, due to lack of information from the manufacturer. This can generate some inconsistencies at low values of cell SOC that, however, can be corrected with clipping before programming the

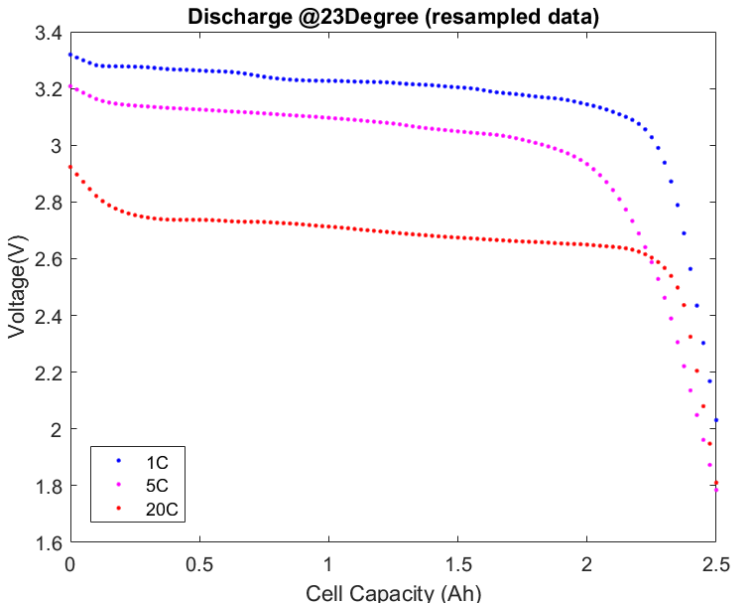

(a) Re-sampled voltage vs. capacity curves from the datasheet

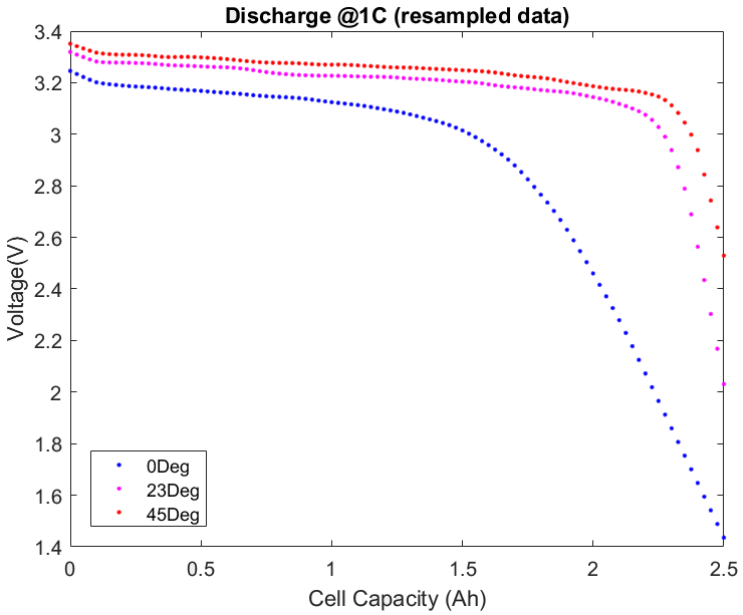

(b) Filtered curves voltage vs. capacity curves from the datasheet

Figure 5.5: Data preparation

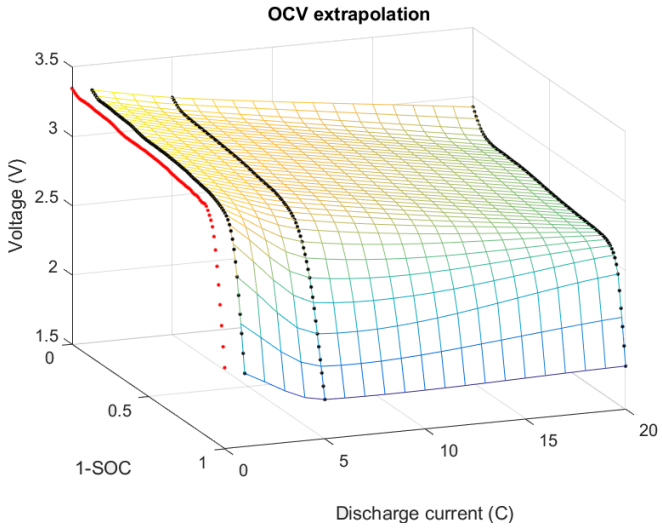

Figure 5.6: OCV at zero current extrapolation

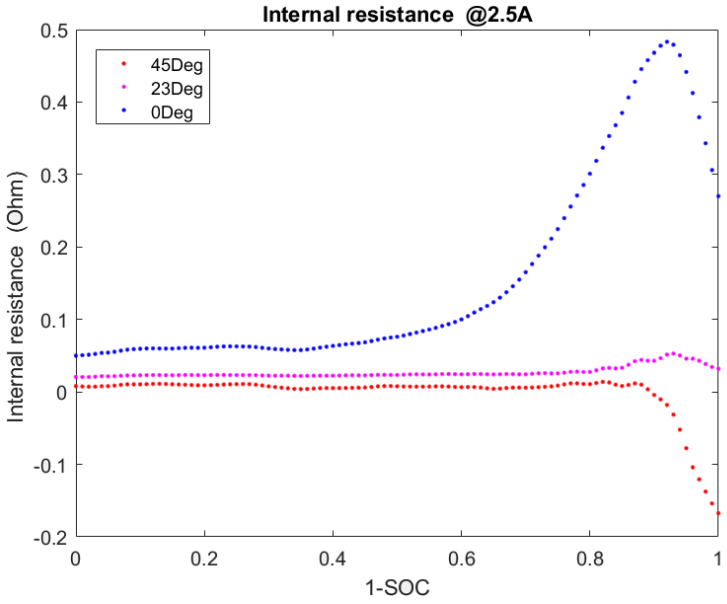

Figure 5.7: R_0 computation from datasheet data

R_0 parameter of the Datasheet Battery Block.

5.4 Extracting Data from Laboratory data collection

If laboratory equipment is available, it is possible to collect customized datasheet-like data. The official data provided by the manufacturer are usually averaged on the characteristics of the batteries produced; furthermore every company uses their own procedure since standard procedures do not exist. Performing a data collection campaign in the lab has, therefore three main advantages:

1. the data are specific to the selected battery cell
2. the ambient temperature and C-rates can be customized
3. more extensive tests can be tailored to the final applications, including dynamic behavior and cycling ageing

The capacity of the A123 LFP-based Lithium-ion batteries was measured both during charging, using a standardized constant current – constant voltage (CC-CV) procedure, and discharging, using a CC procedure, at four different temperatures $T = \{15°C, 25°C, 35°C, 45°C\}$. At each temperature, the battery capacity was measured at six different C-rates $C-rates = \{0.25C, 0.5C, 1C, 2C, 3C, 4C\}$ [5]. Prior to each charging or discharging capacity measurement, the battery cell was kept for one hour at open circuit voltage condition, in order to ensure that it reached a thermo-dynamical stable condition. During all the measurements, the battery cell was placed into a climatic chamber to ensure stable and reliable temperature; furthermore, the mentioned temperature is the one measured on the surface of the cell using a type-k thermocouple.

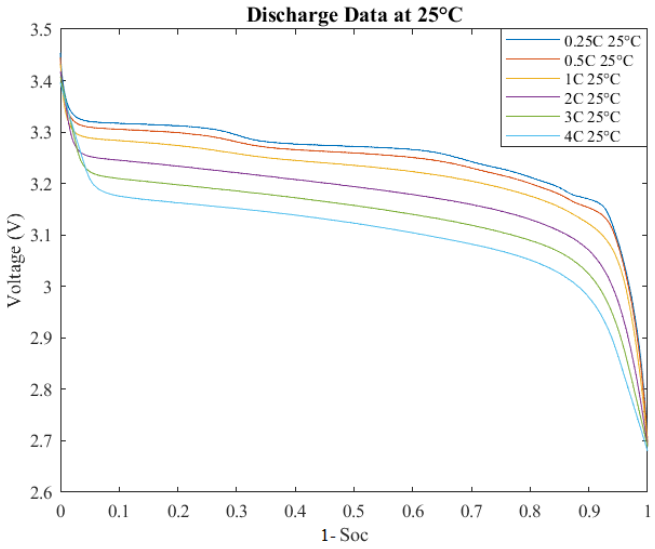

Figure 5.8: Laboratory collected data showing discharge voltage vs. SoC at $25°C$ at different C-rates

The discharge voltage data at different C-rates and at a constant temperature of $25°C$ are shown in Fig. 5.8 while the discharge voltage at constant $1C$ and at different temperatures are shown in Fig. 5.9. The same procedure has been performed at different aging states, with charge and discharge battery voltage profiles for temperature ranging from $15°C$ to $45°C$ and C-rates varying from 0.25 C to 4 C.

5.5 Results

Using the battery manufacturer data we are able to validate battery behavior for limited test conditions. However, using the advanced battery model with the laboratory measurements we have been able to replicate battery behavior under varied operating conditions. Fig. 5.10 shows the results of the datasheet battery block obtained by using the manufacturer's data. The A123 batteries have been tested by the manufacturer using two test cases: (1)

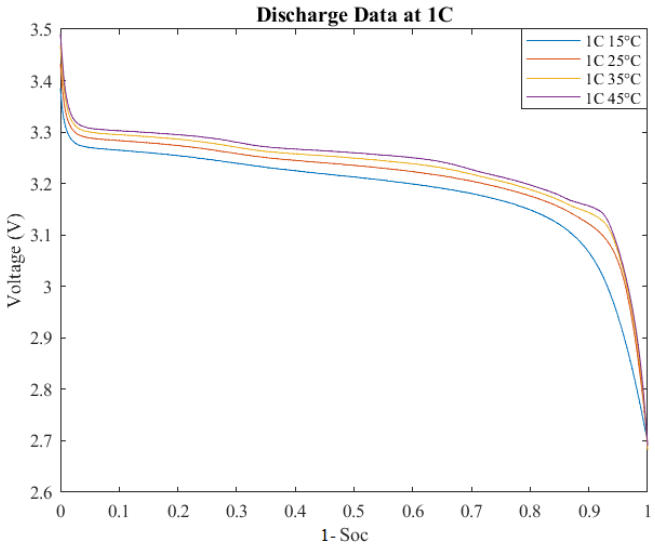

Figure 5.9: Laboratory collected data showing discharge voltage at $1C$ at different temperatures

Ambient temperature of $23°C$ and $\mathrm{C-rates} = \{1C, 5C, 20C\}$; (2) 1C rate and temperatures $T = \{0°\mathrm{C}, 23°\mathrm{C}, 45°\mathrm{C}\}$ as shown in Fig. 5.10a. These data have then been normalized with respect to 1-SOC, as shown in Fig. 5.10b, 5.10c. Fig. 5.10d, 5.10e show the obtained internal resistance as a function of SoC and temperature, while Fig. 11(f) shows the extrapolated OCV, indicated by the symbol E_m: A thorough battery behavior is studied in the laboratory, using which a more robust model is made. Fig. 12 shows the results of the datasheet battery block obtained using data collected in the lab. The A123 batteries have been tested at more operating conditions. In this case, we have: (1) Ambient temperature of 25°C and $\mathrm{C-rates} = \{0.25\mathrm{C}, 0.5\mathrm{C}, 1\mathrm{C}, 2\mathrm{C}, 3\mathrm{C}, 4\mathrm{C}\}$; (2) 1C rate and temperatures $T = \{15°\mathrm{C}, 25°\mathrm{C}, 35°\mathrm{C}, 45°\mathrm{C}\}$as shown in Fig. 5.11a. These data have then been normalized with respect to 1-SOC, as shown in Fig. 15.11b, 5.11c. Fig. 5.11d, 5.11e show the obtained internal resistance as a function of SoC and temperature, while Fig. 5.11f shows the extrapolated OCV, indicated

by the symbol E_m. To compare the two models, we have computed the relative error RE between the original voltage curves used to parametrize the datasheet battery block V_{exp} (i.e. either the data extracted from the manufacturer's datasheet or the laboratory measurements), and the voltage simulated by the configured block V_{sym}, according to this formula:

$$RE = 100 \cdot {}^{(V_{sym} - V_{exp})}/_{V_{exp}}$$

The datasheet battery block configured using data extracted from the manufacturer data has $RE \leq 2.8\%$ for SoC $10\% \leq$ SoC $\leq 100\%$,while the battery block configured using customized laboratory measurements has a $RE \leq 1.05\%$ for SoC $10\% \leq$ SoC $\leq 100\%$.

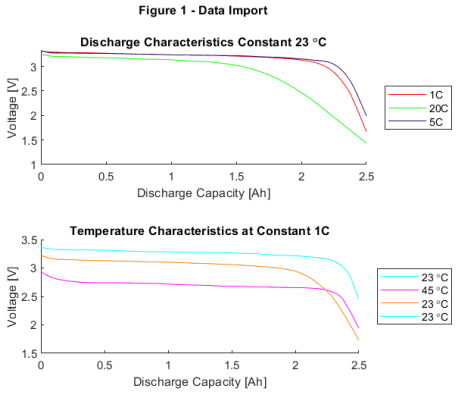

(a) Discharge Data

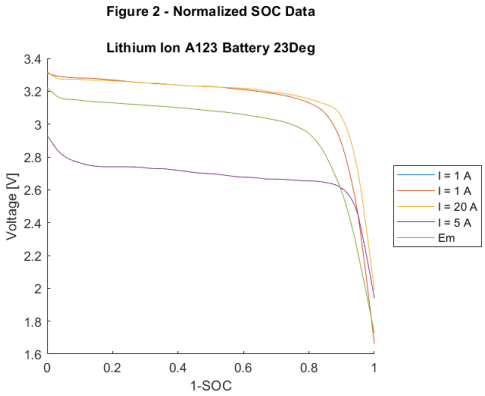

(b) SoC normalized voltage at 23°C

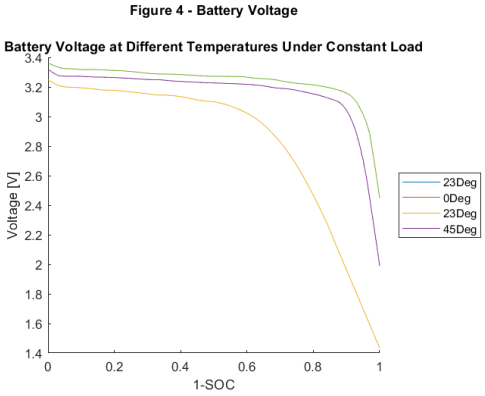

(c) SoC normalized voltage at 1C

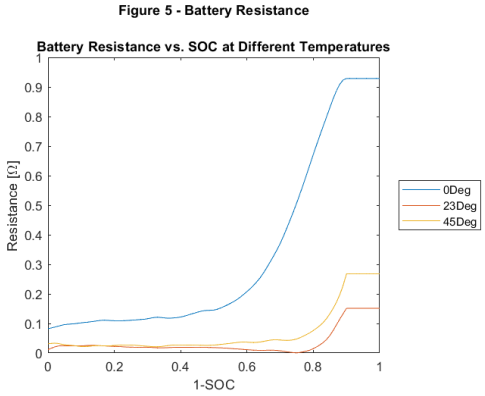

(d) Internal Resistance

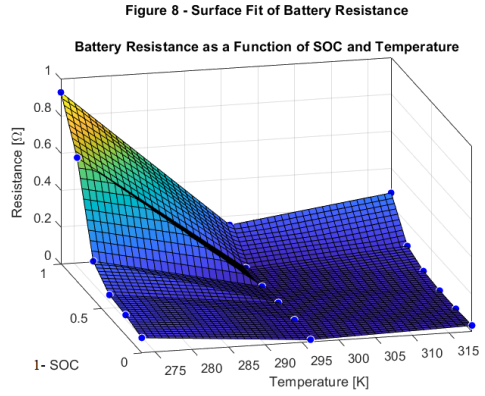

(e) Internal resistance surface

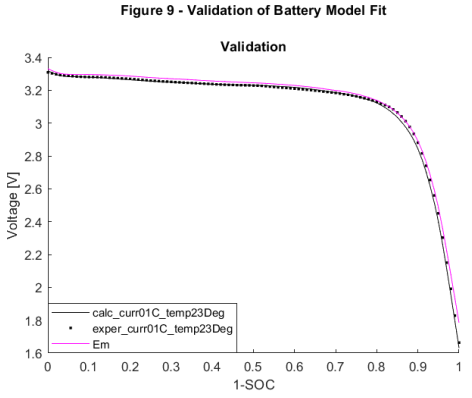

(f) Voltage validation

Figure 5.10: Datasheet Model based on manufacturer's specification data

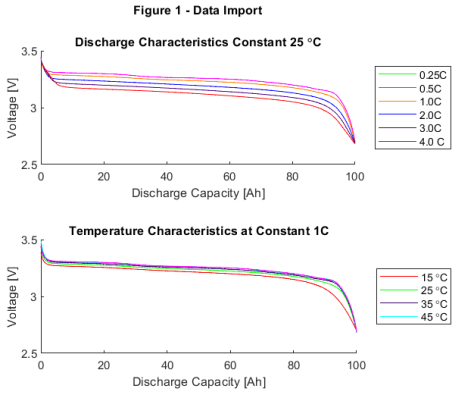

(a) Discharge Data

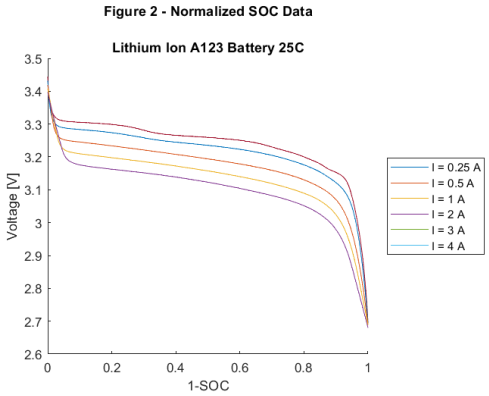

(b) SoC normalized voltage at 23°C

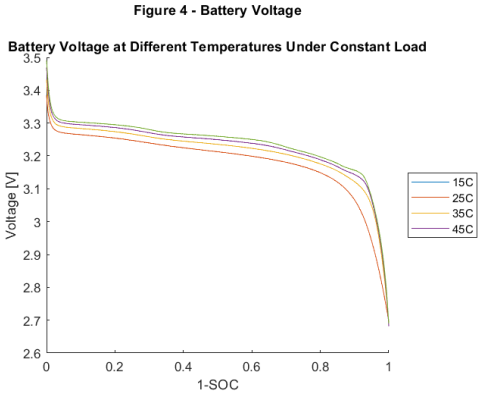

(c) SoC normalized voltage at 1C

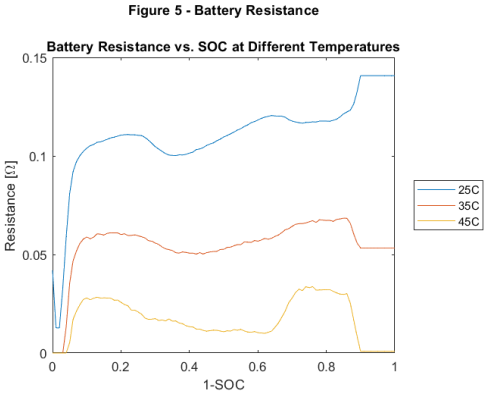

(d) Internal Resistance

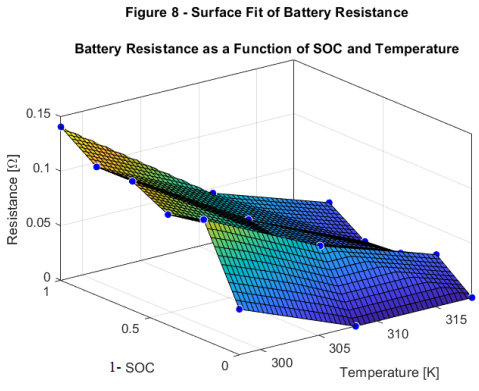

(e) Internal resistance surface

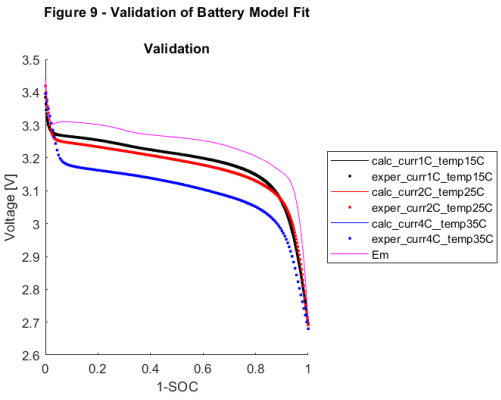

(f) Voltage validation

Figure 5.11: Advanced datasheet battery model using laboratory measurements

5.6 Summary

This chapter presents a data-driven approach for modelling the behavior of a Li-ion battery. Here we showed a systematic methodology of using the manufacturer's datasheets for available simulation platforms, such as Matlab-Simulink. In order to overcome the limited data availability in manufacturer's datasheets we have enhanced the model by including extensive laboratory measurements for building a robust advanced battery datasheet model that can predict battery behavior under varied field applications. The model was validated by using data collected on two test cases: (1) ambient temperature of $25°C$ and $\mathrm{C-rates} = \{0.25\mathrm{C}, 0.5\mathrm{C}, 1\mathrm{C}, 2\mathrm{C}, 3\mathrm{C}, 4\mathrm{C}\}$; (2) 1C rate and temperatures $T = \{15°\mathrm{C}, 25°\mathrm{C}, 35°\mathrm{C}, 45°\mathrm{C}\}$. The advanced datasheet battery model using laboratory measurements is 99% accurate.

References

[1] Mathworks. https://www.mathworks.com/help/matlab/ref/interp1.html.

[2] Mathworks. https://www.mathworks.com/help/matlab/ref/interp2.html.

[3] Mathworks. Datasheet battery block. https://www.mathworks.com/help/autoblks/ref/datasheetbattery.html.

[4] Ankit Rohatgi. Webplotdigitizer. https://automeris.io/WebPlotDigitizerVersion4.3, 2020.

[5] Daniel Ioan Stroe. *Lifetime Models for Lithium-ion Batteries used in Virtual Power Plant Applications*. PhD thesis.

Chapter 6

Extracting the ECM model using wavelet analysis

6.1 Background

There are many techniques for the identification of equivalent circuit parameters such as Electrochemical Impedance Spectroscopy (EIS) . Traditional EIS is a technique to measure the real and imaginary parts of impedance Z as a function of frequency. EIS is an expensive lab activity that requires a scanning sine wave generator, powerful enough to stimulate the battery at different frequencies, from milliHz to kiloHz. The result is a Nyquist plot that is only valid for well-defined values of T, SoC and SoH. The Nyquist plot is then fitted with a circuit containing resistors, capacitors and even exotic components like Warburg impedance or Constant Phase Element (CPE) [1, 3]. Unfortunately, Z is a function of T, SoC and SoH and a complete estimation of the components would require a massive use of EIS. An alternative solution to the frequency scanning stimulus of EIS could be the injection of a wide spectrum current signal to the battery. Then, the resulting voltage drop could be analyzed in frequency with signal processing techniques [5]. The wide spectrum signal could be designed ad-hoc as a pseudorandom bi-

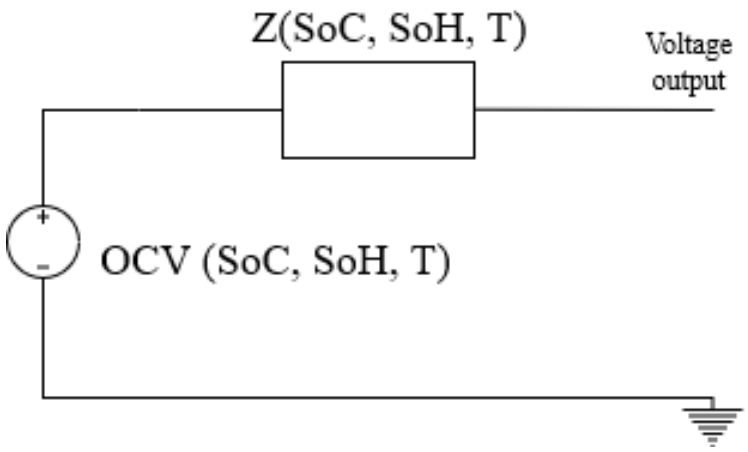

Figure 6.1: A more accurate ECM model

nary sequence. However, EIS-based methodologies for impedance evaluation are not very useful for EVs, because the identification is mainly offline. Moreover, the internal impedance is different when measured under load and this is especially true for the internal resistance, that is responsible for the voltage drop when a current pulse is applied. An online identification would be more useful since it can provide real-time information that could be used to operate the battery optimally.

6.2 A more accurate ECM model

The ECM is an electrical model based on common circuit elements, like voltage generators, resistors and capacitors, and its overall complexity can be tailored to the application. A battery is a voltage source whose electrical behavior can be summarized by an equivalent Thevenin circuit, as shown in Fig. 6.1 The ideal generator, labelled as OCV, is a non-linear function of temperature (T), SoC and SoH. As the name implies, the OCV generator can be easily measured at zero or low currents, but the complete function characterization requires a time-consuming process in the lab. An alternative

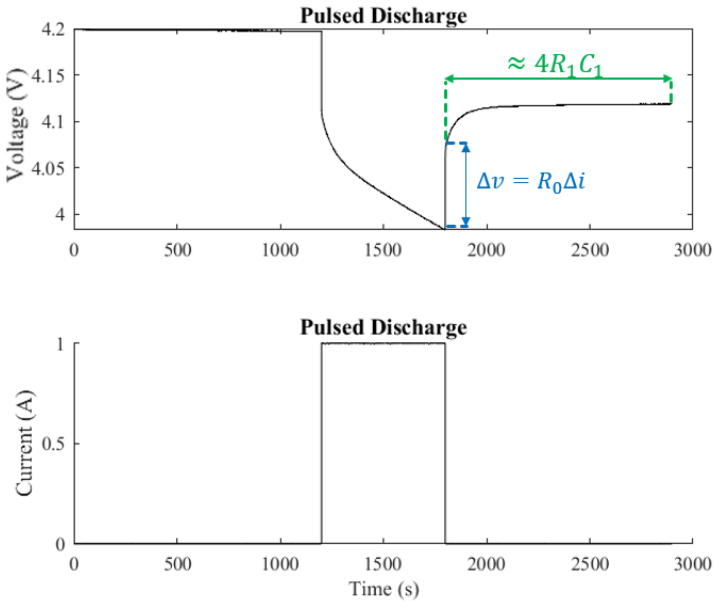

Figure 6.2: Pulsed current discharge

solution will be provided at the end of this chapter. The internal impedance Z is as well a non-linear function of T, SoC and SoH, but it is not accessible and cannot be easily measured. Moreover, the inside equivalent circuit of Z is not known. However, the effect of Z is fully observable as an output voltage drop when the battery supplies current to an external load. Just as an example, Fig. 6.2 shows the voltage drop when the battery supplies an impulse current of 1 A. Under the assumption that Z has inside a first-order equivalent circuit made of R_0 in series with an R_1, C_1 pair, it is possible to estimate the values of components observing the time domain response: R_0 can be estimated as $R = -dV/dI$ at the falling edge of the current; the R_1, C_1 time constant can be estimated from the duration of the exponential rise of the voltage signal. For now, it is useful to note that R_0 is related to the fast change of the signal, i.e. to high frequencies, and the pair R_1, C_1 is related to the relative slow change of the signal, i.e. to low frequencies. In general, Z has a much more complex equivalent circuit and the identification

of components requires a time-frequency analysis of the current and voltage signals.

6.3 Time-frequency analysis of battery signals

As we introduced in Section 6.1, an alternative solution to the frequency scanning stimulus of EIS could be the injection of a wide spectrum current signal into the battery. Then, the resulting voltage drop could be analyzed in frequency with signal processing techniques. The wide spectrum signal could be designed ad-hoc as a pseudorandom binary sequence, but in this Chapter we show that a simple current pulse is enough to draw a partial Nyquist plot over at least two decades of frequencies. This opens the possibility to test the battery in the application field, not only in the lab. In summary, we propose to analyze common pulsed discharge signals of a battery in order to recover multiple Nyquist plots, one for each current pulse, corresponding to different SoC. If the process is repeated at different SoH and different T, we obtain a complete characterization of the battery's internal impedance as a function of T, SoC and SoH. The overall frequency analysis of the signals cannot be done with a simple FFT because this transform locates the signal only in frequency and loses the time information related to SoC. Instead, the frequencies of each pulse must be distinguished by the others in order to draw different Nyquist plots at diffent SoC. The solution is a Continuous Wavelet Transform (CWT) that allows a time-frequency localization of signals. The CWT analyzes a signal with a wavelet, a waveform that is concentrated both in time and in frequency domain. A measure of the concentration is the so-called Heisenberg area, defined as the product of standard deviations in time domain and in frequency domain respectively. A suitable wavelet, called the Generalized Morse Wavelet [4] is shown in Fig. 6.3. Here the parameters gamma and beta have been chosen in order to obtain a small Heisenberg area.

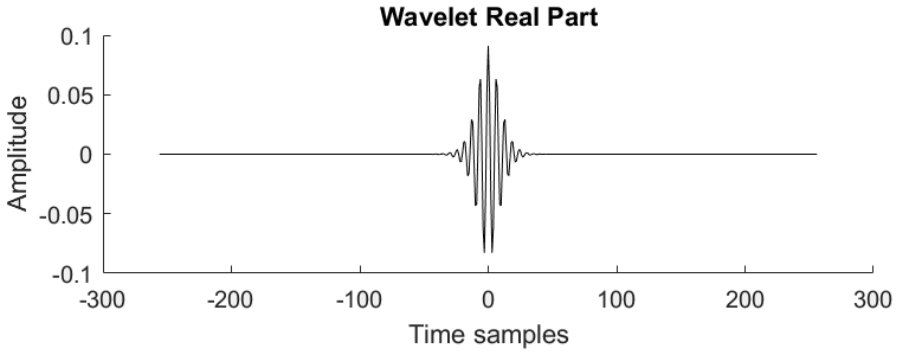

(a) Wavelet real part

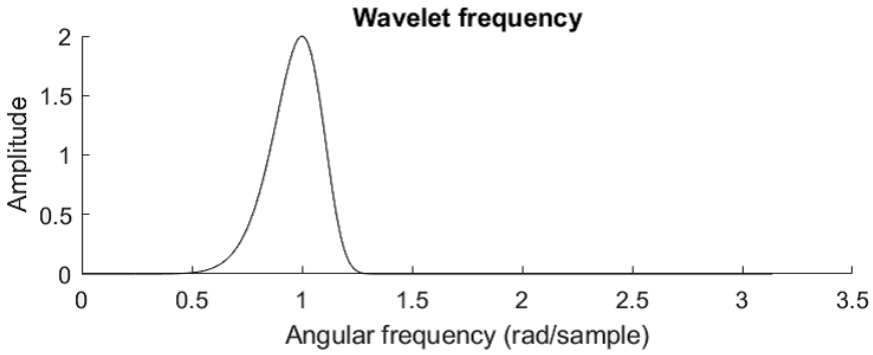

(b) Wavelet imaginary part

Figure 6.3: Generalized Morse wavelet

This wavelet in time domain can be thought as the impulse response of a bandpass filter. Then the CWT output can be thought as a filtered version of the input signal. In this manner, by changing the wavelet frequency we can perform a time-frequency analysis of a signal. The highest possible wavelet frequency is established by half of the sampling frequency of signals (or $\omega = \pi f_s$). The lowest possible frequency for pulsed discharge signals must avoid the overlapping of wavelets located at adjacent fronts of current pulses. Fig. 6.4 shows a zoomed view of a wavelet located to a rising edge of the battery's voltage signal (falling edge of battery current).

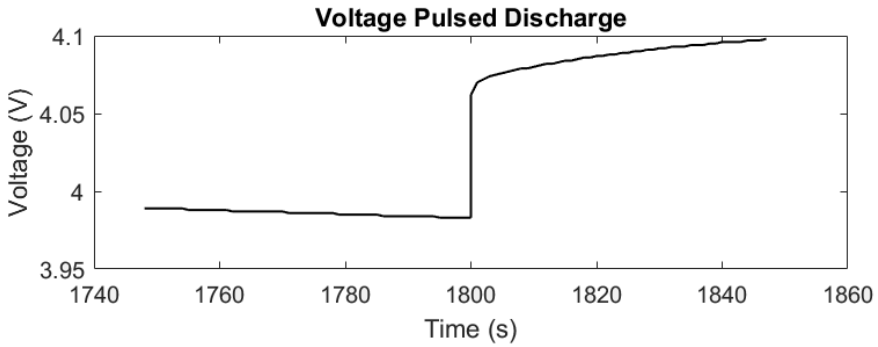

(a) Pulsed voltage discharge

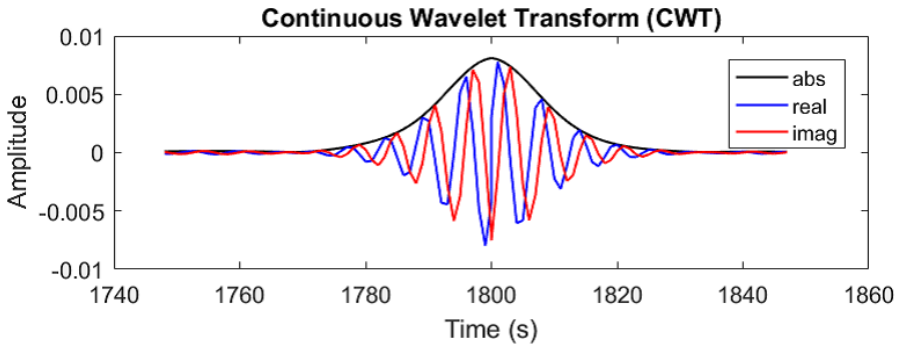

(b) CWT

Figure 6.4: CWT of the pulsed discharge voltage

The wavelet is complex in time domain and has a real and imaginary part. When we divide the CWT of battery voltage and the CWT of battery current at each falling edge, we obtain a single point on multiple Nyquist plots, each corresponding to a falling edge of current, i.e. at different SoC. Changing the wavelet frequency, we can complete all Nyquist plots over a range of frequencies within the limits explained.

6.4 Experimental Data

The proposed methodology has been applied to the NASA dataset [2]. A series of charging and discharging currents between -4.5 A and 4.5 A were

used to continuously operate a set of four 18650 Li-ion batteries. Random walk (RW) operation is the term used to describe this kind of charging and discharging process. Five minutes were allotted for each loading period, and after 1500 of them (about five days), a set of reference charging and discharging cycles were carried out in order to give benchmarks for battery state health. To measure changes in battery transient dynamics, fully charged batteries are discharged with pulsed current after every 3000 RW steps. The pulsed current discharge consists of 10 minutes with a 1 A load applied and 20 minutes with no load. This dataset has 21 pulsed discharge sequences of cell voltage and current, recorded at different ageing times, synchronously sampled at 1 Hz. In Fig. 6.5 only 4 sequences, at different aging times, are superimposed for better visualization. Each current pulse extracts from the cell a charge of 1/6 Ah. The process is repeated until the depletion of the cell. The last current pulse of a sequence can be shorter than 10 minutes. Integrating the current, we obtain the charge capacity of the cell. The fresh cell has a total capacity of 2.1Ah (sequence 1, longest), the aged cell at end of life has a total capacity of about 0.9Ah (sequence 21, shortest). To apply the CWT, we have to establish the range of frequency that the chosen wavelet can analyze.

6.5 Wavelet analysis of Nasa data set

The wavelet is complex in the time domain and thus has a real and imaginary part. When we divide the CWT of battery voltage and the CWT of battery current at each falling edge of the current and voltage signals taken from the NASA dataset, we obtain a single point on multiple Nyquist plots, each corresponding to a falling edge of current, i.e. at different SoC. Changing the wavelet frequency, we can complete all Nyquist plots over a range of frequencies within the limits previously explained. The Nyquist plots have been calculated at each current front. For visualization clarity, the next

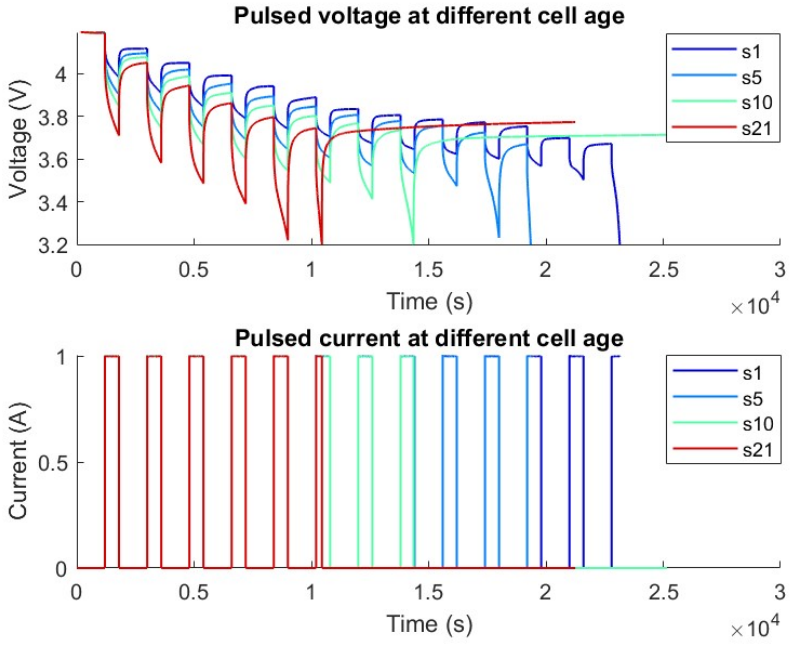

Figure 6.5: Selected pulsed voltages and currents sequences from the NASA dataset

graphs are shown only in correspondence with the falling edge of the third pulse (from the left). At this edge, the total charge extracted from the cell is 0.5Ah. The Nyquist plots have each 30 points, corresponding to log spaced frequencies from $\omega = 2$ to $\omega = 0.02$ (two decades). Fig. 6.6 shows the results only for the sequences of Fig. 6.5, with the same colors for the identification. It is apparent the increase of the impedance as the cell ages and the charge capacity fades (decrease of SoH). The Nyquist plots from traditional EIS are computed over a wider frequency range. For example, the intersection with the real axis cannot be computed with CWT due to the limits of the sampling frequency of the cell signals. However, this reduced view of plots has enough information and makes it possible to extract equivalent circuit elements.

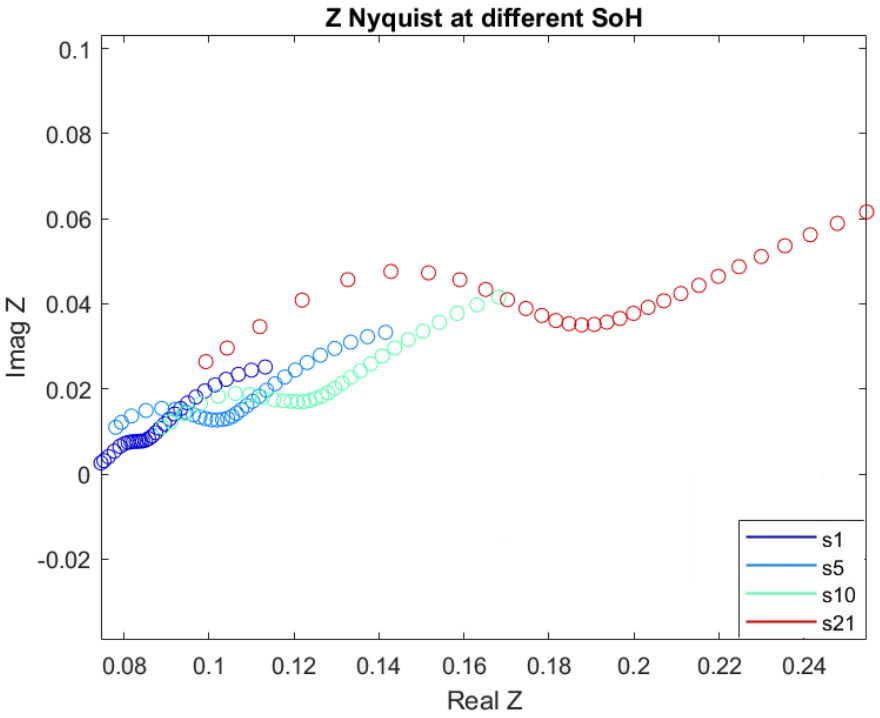

Figure 6.6: Nyquist plots of selected pulsed discharge sequencies from the NASA dataset

6.6 Fitting the Nyquist plots

Nyquist plots show complex impedance values measured at different frequencies. We want to find an equivalent circuit that exhibits the same impedance behavior as closely as possible. We know that for batteries the circuit elements are mainly resistors and capacitors. Small inductances are only due to battery terminals and are present only at high frequencies, which are not considered in this work. Even complex components like Warburg impedance or CPE can be approximated by RC circuits, as they can be modelled by a large number of RC branches, as in an equivalent transmission line. For batteries, the simplest equivalent circuit is shown in Fig. 6.7.

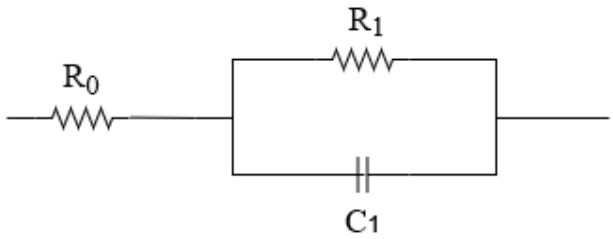

Figure 6.7: First order equivalent circuit

The corresponding Nyquist plot is a semi-circle with center at $R_0 + R_1/2$ and radius $R_1/2$. C_1 has effects on the frequency behavior. For this simple Nyquist plot, it is possible to derive some formulas to fit the equivalent R_0, R_1 and C_1 circuit elements.

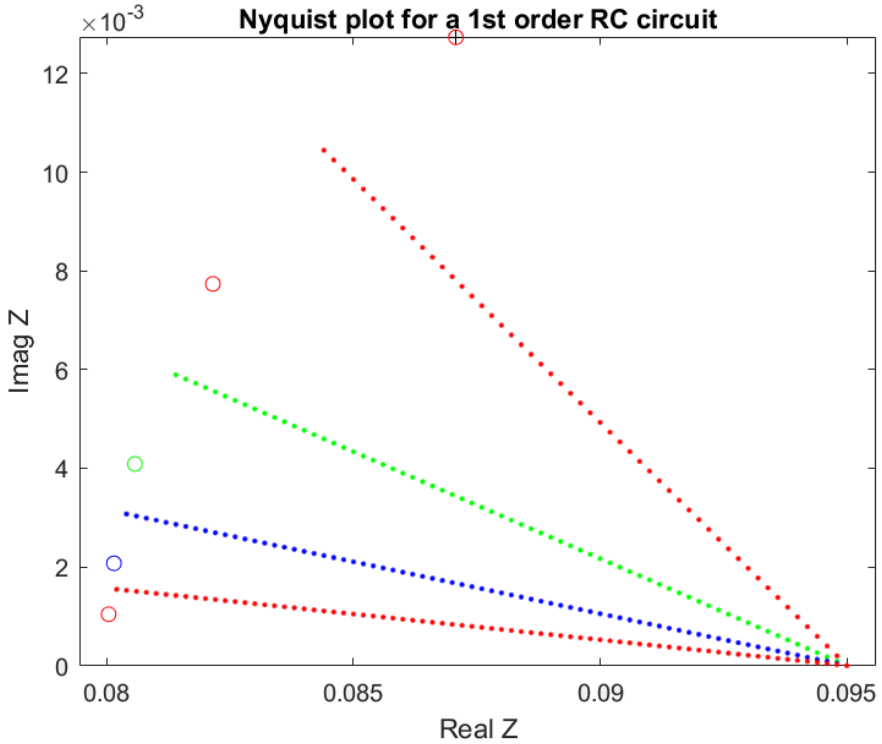

Figure 6.8: Some Nyquist points on the semicircle

Fig.6.8 shows some semi-circle points computed with the CWT method at known frequencies and also the bisects of cords between adjacent points. The bisects intersect at the center of the semi circle, also laying on the real Z axis. With simple geometric considerations, the following formulas can be derived:

$$\mathrm{Z} = \mathrm{R}_0 + \frac{\mathrm{R}_1}{(1 + \mathrm{sR}_1\mathrm{C}_1)} \qquad \text{where } \mathrm{s} = j\omega \tag{6.1}$$

the real part $Re(\mathrm{Z})$ and the imaginary part $Im(\mathrm{Z})$ are, respectively:

$$\begin{aligned} Re(Z) &= R_0 + \tfrac{R_1}{1+(\omega R_1 C_1)^2} \\ Im(Z) &= \tfrac{-\omega R_1^2 C_1}{1+(\omega R_1 C_1)^2} \end{aligned} \tag{6.2}$$

If we consider two different frequencies ω_1 and ω_2, and their respective imaginary parts $Im\left(\mathrm{Z}_{\omega_1}\right)$ and $Im\left(\mathrm{Z}_{\omega_2}\right)$, we obtain:

$$\mathrm{C}_1 = \frac{\frac{\omega_2}{Im2} - \frac{\omega_1}{Im1}}{\omega_1^2 - \omega_2^2} \tag{6.3}$$

The semi circular Nyquist plot has center $\mathrm{C}_N = \mathrm{R}_0 + \frac{\mathrm{R}_1}{2}$ and radius $\mathrm{R}_N = \frac{\mathrm{R}_1}{2}$. We know that a perpendicular that bisects a chord passes for the center of the circle. The mid point P on the chord has the following coordinates:

$$\begin{aligned} px &= Re\left(\mathrm{Z}_2\right) + \tfrac{\mathrm{DR}}{2} \\ py &= Im\left(\mathrm{Z}_1\right) + \tfrac{\mathrm{DI}}{2} \end{aligned} \tag{6.4}$$

where:

$$\begin{aligned} DR &= abs\left(Re\left(\mathrm{Z}_1\right) - Re\left(\mathrm{Z}_2\right)\right) \\ DI &= abs\left(Im\left(\mathrm{Z}_1\right) - Im\left(\mathrm{Z}_2\right)\right) \end{aligned} \tag{6.5}$$

the angular coefficient of the perpendicular is:

$$\begin{aligned} m &= \tan\left(\tfrac{\pi}{2} + \arctan\left(\tfrac{\mathrm{DI}}{\mathrm{DR}}\right)\right) \\ y &= m \cdot (x - p_x) + p_y \end{aligned} \tag{6.6}$$

and the circle center on the horizontal axis of the Nyquist plot is:

$$\mathrm{C}_N = \frac{m \cdot (p_x - p_y)}{m} \tag{6.7}$$

and finally we can obtain R_1 :

$$\mathrm{R}_1 = \sqrt{(c_x - Re\,(\mathrm{Z}_1))^{\,2} + Im\,(\mathrm{Z}_2)^{\,2}} \tag{6.8}$$

These formulas require only two Nyquist points, with better results for bisects near 45 degrees. The components values corresponding to the Nyquist plot of Fig.6.8 are: $R_0 = 0.08\ \Omega$; $R_1 = 0.03\ \Omega$; $C_1 = 600\ F$. Real cells have more complicated Nyquist plots and circuit fitting is much more challenging. Nyquist plots computed from the Nasa dataset and shown in Fig. 6.6 require higher-order RC circuits for which geometric considerations to derive simple formulas for the computation of the components is not possible. The solution is to fit RC values with known optimization techniques that minimize the distance between the Nyquist plot and the Z behavior of the tentative circuit. To fit the data from the NASA repository, we propose a 3rd order circuit, as shown in Fig.6.9.

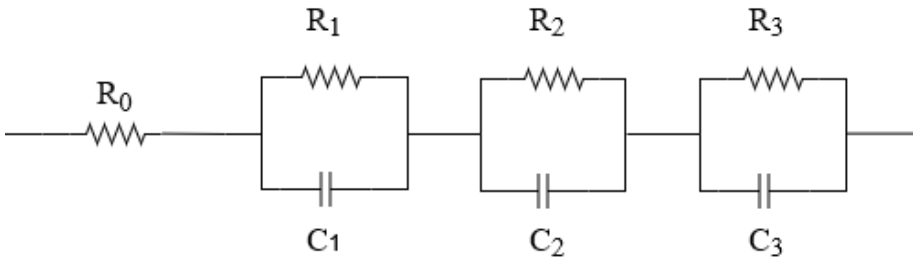

Figure 6.9: Third order equivalent circuit

In the Matlab environment, the *fminsearch* function can perform the fitting of the Nyquist plots. *fminsearch* makes a guess for the seven $R_0, R_1, C_1, R_2, C_2, R_3, C_3$ parameters and then call a user callback function that must

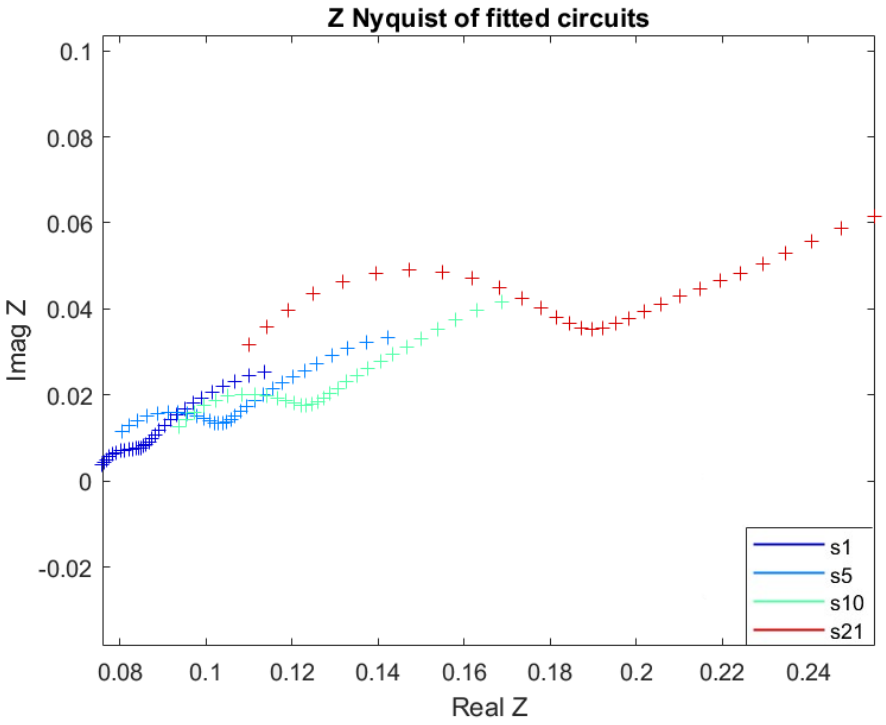

Figure 6.10: Fitting results for Nyquist plots

return a scalar as a measure of distance. The scalar returned has been computed as the unweighted squared distance between the Nyquist points and the corresponding guessed points. Due to the large search space, it is important to start from a good starting guess for a successful fitting. The first guess has been computed with the formulas (6.1)-(6.8) shown above for the 1st order circuit. The fitting results for Nyquist plots of Fig. 6.6 are shown in Fig.6.10, with the same colors for identification. The $R_0, R_1C_1, R_2C_2, R_3C_3$ have been computed for all the current fronts of all the 21 NASA sequences, obtaining seven functions of cell parameters dependent on SoC and SoH. The dependability from temperature T cannot be computed as all the NASA sequences are taken at room temperature. The complete results of the analysis on all the sequences of the NASA dataset are shown with normalized SoC and SoH. The plots contain 21 values, each corresponding to a sequence of

the NASA dataset. The SoH points are computed as the ratio of the charge capacity of the aged cell (sequence 2 to 21) over the charge capacity of the fresh cell (sequence 1). Fig. 6.11 shows the SoH of the NASA dataset.

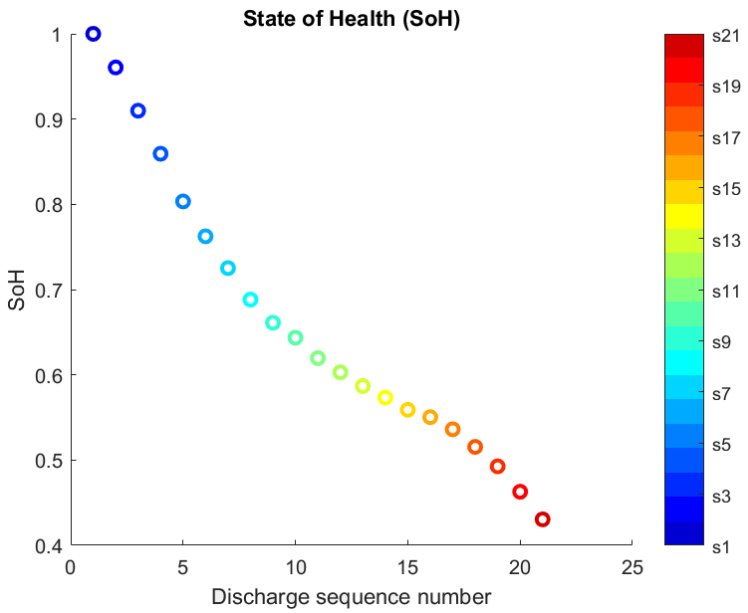

Figure 6.11: Normalized SoH of the NASA dataset

The color sidebar helps in identifying the pulsed discharge sequences: the color identified with 's1' indicates sequence 1 of the fresh cell (longest sequence), the color identified with 's21' color indicates sequence 21 of the end-of-life cell (shortest sequence). The same color code has been used for Figs. 6.12 - 6.15, which show the results for the seven parameters R0, R1, C1, R2, C2, R3, C3 as functions of SoC, SoH.

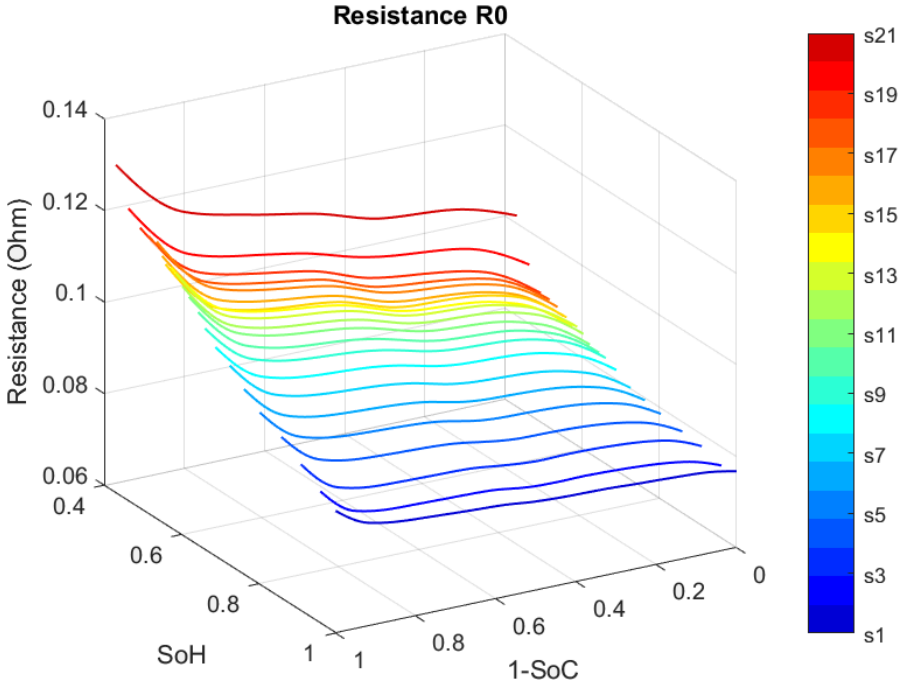

(a) $R_0(SoC, SoH)$

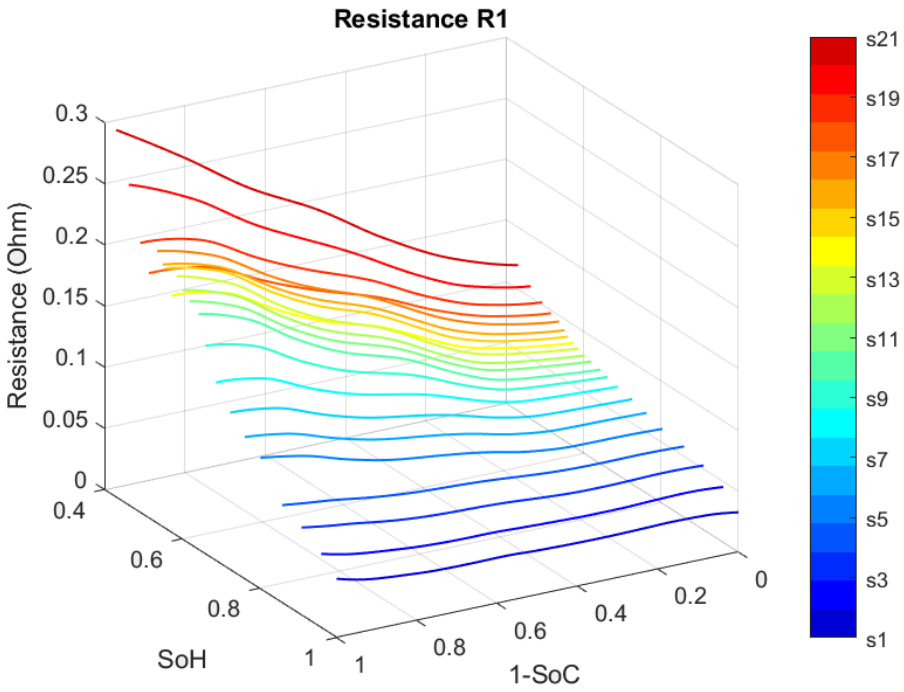

(b) $R_1(SoC, SoH)$

Figure 6.12: ECM parameters values using wavelet analysis on the NASA dataset

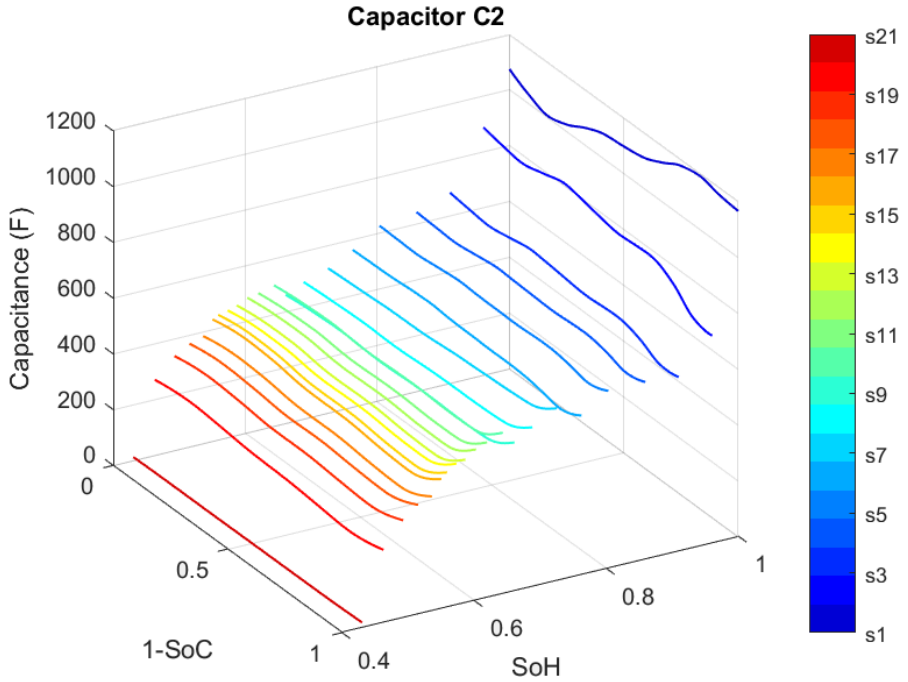

(a) $C_2(SoC, SoH)$

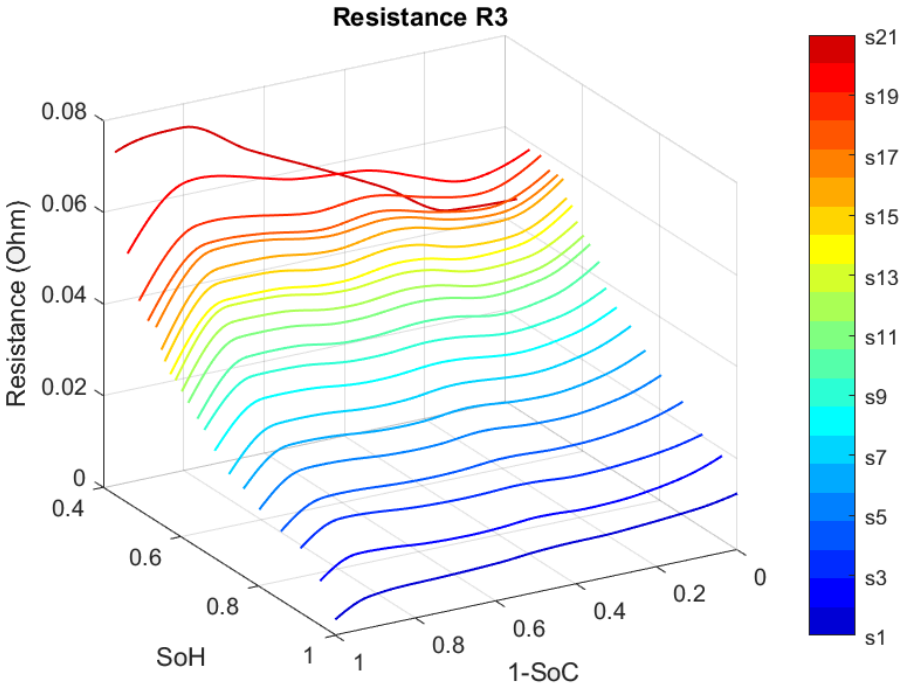

(b) $R_3(SoC, SoH)$

Figure 6.14: ECM parameters values using wavelet analysis on the NASA dataset

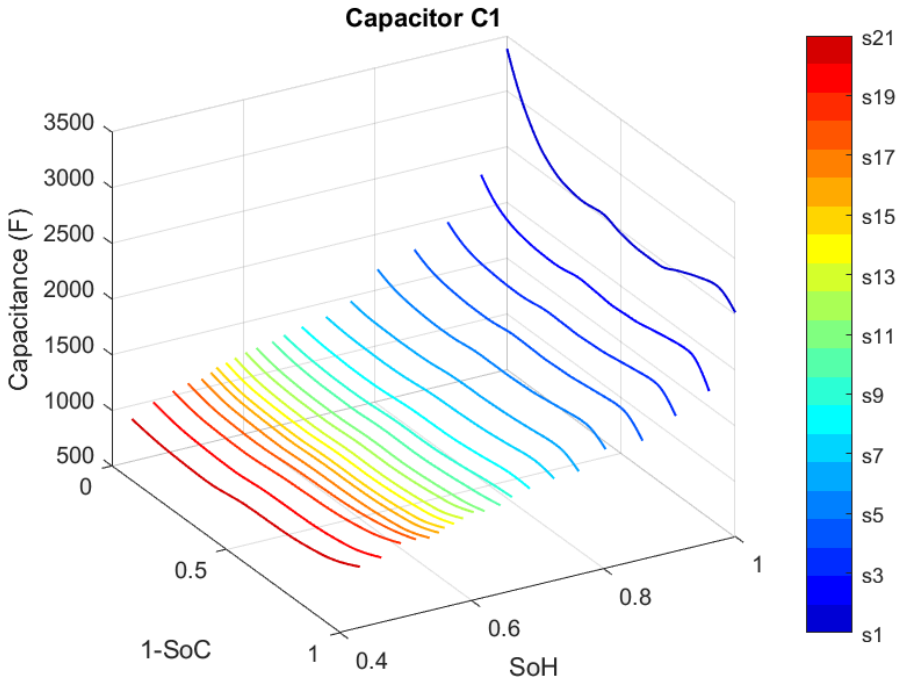

(a) $C_1(SoC, SoH)$

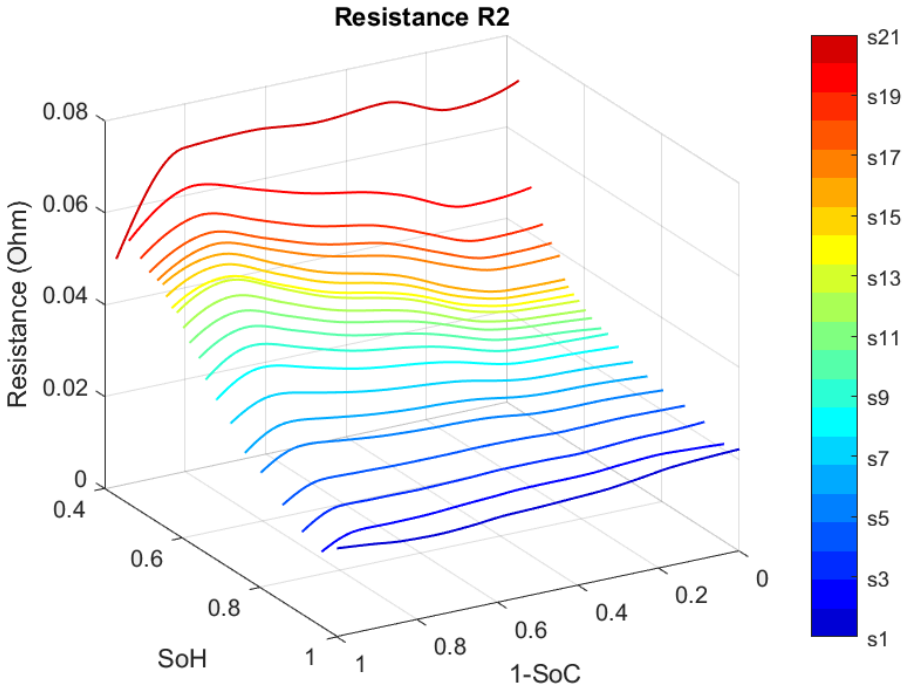

(b) $R_2(SoC, SoH)$

Figure 6.13: ECM parameters values using wavelet analysis on the NASA dataset

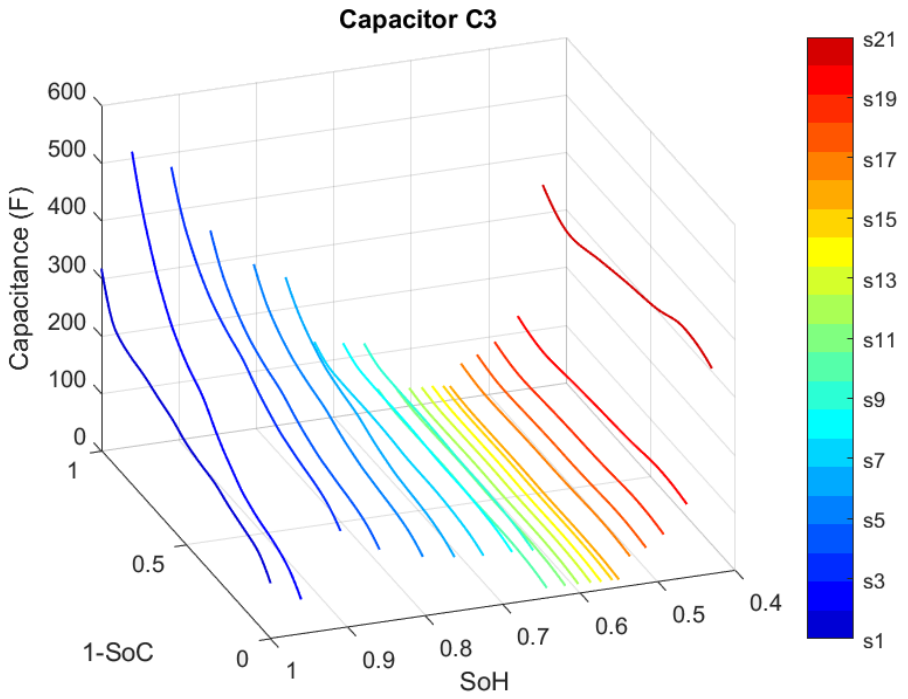

(a) $C_3(SoC, SoH)$

Figure 6.15: ECM parameter values using wavelet analysis on the NASA dataset

Note that Figs. 6.12-6.15 have different angle of view for resistors and capacitors, to aid the visualization of values. It is quite reasonable that internal resistance values increase as the cell ages. Less obvious is the simultaneous decrease of capacitors values, presumably related to the lithium ion diffusion process inside the cell.

6.7 Estimating the OCV from experimental data

The Open Circuit Voltage (OCV) of a cell, at a fixed temperature and at a defined lifetime, is a non-linear function of SoC. This means that the dV drop after the a discharge dQ depends on the state of charge. The ratio dQ/dV

has a dimension of a capacitance and has a finite value (dV is not zero as in an ideal voltage generator). Thus the OCV generator can be thought of as a non-linear supercapacitor. Its reactance at the frequencies of the previous Nyquist plots is low, but it has been taken into account by correcting the imaginary part of the internal impedance Z. Here we want to estimate the OCV generator as a function of SoC and SoH in order to be able to simulate it as a Voltage Controlled Voltage Source (VCVS). Thanks to the previous analysis, we now know the values of the complex internal impedance Z. We can reverse engineer the voltage pulsed discharge signal and subtract the dynamic effects of Z traversed by the pulsed current. Fig. 6.16 shows the 3rd order equivalent circuit of Z.

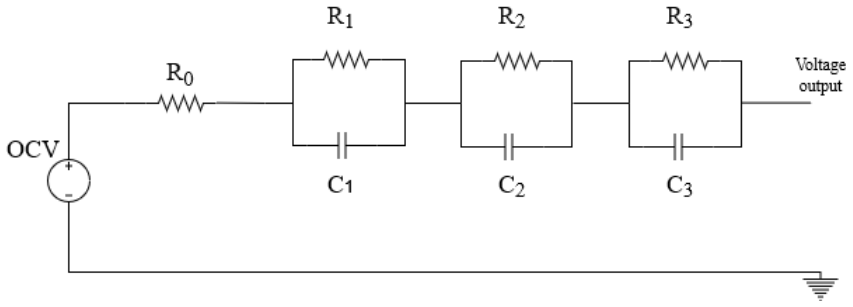

Figure 6.16: Complete 3RC ECM model

The voltage contribution of R_0 is simply the instantaneous product $R_0 i(t)$. The voltage contribution of each pair $R_i C_i$ $(i = 1, 2, 3)$ can be computed by the following recursive formula:

$$v_{RC}(k+1) = \exp(-dt/RC) v_{RC}(k) + (1 - \exp(-dt/RC)) R \cdot i(k) \qquad (6.9)$$

where dt is the sampling period and k is the sample index at time kdt. The total voltage effect of Z is the sum of the four contributions. When this total voltage is summed to the original pulsed voltage of Fig. 6.5, we obtain the

results shown in Fig. 6.17 (for a clear visualization only sequence 1 and 21 are shown).

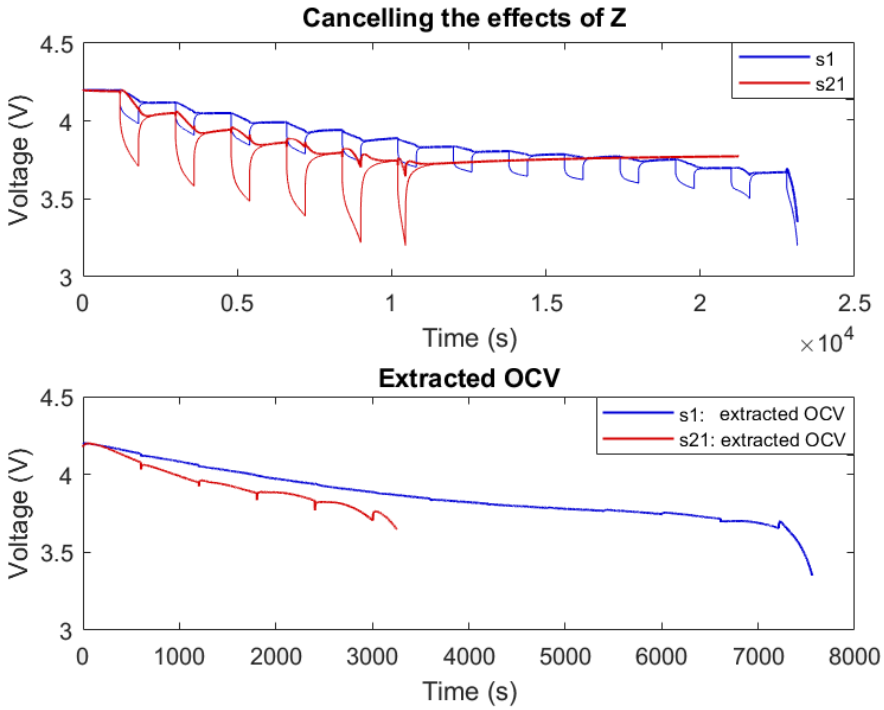

Figure 6.17: OCV reconstruction for sequences 1 and 21 of the NASA dataset

Now, recording the voltage output only when the current is 1A (i.e. during the current pulses), we obtain the classical OCV plot. The horizontal axis shows time, but it can be easily converted to Ah and thus to SoC. The results for all 21 sequences are shown in Fig. 6.18

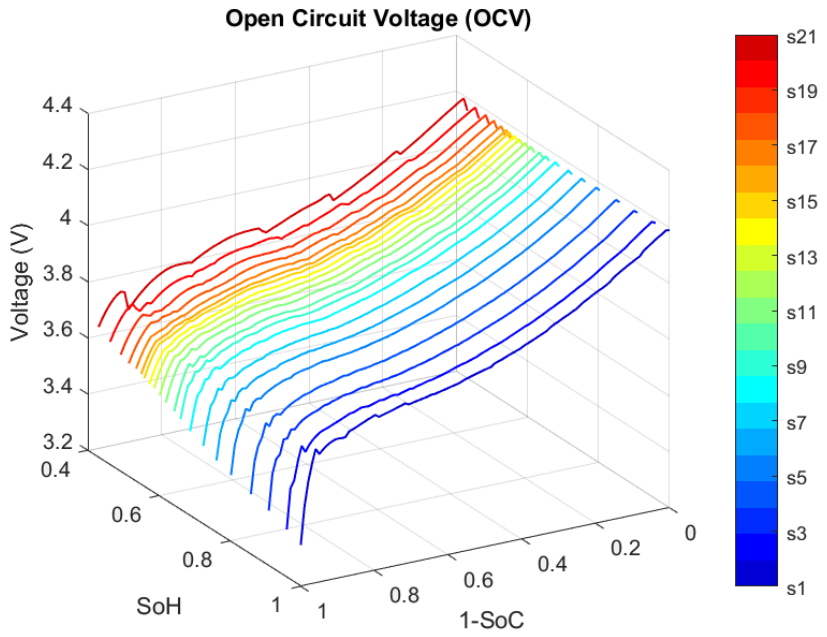

Figure 6.18: OCV reconstruction results on the NASA dataset

It is worth noting that the extracted parameters $R_0, R_1, C_1, R_2, C_2, R_3, C_3$ are indirectly proven to be correct as the voltage pulses due to internal Z on Fig. 6.17 are almost completely canceled.

6.8 Summary

We presented an innovative methodology to extract ECM model parameters as a function of the SoC and SoH of battery cells. The methodology is based on wavelet analysis of the pulsed discharge voltage and current signals from the publicly available Prognostic data repository of NASA. The circuit parameters were fitted using optimization techniques. These parameters were used to cancel the discharge voltage pulses and to recover the OCV curve. $R_0, R_1C_1, R_2C_2, R_3C_3$ and OCV will used in the next Chapter to synthesize a Battery Digital Twin.

References

[1] Empirical modeling of lithium-ion batteries based on electrochemical impedance spectroscopy tests. *Electrochimica Acta*, 160:169–177, 2015.

[2] B. Saha and K. Goebel, NASA Ames Prognostics Data Repository, NASA Ames Research Center, Moffett Field, CA . Battery data set.

[3] Analog Devices. Cn0510 electrochemical impedance spectroscopy(eis) for batteries, circuit notes, 2020.

[4] Jonathan M. Lilly and Sofia Charlotta Olhede. Generalized morse wavelets as a superfamily of analytic wavelets. *IEEE Transactions on Signal Processing*, 60:6036–6041, 2012.

[5] Gjorgji Nusev, Dani juricic, Miran Gaberscek, Joze moskon, and Pavle Boskoski. Fast impedance measurement of li-ion battery using discrete random binary excitation and wavelet transform. *IEEE Access*, 9:46152–46165, 2021.

Chapter 7

Synthesis of a Battery Digital Twin

7.1 Background

Artificial Intelligence (AI) has progressively become a very attractive tool to be applied to batteries, mostly to the estimation of battery parameters[2, 4]. The data preparation phase is the most critical and it is of fundamental importance to insure a successful and trustworthy application of AI techniques. Neural Networks (NN) are broadly used for their capability to infer the input-output relationship between data in an automated way, a process known as black-box modelling. A successful application of NN, requires a lot of training data taken from field-specific applications. To aid the training phase, which can require a lot of time depending on the chosen NN structure, the input data are usually pre-processed using domain-specific knowledge by researchers. This process requires a great deal of time and effort since the data need to be fully understood and cleaned of all the parts that are not necessary to understand the data input-output relationship. Therefore, the development of domain-targeted tools for automating the data preparation phase for NN is needed to speed up the data preparation phase and to be sure to cap-

ture the significant parts of the training data. NNs can exactly fit the training points and, thanks to their interpolation generalization properties, can compute the output also for intermediate points. As previously stated the battery cell is a complex non-linear system. Its parameters change dynamically as a function of SoC, SoH and T. It would be useful to have a digital twin of a real battery cell, chosen for a specific application [3]. Such battery model would be useful to simulate the whole system application in accelerated time taking into account the battery ageing avoiding time-consuming and costly experiments in the laboratory. At this point, we have developed a methodology to extract equivalent ECM parameters from the pulsed voltage and current discharge signals of a real battery. We now need to build a simulation model that behaves like a real battery. The implementation can be carried out using Neural Networks (NN) to compute the instant values of the circuit elements. The solution could thus be an ensemble of NNs that drives variable RC elements and OCV generator. The aim of this Chapter is thus to develop a NN-based Battery Digital Twin (BDT) that receives normalized SoC, SoH parameters as inputs, and produces a realistic voltage output signal in response to a load current waveform of any shape. In this way the output voltage will be a function of cell current and known charges and ageing states, thereby providing a platform to test algorithms that must reconstruct the cell states from only the voltage and current signals. The BDT has many purposes: it can be used as a simulator for fast testing of state estimation algorithms, or for battery monitoring or diagnostic when run in parallel with the real battery. This BDT is very useful in SB, where the single cells inside the pack can be used according to their states (SoC, SoH), possibly leading to a longer lifetime of the battery. It is therefore essential, especially in SB, to have a tool that is able to simulate cells at different SoC and SoH. Since the BDT allows to simulate a smart battery pack with cells at different charge and ageing states, it can be used for the validation of different SB balancing algorithms, consequently allowing to test the optimization of the lifetime of the SB.

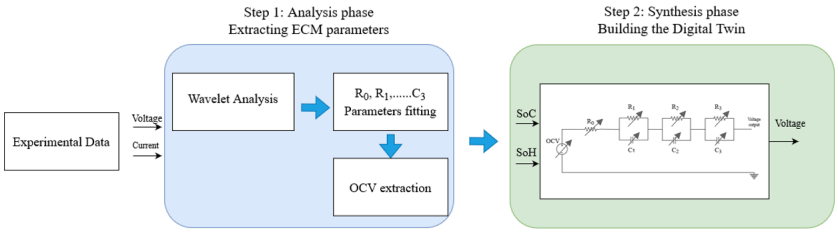

Figure 7.1: BDT development process

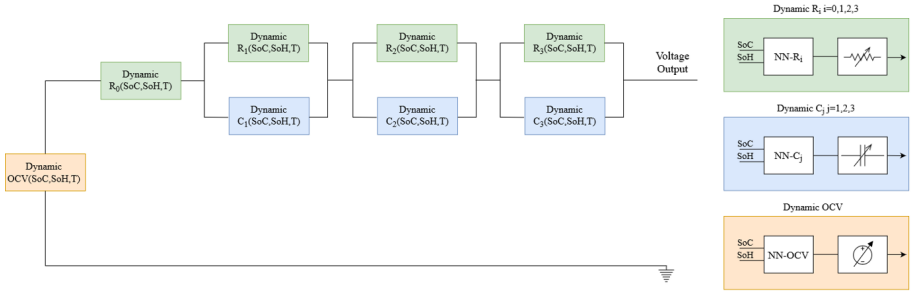

Figure 7.2: The NN-based dynamic ECM model

7.2 Battery Digital Twin

We will syntesize a BDT using the 3RC ECM model presented in Section 4.2. Developing a BDT starting from pulsed discharge experimental data is a two step process, as shown in Fig. 7.1. In the Analysis phase, experimental data are analyzed to extract only the relevant parts of the data needed to train the NN. This phase is performed with wavelet analysis. The data coming from the analysis step, are used in the synthesis step, to train the NNs. The results of the wavelet analysis presented in Chapter 6 will be used to train NNs to synthesize the BDT. Each NN will receive as input the SoH and SoC values and computes the output values for the OCV, R_0, R_1, C_1, R_2, C_2, R_3, C_3, as shown in Fig. 7.2.

7.3 Synthesis of the ECM model with feed forward neural networks

Now we want to implement all the nonlinear functions R_0, R_1, C_1, R_2, C_2, R_3, C_3,OCV for the realization of a cell model that can accurately reproduce the pulsed discharge waveforms and mimic the real cell as a digital twin. The solution is based on feed-forward neural networks that drive controlled RC elements for the simulation of the internal Z and a controlled VCVS for the simulation of the OCV generator. Neural networks can exactly fit the training points and moreover, they can compute the output for intermediate points, thanks to their interpolation and generalization properties. The neural network training has been done in the Matlab environment with the tools of the Deep Learning Toolbox. After several trials on different partitions of RC elements, it turns out that the best generalization results can be obtained by training a neural network for each function $R_0, R_1, C_1, R_2, C_2, R_3, C_3$, OCV. In this way, each neural network needs only few neurons (10-20) and the optimization can be carried out without interference from the other parameters. Other choices lead to bulk neural networks with many neurons and with poor generalization. Each NN has as input two rows vector [SoC; SoH] and outputs the control for the corresponding circuit parameter. The networks were trained with Levenberg-Marquardt backpropagation algorithm [1]. The training can be run several times. The best result must have the lowest Mean Squared Error (MSE) between the Neural Network outputs and the target values. The NNcell trained with the data shown in Section 6.6 and 6.7 have an MSE in the range $10^{-6} \leq \text{MSE} \leq 10^{-4}$. The Simulink scheme of the cell model is shown in Fig. 7.3. On the right side of Fig. 7.3 we can recognize the RC circuit for the realization of the complex internal impedance of the cell. All elements are variable and are controlled by an ensemble of neural networks. The OCV generator is realized by a controlled voltage source, again controlled by a neural network. All neural networks receive in input

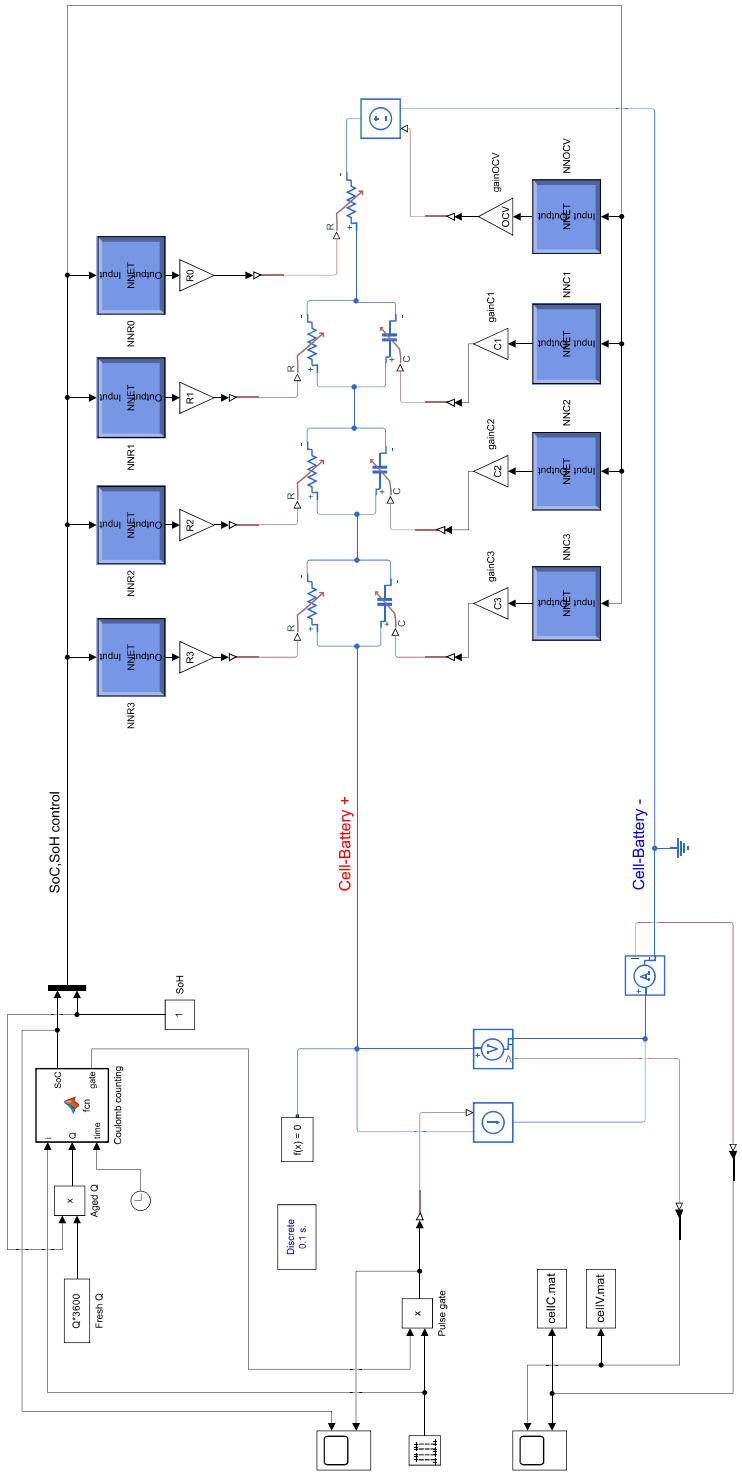

Figure 7.3: BDT Simulink model

the same SoC and SoH control signals. All electrical components are taken from the Simscape library and are simulated as physical elements (note the blue color of the scheme). On the left side of Fig 7.3 we can see a Simulink test circuit of the cell model. The test performs a pulsed discharge of the cell with a current of 1A, with the same timings of the NASA signals (10 minutes on, 20 minutes off). The charged fresh cell has a charge capacity of Q (2.1 Ah in the example). A Coulomb counting function computes the SoC and sends it to the neural networks. For simplicity, SoH is fixed as a constant. In a more sophisticated simulation, SoH can be computed from calendar ageing and/or from cycling ageing. The cell model outputs a realistic voltage signal according to the SoC and SoH states. By reversing the input current, the cell model can be used also for charging simulation. The blocks CellC.mat and CellV.mat record the current and voltage signals on files, for later offline post-processing. The gain blocks between neural networks and variable elements determine the actual values of the circuit components. The gains can be set up at the start of the simulation by an init.m program that writes variable values in the Matlab workspace. The gains are present because the neural networks are normalized to the component values at SoC = 1, SoH = 1 (see values in Figs. 6.11 -6.15a). This solution has been adopted in order to allow the BDT to simulate not only a single cell but a complete battery system consisting of a stream of s series connected cells and p parallel connected streams. With the hypothesis of identical cells, the battery can be simulated after multiplying gainOCV by s, gainRi by s/p and gainCi by p/s (i=1,2,3). In simulations where the cells are not identical, the series connection of cells must be really done and thus the BMS must send multiple SoC, SoH control signals.

The cell model of Fig. 7.3 can reproduce the NASA signals with the same pulsed currents and with the same SoH state, as shown on Fig.7.2 and 7.3 for SoH=1 and SoH=0.45, respectively. However, the cell model can now produce any signal waveform, so it is as if we can perform tests in the

laboratory on the same NASA battery cell without any hardware requirement using the developed battery digital twin.

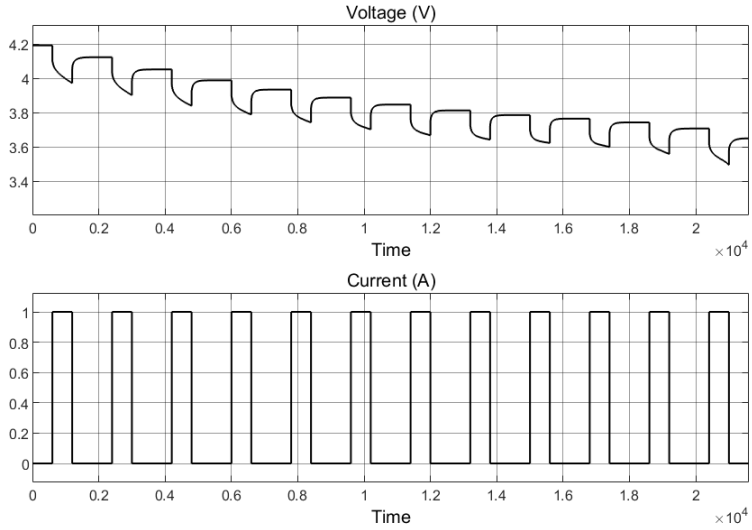

(a) BDT current input and voltage output at SoH = 1

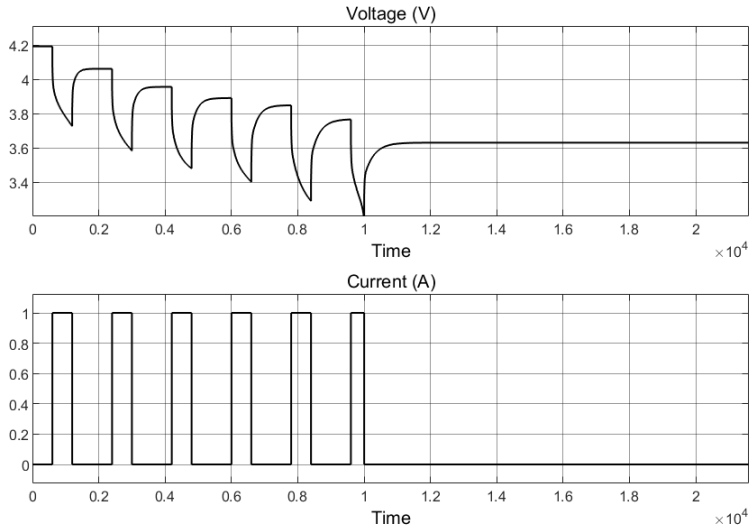

(b) BDT current input and voltage output at SoH = 0.45

Figure 7.4: BDT generating voltage signals for different SoH

7.4 Summary

The BDT produces a realistic voltage signal as a function of input current, SoC and SoH. The non-linear behavior of the OCV and of the internal impedance parameters versus SoC and SoH are simulated by feed-forward Neural Networks, trained with data extracted by wavelet analysis. This BDT has many useful applications. It could be used: to produce data signals for testing SoC and SoH algorithms; to simulate a battery pack with cells at different states of charge and/or ageing states to develop and test cell balancing algorithms. Moreover, the BDT could be run in parallel with a real battery for monitoring and diagnostic purposes.

References

[1] Pallavi Bharadwaj, Kunal Narayan Chaudhury, and Vinod John. Sequential optimization for pv panel parameter estimation. *IEEE Journal of Photovoltaics*, 6(5):1261–1268, 2016.

[2] Mohammad Charkhgard and Mohammad Farrokhi. State-of-charge estimation for lithium-ion batteries using neural networks and ekf. *IEEE Transactions on Industrial Electronics*, 57(12):4178–4187, 2010.

[3] Roberta Di Fonso, Pallavi Bharadwaj, Remus Teodorescu, and Carlo Cecati. A battery digital twin based on neural network for testing soc/soh algorithms. In *2022 IEEE 20th International Power Electronics and Motion Control Conference (PEMC)*, pages 655–660, 2022.

[4] Nitikorn Junhuathon, Guntinan Sakunphaisal, and Keerati Chayakulkheeree. Li-ion battery aging estimation using particle swarm optimization based feedforward neural network. In *2020 International Conference on Power, Energy and Innovations (ICPEI)*, pages 73–76, 2020.

Chapter 8

Main contributions and conclusions

8.1 Main contributions

This thesis gave the main contribution to the following topics:

- **Multilevel battery system for EVs:** a solution for the synthesis of the AC driving voltage for a PMSM motor inside an electric car. The proposed topology has been exploited to develop a regenerative braking system for an EV. Results on the WLTC test cycle show that the proposed system allows to recover up to 41% of the kinetic energy of the car. The paper has been published in [2] and Best Student Paper Award.

- **Multidimensional Machine Learning balancing in Smart Battery Packs (SBP):** Smart Battery Packs are a redundant battery topology based on the series connection of individual cell modules. Each module is formed by a cell with an insertion/bypass circuit and a wireless processor that monitors cell states and communicates with a Master controller. Ideally, the cells in the SBP should be identi-

cal. However, parameter variations of cells in EVs, along with different working conditions can cause SoC and temperature imbalances that shorten battery lifetime. A Machine Learning based control algorithm is proposed and tested in Matlab to insert/bypass the cells and reach simultaneous balancing of both SoC and temperature. The new method based on the K-nearest algorithm has been compared in simulation with a conventional sorting balancing method and showed superior performance, especially in temperature balancing. The results of this work have been published in [3].

- **Data-driven Modeling of Li-ion Battery:** The Simulink Datasheet Battery block is a ready-to-use subsystem that can simulate an ECM model, customized with look-up tables. Two different ways of creating the model are explored: using datasheets provided by the manufacturer and using more extensive laboratory measurements. This hybrid method of using the laboratoty data on datasheet battery model is named here as advance datasheet battery model. Results show that the measurements-based advanced datasheet battery model is more robust to model battery behavior, improving significantly the modelling accuracy compared to a pure datasheet-based approach. The results of this work have been published in [6].

- **Battery internal impedance estimation using Wavelet Analysis:** Battery performances degrade with usage and time and this translates into a decreased charge capacity and an increased internal impedance. Internal resistance is directly related to the amount of deliverable power, therefore its estimation is of particular interest for EVs. Observing the ageing effects on real batteries, however, is very time-consuming since many charge-discharge cycles need to be performed in the laboratory. The internal impedance effects are best seen on the output voltage of the battery when the input is a current pulse.

The wavelet time-frequency analysis can be used to filter the output voltage of the battery in order to estimate the internal impedance as a function of SoC and SoH. The wavelet analysis is a software tool to reconstruct the Nyquist plots of a battery cell, according to ageing conditions. Moreover, if applied to SB, the wavelet analysis is an online tool for internal impedance estimation. The results of this work have been published in [4].

- **Open Circuit Voltage (OCV) extraction methodology from pulsed discharge data:** OCV depends on SoC and SoH. Its measurement in the lab is very delicate and time-consuming. It requires putting the cell at rest for many hours and is also prone to measurement errors. A software procedure to extract OCV from pulsed discharge laboratory measurements is developed. The results of this work will be publised in [7].

- **Building a Battery Digital Twin (BDT):** To avoid working conditions that can accelerate irreversible degradation reactions, SoC and SoH must always be known. Since they cannot be measured directly with sensors on cells, they must be derived from the observation of voltage and current at the accessible connections. Testing of algorithms on real batteries is very time-consuming due to the need for many charge-discharge cycles in order to observe ageing effects. A Battery Digital Twin (BDT) that receives normalized SoC, SoH parameters as inputs, and produces a realistic voltage output signal in response to a load current waveform of any shape, is developed in this work. This BDT is a dynamic ECM-based built with feed-forward Neural Networks (NN). The time-frequency wavelet analysis is used as a domain-specific, automated pre-processing tool to prepare NNs training data. The BDT is essentially a battery simulator that is accelerated in time with respect to the SoH, so it is able to simulate both a cell at any given age, and

a cell that ages in seconds, not months. The BDT can be used for many purposes: (i) as a simulator for fast testing of state estimation algorithms; (ii) for the validation of balancing or other optimization algorithms (iii) for battery monitoring or diagnostic when run in parallel with the real battery. Partial results of this work have been published in [5] and the full BDT development procedure will be publised in [7].

8.2 Conclusions and future work

Thanks to their high energy density, high energy efficiency and long cycle life LIBs are employed in a broad range of applications: they are an effective solution for the integration of renewable energy sources in the smart grid and they are the preferred solution for electric mobility, ranging from Electric Vehicles (EVs) to mobile robots. In many applications, the battery is seen as a raw energy source, unsuitable to directly power the load. Thus, a converter/inverter is usually put as an interface between the battery and the final load to assure the required quality of output voltage. The first part of this thesis explored the advantages of using innovative battery topologies that integrate the multilevel inverter concept. Instead of a fixed stream of cells, the battery contains a stream of modules. Each module has insert/bypass power switches and one or more cells. By properly driving the switches at sampling times, the battery can synthesize a desired DC or even an AC output voltage, as well as perform cell balancing, charge control and subsequent thermal management. The number of modules can be redundant in order to assure fault tolerance against cell failures and/or to accommodate a greater total charge capacity. In the Chapter 1 a bidirectional 9-level cascaded H-bridge converter with batteries was proposed to synthesize the AC output voltage to control a PMSM motor of an electric car. A regenerative braking system has been developed, with the aim of recovering part of the kinetic energy of the car during braking. The proposed solution allowed to recover up to 41% of the energy of the car, compared to pure mechanical braking. Chapter 2 focused on another multilevel battery system: the smart battery. Since the SB has more cells than strictly necessary, at a given time only a subset of cells are series-connected. This topology has many useful features like modularity, reconfigurability, cell fault tolerance and greater useful capacity. In order to achieve optimal balancing in operation for both temperature and SoC, a multidimensional K-nearest control algorithm (MKNA) was developed and simulated with the aim to limit the spread of cell SoCs and temperatures.

The MKNA algorithm chooses the cells to be inserted/bypasses based on their "distance" from a virtual point that is dynamically computed at sampling time. The algorithm uses weighting factors to give more importance to SoC or temperature. This operation has the potential to extend the lifetime of the battery pack, which will be evaluated in future work. The structure of the MKNA algorithm allows to easily add other dimensions to the control strategy, such as the internal resistance or the SoH of the cells. The second part of the thesis focused on cell models. Chapter 3 presented an overview of how Li-ion cells work, and how the internal electrochemical reactions have effects on their operativity. Chapter 4 offered an overview of battery models and presented the ECM model adopted in this work. In Chapter 5, we presented a data-driven approach for modelling the behavior of a Li-ion battery using a ready-to-use model available in Simulink. We showed a systematic methodology of using the manufacturer's datasheets for available simulation platforms, such as Matlab-Simulink. In order to overcome the limited data availability in manufacturer's datasheets we have enhanced the model by including extensive laboratory measurements for building a robust advanced battery datasheet model that can predict battery behavior under varied field applications. In future work, we will further enhance the proposed model by incorporating different ageing cases for a more complete approach. Chapter 6 presented the wavelet time-frequency analysis as a software alternative to EIS-based experimental techniques. The proposed methodology was applied to pulsed discharge signals from the publicly available prognostic data repository of NASA. Furthermore, a methodology for OCV extraction was presented. Future work will explore the potential to use the wavelet analysis in SB topologies, where it could be used for online estimation of the cell parameters and SoH. This knowledge can then be used to develop strategies to use the cell in the pack optimally with the goal of maximizing the battery lifetime. Furthermore, we will explore how to use the wavelet analysis to extract other parameters of interest, such as temperature. Chapter 7 presented

the battery digital twin. The BDT produces a realistic voltage signal as a function of current and SoC and SoH states. The non-linear behavior of the OCV and the internal impedance parameters versus SoC and SoH are simulated usding feed-forward Neural Networks. In this work, we developed a battery digital twin using the experimental data from the publicly available Prognostic data repository of NASA. By collecting pulsed discharge data from a specific battery of interest, the whole developing process can be repeated, obtaining a BDT tailored to the battery of interest. Future work will focus on the BDT applications: (i) for the testing of SoC and SoH estimation algorithms (ii) to simulate cells of different charge capacities and aging times in battery packs (iii) to be used in a battery cell simulators for testing Battery Management Systems as Hardware-in-the- Loop systems (BMS HiL) (iv) to be run in parallel with real battery in on-field applications, such as EVs and smart grids for monitoring/diagnosis purposes.

References

[1] Roberta Di Fonso and Carlo Cecati. Navigation and motors control of a differential drive mobile robot. In *2023 International Conference on Control, Automation and Diagnosis (ICCAD)*, pages 1–6, 2023.

[2] Roberta Di Fonso and Carlo Cecati. Test cycle simulation of an electric car with regenerative braking. In *2020 AEIT International Conference of Electrical and Electronic Technologies for Automotive (AEIT AUTOMOTIVE)*, pages 1–5, 2020.

[3] Roberta Di Fonso, Xin Sui, Anirudh Budnar Acharya, Remus Teodorescu, and Carlo Cecati. Multidimensional machine learning balancing in smart battery packs. In *IECON 2021 47th Annual Conference of the IEEE Industrial Electronics Society*, pages 1–6, 2021.

[4] Roberta Di Fonso, Pallavi Bharadwaj, Remus Teodorescu, and Carlo Cecati. Internal resistance estimation of li-ion batteries using wavelet analysis. In *2022 IEEE 13th International Symposium on Power Electronics for Distributed Generation Systems (PEDG)*, pages 1–5, 2022.

[5] Roberta Di Fonso, Pallavi Bharadwaj, Remus Teodorescu, and Carlo Cecati. A battery digital twin based on neural network for testing soc/soh algorithms. In *2022 IEEE 20th International Power Electronics and Motion Control Conference (PEMC)*, pages 655–660, 2022.

[6] Roberta Di Fonso, Remus Teodorescu, Daniel-Ioan Stroe, Carlo Cecati, and Pallavi Bharadwaj. Data-driven modeling of li-ion battery based on the manufacturer specifications and laboratory measurements. In *2022 IEEE Power Electronics, Drives and Energy Systems (PEDES)*, 2022.

[7] Roberta Di Fonso, Remus Teodorescu, Carlo Cecati, and Pallavi Bharadwaj. A battery digital twin from pulsed laboratory data using wavelet analysis and neural networks. *Submitted for publication to IEEE Transaction on Industrial Informatics*, 2023.

Appendix

Wavelet theory

The Continuous Wavelet Transform (CWT) of a finite energy signal $x(t)$ is [12]:

$$W_\Psi(u,s) = \frac{1}{\sqrt{s}} \int_{-\infty}^{+\infty} x(t)\Psi^* \frac{(t-u)}{s} dt \tag{1}$$

Where $\Psi(t)$ represents the mother wavelet, i.e. a complex-valued time-frequency filter; u is the time shift parameter (for time localization) and s is a scaling parameter (for frequency localization). The CWT can be thought as the output of a bandpass filter whose input is the signal $x(t)$. By choosing a suitable mother wavelet, we can compute the time-frequency content of the signal as coefficients of the CWT. The choice of which wavelet to use depends on its time and frequency resolution. Only analytic wavelets will be considered, i.e. wavelets whose spectrum is zero for negative angular frequencies: $\Psi(\omega) = 0, \quad \omega < 0$. In this work, we will use the Generalized Morse Wavelet :

$$\Psi(\omega) = U(\omega) K_{(\beta,\gamma)} \omega^\beta e^{-\omega^\gamma} \tag{2}$$

Where $U(\omega)$ is the Heaviside function, and $K_{(\beta,\gamma)}$ is a normalizing factor. Unlike other mother wavelets, the Generalized Morse wavelet is defined by two parameters $\beta, \gamma > 0$ that allow to change the wavelet properties, while remaining exactly analytic [9, 10, 11, 12]. By properly choosing β, γ, ω we

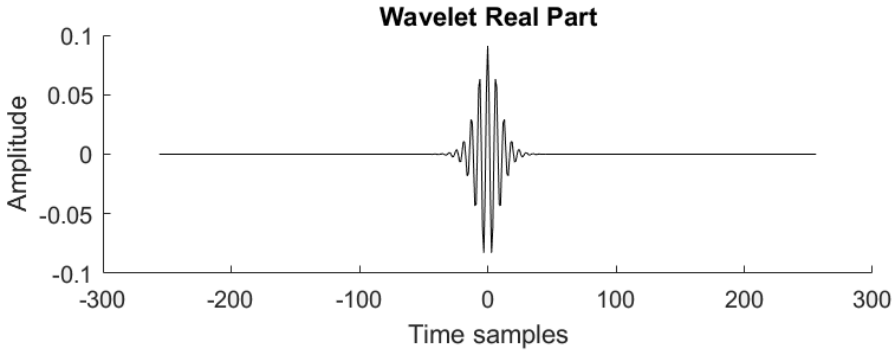

(a) Wavelet real part

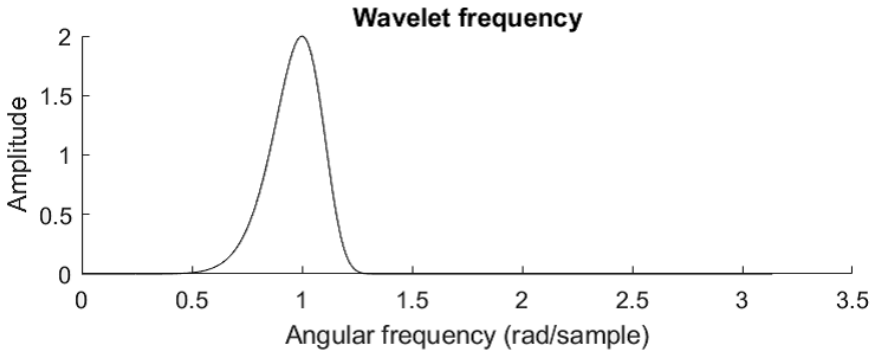

(b) Wavelet imaginary part

Figure 1: Generalized Morse wavelet

can tune the frequency and the bandpass resolution.

Fig. 1 shows an example of the generalized Morse wavelet plotted using the MATLAB toolbox JLAB, freely available online [8]. The wavelet can be thought as the impulse response of a bandpass filter. Fig. 2b shows the zoomed output of this filter (i.e. CWT) when the input is the voltage signal of Fig. 2a. As the wavelet is complex in the time domain, Fig. 2b shows the real and imaginary part, as well the absolute value, which peaks at the rising transition of the voltage signal. Knowing this behavior, the wavelet transform is applied to voltage and current signals $v(t), i(t)$ of the cell battery

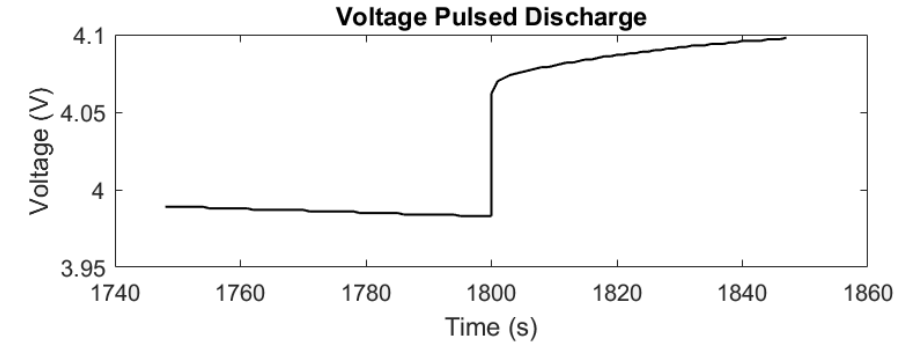

(a) Pulsed voltage discharge

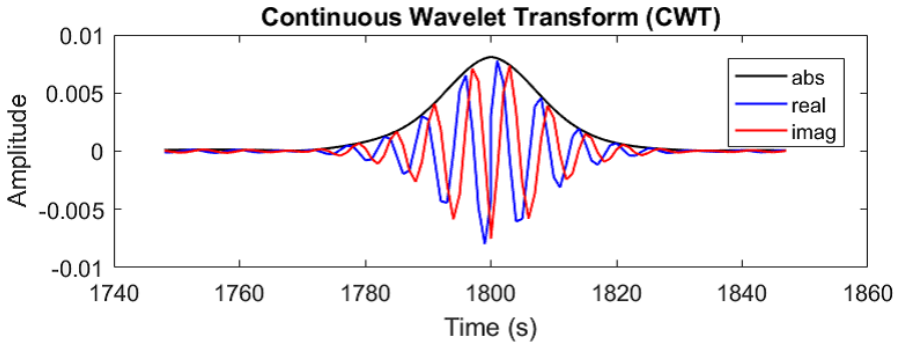

(b) CWT

Figure 2: CWT of the pulsed discharge voltage

in order to obtain a set of coefficients:

$$\begin{aligned} W_i(t,\omega) &= Re\left\{W_i(t,\omega)\right\} + jIm\left\{W_i(t,\omega)\right\} \\ W_v(t,\omega) &= Re\left\{W_v(t,\omega)\right\} + jIm\left\{W_v(t,\omega)\right\} \end{aligned} \tag{3}$$

where $W_v(t,\omega)$ is the wavelet transform of the signal $v(t)$ as a function of time t and angular frequency ω. Since the transform is a linear operation, the cell impedance Z can be then identified by a division between the CWT coefficients of voltage and current:

$$Z(t,\omega) = \frac{W_v(t,\omega)}{W_i(t,\omega)} \tag{4}$$

$Z(t,\omega)$ is the instantaneous amplitude and phase of impedance Z at angular frequency ω. By changing the wavelet frequency we can perform a time-frequency analysis of a signal to identify the whole ECM model.

References

[8] J. M. Lilly. jlab: A data analysis package for matlab.

[9] Jonathan M. Lilly and Sofia C. Olhede. Higher-order properties of analytic wavelets. *IEEE Transactions on Signal Processing*, 57(1):146–160, 2009.

[10] Jonathan M. Lilly and Sofia C. Olhede. On the analytic wavelet transform. *IEEE Transactions on Information Theory*, 56(8):4135–4156, 2010.

[11] Jonathan M. Lilly and Sofia Charlotta Olhede. Generalized morse wavelets as a superfamily of analytic wavelets. *IEEE Transactions on Signal Processing*, 60:6036–6041, 2012.

[12] Gjorgji Nusev, Dani juricic, Miran Gaberscek, Joze moskon, and Pavle Boskoski. Fast impedance measurement of li-ion battery using discrete random binary excitation and wavelet transform. *IEEE Access*, 9:46152–46165, 2021.

La borsa di dottorato è stata cofinanziata con risorse del Programma Operativo Nazionale 2014-2020 (CCI 2014IT16M2OP005), Fondo Sociale Europeo, Azione I.1 “Dottorati Innovativi con caratterizzazione industriale”